AN EMPIRICAL RELATIONSHIP BASED ON HIGH-PASS FILTERING TO ESTIMATE USABLE PERIOD RANGE FOR NONLINEAR SDOF RESPONSE

A THESIS SUBMITTED TO
THE GRADUATE SCHOOL OF NATURAL AND APPLIED SCIENCES
OF
MIDDLE EAST TECHNICAL UNIVERSITY

BY

ÖZKAN KALE

IN PARTIAL FULFILLMENT OF THE REQUIREMENTS
FOR
THE DEGREE OF MASTER OF SCIENCE
IN
CIVIL ENGINEERING

DECEMBER 2009

Approval of the thesis:

AN EMPIRICAL RELATIONSHIP BASED ON HIGH-PASS FILTERING TO ESTIMATE USABLE PERIOD RANGE FOR NONLINEAR SDOF RESPONSE

submitted by **ÖZKAN KALE** in partial fulfillment of the requirements for the degree of **Master of Science in Civil Engineering Department, Middle East Technical University** by,

Prof. Dr. Canan ÖZGEN ____________________
Dean, Graduate School of **Natural and Applied Sciences**

Prof. Dr. Güney ÖZCEBE ____________________
Head of Department, **Civil Engineering**

Assoc. Prof. Dr. Sinan AKKAR
Supervisor, **Civil Engineering Dept., METU** ____________________

Examining Committee Members:

Prof. Dr. Polat GÜLKAN ____________________
Civil Engineering Dept., METU

Assoc. Prof. Dr. Sinan AKKAR ____________________
Civil Engineering Dept., METU

Assist Prof. Dr. Ayşegül ASKAN GÜNDOĞAN ____________________
Civil Engineering Dept., METU

Assist Prof. Dr. M. Tolga YILMAZ ____________________
Engineering Sciences, METU

Assist Prof. Dr. Zehra ÇAĞNAN ____________________
Civil Engineering Dept., METU, (NCC)

Date: 21.12.2009

I hereby declare that all information in this document has been obtained and presented in accordance with academic rules and ethical conduct. I also declare that, as required by these rules and conduct, I have fully cited and referenced all material and results that are not original to this work.

Name, Last name: Özkan KALE

Signature :

ABSTRACT

AN EMPIRICAL RELATIONSHIP BASED ON HIGH-PASS FILTERING TO ESTIMATE USABLE PERIOD RANGE FOR NONLINEAR SDOF RESPONSE

Kale, Özkan
M. Sc., Department of Civil Engineering
Supervisor: Assoc. Prof. Dr. Sinan Akkar

December 2009, 115 pages

High-pass filtering that is one of the most efficient methods in removing long-period noise of accelerograms is investigated for its effect on nonlinear oscillator deformation response. Within this context, uncertainty in filter cut-off periods that would significantly modify the low-frequency content of accelerograms come into prominence for obtaining reliable long-period displacement response. Analog and digital ground-motion records from recently compiled Turkish strong-motion database are used and these records are high-pass filtered with a consistent methodology by randomly generated filter cut-offs that represent different filter cut-off decisions of the analysts. The uncertainty in inelastic spectral and residual displacements (SD_{IE} and SD_R, respectively) due to variations in filter cut-offs is examined to derive the usable period ranges where the effect of high-pass filtering is tolerable. Non-degrading, stiffness degrading and stiffness and strength degrading oscillator behavior are considered in these analyses. The level of nonlinear behavior in single degree of freedom (SDOF) response is described by varying the yield strength (R, normalized yield strength) and displacement ductility (μ) levels. The usable period ranges that depend on magnitude, recording quality,

level of inelasticity and level of degradation are determined for SD_{IE} through robust probabilistic methodologies.

Keywords: Strong-motion, high-pass filtering, filter cut-off period, nonlinear oscillator response, hysteretic model, probability, usable period.

ÖZ

DOĞRUSAL OLMAYAN TEK SERBESTLİK DERECELİ SİSTEM DAVRANIŞININ KULLANILABİLİR PERİYOT ARALIKLARININ YÜKSEK GEÇİRİMLİ FİLTRELEMEYE DAYALI BELİRLENMESİNE YÖNELİK AMPİRİK İLİŞKİSİ

Kale, Özkan
Yüksek Lisans, İnşaat Mühendisliği Bölümü
Tez Yöneticisi: Doç. Dr. Sinan Akkar

Aralık 2009, 115 sayfa

Uzun periyot gürültüsünün ivme kayıtlarından arındırılması için en etkili yöntemlerden biri olan yüksek geçirimli filtrelemenin doğrusal olmayan osilatör tepki deformasyonuna etkileri incelenmiştir. Bu bağlamda, güvenilir uzun periyot tepki yer değiştirmesi elde edebilmek için kayıtların düşük frekans içeriğini önemli ölçüde değiştiren filtre periyodundaki değişkenlik önem kazanmaktadır. Yeni derlenen Türk ulusal kuvvetli yer hareketi veritabanına ait analog ve dijital ivme kayıtları ele alınmıştır ve bu kayıtlar araştırmacıların değişik filtre periyodu seçimlerini temsil eden rastgele türetilmiş filtre periyotlarıyla tutarlı bir yönteme göre yüksek geçirimli filtrelenmiştir. Filtre periyodundaki farklılıklardan kaynaklanan elastik olmayan yer değiştirme spekturumundaki ve kalıcı yer değiştirmedeki (sırasıyla SD_{IE} ve SD_R) değişkenlik, yüksek geçirimli filtre etkisinin tolere edilebilir olduğu periyot aralığını belirleyebilmek için incelenmiştir. Analizlerde azalımsız, rijitlik azalımlı ve rijitlik ve kapasite azalımlı osilatör davranışı göz önüne alınmıştır. Tek serbestlik dereceli sistemlerin doğrusal olmayan davranış düzeyi, akma kapasitesi (R, normalize edilmiş akma kapasitesi)

ve süneklik (μ) düzeyindeki değişimlerle ifade edilmiştir. Deprem büyüklüğü, kayıt kalitesi, elastik olmama derecesi ve azalıma bağlı olan kullanılabilir periyot aralıkları, güçlü olasılıksal yöntemlerle elastik olmayan tepki yer değiştirmeleri için belirlenmiştir.

Anahtar Kelimeler: Kuvvetli yer hareketi, yüksek geçirimli filtreleme, filtre periyodu, doğrusal olmayan osilatör tepkisi, malzeme davranım modeli, olasılık, kullanılabilir periyot.

To My Parents

ACKNOWLEDGMENTS

I would like to express my endless thanks to my supervisor Dr. Sinan Akkar for his support, guidance, advice, criticism, encouragement and insight throughout the study.

I would like to express my sincere thanks to Dr. Sinan Akkar and Dr. Polat Gülkan for supplying the office facilities at Civil Engineering Department.

This work is supported by Scientific Research and Technical Council of Turkey (TÜBİTAK) under Award No. 105G016. The funding provided by TÜBİTAK is gratefully acknowledged.

I also would like to express my deepest thanks to Dr. M. Altuğ Erberik for his valuable support and comments on hysteretic model studies.

I am grateful to Abdullah Sandıkkaya, Bekir Özer Ay, Emrah Yenier, Koray Kadaş, Özgür Erdoğan, and Tuba Eroğlu for their friendship, assistance and encouragement during the thesis study. I also owe thanks to İlker Kazaz for his friendship and support.

I wish to thank to Gökalp Ulucan and Doruk Doğanay for their friendship during my social life. I also thanks to Nazile Tekin for her special coffees.

Finally, endless thanks to my father Ethem Kale, my mother Melek Kale, my brother Volkan, my uncle Fikri Soyarslan, my aunt İlknur Soyarslan and my cousins Melis and İdil for their encouragement, confidence in me, support and for their love.

TABLE OF CONTENTS

LIST OF TABLES

LIST OF FIGURES

LIST OF ABBREVIATIONS

CDF	Cumulative Distribution Function
d	Joyner and Boore distance (R_{jb})
f	force
f_a	theoretical source spectrum corner frequency
FAS	Fourier Acceleration Spectrum
f_c	high-pass filter frequency
$f_{c,max}$	maximum high-pass filter frequency
$f_{c.min}$	minimum high-pass filter frequency
$f_{c,opt}$	optimum filter cut-off frequency
$f_{c,rlx}$	relaxed filter cut-off frequency
$f_{c,svr}$	severe filter cut-off frequency
f_m	maximum strength
f_r	residual strength
$f_x(i)$	maximum strength after degradation
$f_x(i-1)$	maximum strength before degradation
f_y	yield strength
f_y^+	positive yield strength
f_y^-	negative yield strength
f^2	theoretical decay rate of low-frequency components
GMPEs	ground-motion prediction equations
k_r	post-capping stiffness
k_u	post-yielding stiffness
k_0	initial elastic stiffness
k_1	unloading stiffness
M_w	moment magnitude

n	hysteretic excursion number
ND	non-degrading
NEHRP	National Earthquake Hazard Reduction Program
N/A	not available
PDF	Probability Distribution Function
Pr	probability
R	normalized yield strength
R_{jb}	Joyner and Boore distance (closest distance from site to vertical projection of fault rupture)
SD	stiffness degrading
SD_E	elastic spectral displacement
SD_{IE}	inelastic spectral displacement
SDOF	single degree of freedom
SD_R	residual displacement
SSD	stiffness and strength degrading
T	period
T_c	high-pass filter cut-off period
u	displacement
u_m	maximum displacement
u_r	residual displacement
USDP	Utility Software for Data Processing
u_x	maximum displacement
u_y	yield displacement
u_y^+	positive yield displacement
u_y^-	negative yield displacement
V_{S30}	average shear-wave velocity in the upper 30 m soil profile
α_u	post-yielding stiffness ratio
α_r	post-capping stiffness ratio
β_a	strength degradation factor
β_b	strength degradation factor

β_0	stiffness degradation factor
χ	fractional factor
κ	fractional factor
λ	residual to yielding strength ratio
μ	displacement ductility
$\mu_{SD_{IE}}$	average inelastic spectral displacement
σ	standard deviation

CHAPTER 1

INTRODUCTION

1.1 Background and Literature Survey

The nonlinear response of structures has been a research topic for many years because most structural systems are designed to behave in the post-elastic range under severe seismic action. With advances in displacement-based design and assessment procedures, significant amount of studies in this field have focused on calculating the expected peak nonlinear deformation demands on oscillators (inelastic spectral displacements, SD_{IE}). Recently, the estimation of SD_{IE} has been upgraded to more sophisticated prediction equations in the sense that they account for a more complete suite of seismological estimator parameters for their effects on nonlinear single degree of freedom (SDOF) response (e.g., Tothong and Cornell, 2006). These equations have similar formats to those implemented in the conventional ground-motion prediction equations (GMPEs).

The continuous developments in the SD_{IE} predictive models bring forward the reliability of long-period content of strong motions because recent studies (e.g. Akkar and Boore, 2009) have shown that the uncertainty in the long-period ground-motion components can be a serious limitation for nonlinear oscillator response. The major source of this uncertainty stems from the inherent long-period noise embedded in the strong-motion records. Figure 1.1 shows an example to demonstrate this fact. It presents the variations of elastic (SD_E) and inelastic spectral displacements (left and right panels, respectively) of a record that is subjected to a set of different data processing schemes to remove the existing long-period noise. The dispersion (scatter about the mean spectral curve defined by the solid black line) is more prominent in SD_{IE} and commences at relatively shorter vibration periods when compared to the corresponding deviations in SD_E. Thus, the uncertainty in the long-period ground-motion components is magnified more by nonlinear oscillators with respect to their linear counterparts.

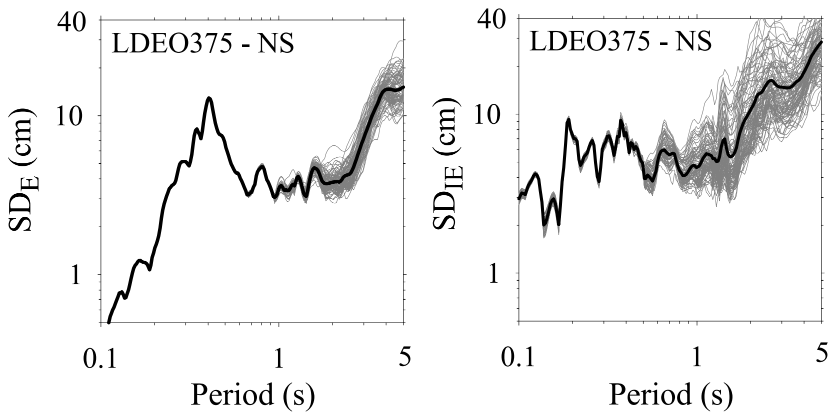

Figure 1.1 Elastic (left panel) and inelastic (right panel) spectral displacements (gray curves) of a digital record subjected to different data processing schemes to remove the long-period noise. Inelastic spectra are calculated for elastoplastic hysteretic behavior with a normalized strength ratio of R=4. Black solid lines show the mean of spectral displacements computed for each processing scheme (modified from Akkar and Boore, 2009).

The influence of long-period noise and high-pass filtering (widely used data processing tool for removing the long-period noise) on reliable SD_E calculations has been discussed in various studies (e.g. Abrahamson and Silva, 1997; Boore and Bommer, 2005; Akkar and Bommer, 2006). Akkar and Bommer (2006) proposed some empirical factors to be used as a fraction of T_c (low-cut filter cut-off period) that vary for different site classes and recording type (i.e. digital vs. analog records). Abrahamson and Silva (1997) also proposed to use elastic spectrum for periods up to $0.8T_c$ based on the theoretical relationship between the oscillator response and digital filter behavior. These studies have revealed practical guidance for determining spectral bands where the peculiarities in elastic spectral response due to high-pass filtering can be disregarded. To the best of author's knowledge, this discussion has not been extended systematically for variations in SD_{IE}. Few studies showed how different filtering techniques (acausal vs. causal or bidirectional vs. unidirectional filter) might affect the nonlinear oscillator displacements (e.g., Boore and Akkar, 2003; Bazzurro et al., 2005) but none of them has gone into the details of interaction between high-pass filter cut-offs and nonlinear deformation demands. These studies only concluded that inelastic spectrum is relatively less sensitive to the high-pass filter values when bidirectional (acausal) filters are used. Akkar and Ozen (2006) acausally filtered a set of analog ground motions using alternative high-pass filter values computed from different noise models. They showed that the elastoplastic spectra of low-magnitude rock site analog records are more sensitive to high-pass filtering such that the influence of filter cut-off commences at spectral periods significantly shorter than the chosen T_c value.

This study contributes to this discussion by investigating the influence of high-pass (low-cut) filter cut-offs (T_c) on the nonlinear spectral and residual displacements. The latter spectral parameter is used to validate the SD_{IE} based observations for another nonlinear sdof deformation quantity. Moreover, the residual displacement spectrum (Kawashima et al., 1998) has recently become an important deformation demand index for verifying the seismic performance of buildings.

1.2 Object and Scope

In the first stage, this study generates random sets of T_c for a suite of ground motions to represent the likely variation in the choice of this parameter while removing the long-period noise. Later, SD_{IE} and SD_R for two commonly used inelastic spectrum types: the constant strength (R) and constant ductility (μ) spectra are calculated to observe whether the level of uncertainty in SD_{IE} and SD_R changes due to the conceptual differences in the calculations of these two spectra. Bilinear hysteretic model and modified version of Clough and Johnston hysteretic model (1966) for representing different degradation levels (stiffness degradation and stiffness and strength degradation) are considered in the spectral calculations. Magnitude and level of inelasticity (different R or μ values) that contribute to the dispersion in SD_{IE} and SD_R are also investigated within the context of the study for a complete picture of shortfalls invoked by high-pass filtering. In the final part of this study, usable spectral period ranges are derived that are based on robust probabilistic methods where the risk of unreliable SD_{IE} due to high-pass filtering is below a certain level. The results and discussions of this thesis are believed to be useful for the improvements of nonlinear spectral displacement GMPEs. The discussions may also be important to understand the limitations of high-pass filtered records for their implementation in the nonlinear response history analysis of long-period structural systems.

1.3 Organization of the Thesis

The study starts by describing the hysteretic models that are used in the nonlinear oscillator response. These hysteretic models are capable of representing different degradation levels (Chapter 2).

General information related to the ground-motion database considered in this study and explanations about the high-pass filtering procedure are the subjects of Chapter 3. The database is presented in terms of magnitude, distance and site class parameters. In the strong-motion data processing part, decisions on high-pass filter cut-offs and their random generation procedure are described.

Chapter 4 introduces and applies the procedure described in Chapter 3 to determine the usable period ranges pertaining to different magnitude and filter cut-off intervals as well as recording type (analog vs. digital). At the beginning of this chapter, the uncertainty on nonlinear oscillator response due to random filter cut-offs is also investigated by illustrations.

The main conclusions as well as future research directions are discussed in Chapter 5. The report includes an appendix displaying dispersion information in SD_{IE} and SD_R due to random variation of low-cut filter values.

CHAPTER 2

NONLINEAR HYSTERETIC MODELS

2.1 General

In this chapter, hysteretic behavior of nonlinear models used in this study is explained by individual illustrations. In order to represent the inelastic behavior of SDOF systems, hysteretic models reflecting different degradation levels are utilized. The degradation levels of the oscillators are defined as non-degrading (ND), stiffness degrading (SD) and stiffness and strength degrading (SSD). Bilinear hysteretic model is employed in order to simulate the seismic response of non-degrading systems whereas degrading models are based on the modified version of Clough model (Clough and Johnston, 1966; Mahin and Bertero, 1976).

2.2 Hysteretic Models

In this section, basic descriptions of the hysteretic models that are used in this study are explained. Non-degrading, stiffness degrading and stiffness and strength degrading oscillator response are represented by these hysteretic models.

2.2.1 Description of Backbone Curve

The backbone curve defines the hysteretic excursion path of force-deformation relationship for a SDOF system with certain parameters. The backbone curve of ND and SD models is shown in Figure 2.1.a whereas the backbone curve for the

SSD model is presented in Figure 2.1.b. The following parameters define the backbone curve.

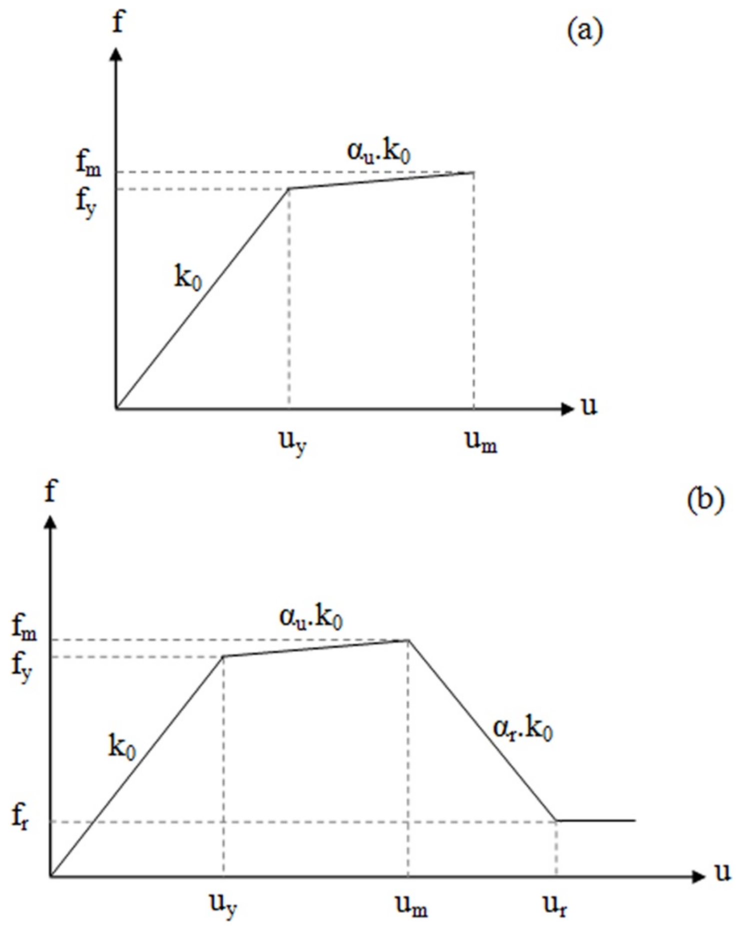

Figure 2.1 Backbone curves for a) ND and SD hysteretic models, b) SSD hysteretic model.

2.2.1.1 Initial Branch

Initial branch continues up to the yield point of the system (u_y, f_y) with an initial stiffness, k_0 that represents the elastic part of hysteretic excursion. The variables u_y and f_y are the yield displacement and yield strength of the oscillator, respectively.

2.2.1.2 Post-yielding Branch

Post-yielding branch begins with the yielding and continues until the starting point of unloading stage (u_m, f_m) for ND and SD systems and post-capping stage (u_m, f_m) for SSD systems. The parameters u_m and f_m are the maximum displacement and maximum strength attained on the related hysteretic cycle, respectively. The post-yielding stiffness (k_u) is defined in terms of post-yielding stiffness ratio (α_u) and the initial stiffness of the system:

$$k_u = \alpha_u \cdot k_0 \tag{2.1}$$

For SSD hysteretic behavior, the fraction of u_m/u_y is called as displacement ductility ratio (μ) of the system. The variable f_m is calculated as:

$$f_m = f_y + k_u \cdot (u_m - u_y) \tag{2.2}$$

2.2.1.3 Post-capping Branch

The post-capping is defined by the branch between (u_m, f_m) and (u_r, f_r) for SSD systems. The post-capping stiffness (k_r) is also defined in terms of post-capping stiffness ratio (α_r) and initial stiffness of the system:

$$k_r = \alpha_r \cdot k_0 \tag{2.3}$$

2.2.1.4 Residual Branch

The residual branch starts with the end point of post-capping section. The residual strength (f_r) of the system is defined as the fraction of yield strength:

$$f_r = \lambda \cdot f_y \tag{2.4}$$

where λ is called as residual to yielding strength ratio. The residual displacement (u_r) corresponding to residual strength is calculated as:

$$u_r = u_m + \frac{(f_m - f_r)}{k_r} \tag{2.5}$$

2.2.2 Bilinear Hysteretic Model

Bilinear hysteretic model that is shown in Figure 2.2 is used for representing the non-degrading (ND) hysteretic behavior in this study. Although the hysteretic energy dissipation is overestimated by this model, it is preferred by many researchers due to its simplicity. This feature of bilinear model constitutes one of the major motivations of its implementation by this study.

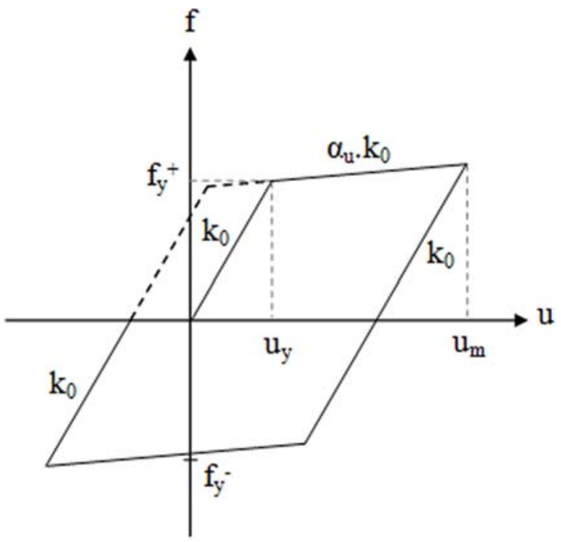

Figure 2.2 Representative force-deformation relationship of ND bilinear hysteretic model.

Non-degrading hysteretic behavior simply indicates that the unloading stiffness does not degrade with yielding. In this model, the loading and unloading stiffness (k_0) values are equal during the hysteretic excursion. The bilinear model with a post-yielding stiffness ratio of 0% is defined as elastic perfectly plastic model in the literature (Otani, 1981). In this study, the post-yielding stiffness ratio is considered as 3% in all nonlinear response history analysis that can be considered as a premise for a wide range of structural behavior.

2.2.3 Clough Hysteretic Model

As stated previously Clough model uses a bilinear backbone curve that represents the stiffness degradation during the reloading stage (Clough and Johnston, 1966). Mahin and Bertero (1976) modified the Clough model by adding stiffness degradation in the unloading stage. In this study, the model proposed by Mahin and Bertero (1976) is implemented to represent the stiffness degradation both in unloading and reloading stages. The hysteretic curve and model parameters are given in Figure 2.3.

During the hysteretic excursions, the reloading shoots for the preceding unloading point in modified Clough model. When reloading reaches the preceding unloading point, the target is previous maximum point. The unloading stiffness after yielding is degraded in accordance with the following equation

$$k_1 = k_0 \cdot \left(\frac{u_y}{u_m} \right)^{\beta_0} \tag{2.6}$$

where k_1, k_0 and β_0 are called as the unloading stiffness, initial elastic stiffness and stiffness degradation factor, respectively. β_0 takes values between 0 (no degradation) and 1.

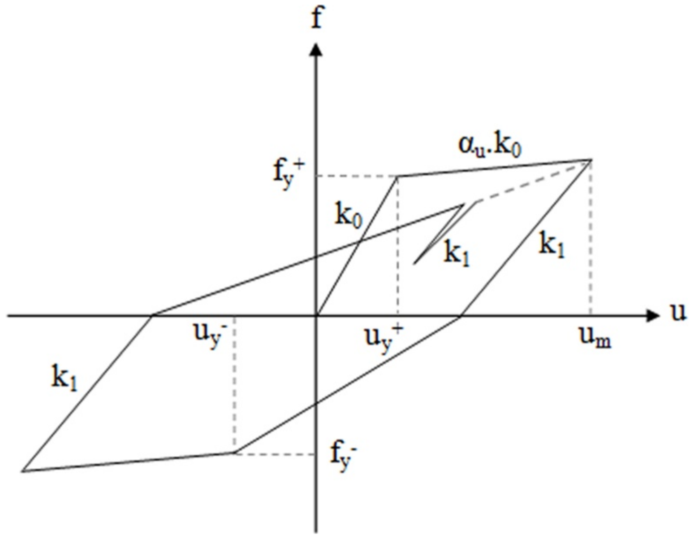

Figure 2.3 Representative force-deformation relationship of SD modified Clough hysteretic model.

2.2.4 Clough Hysteretic Model with Strength Degradation

SSD model is developed by introducing a strength degradation portion to the SD model. The strength degradation occurs in the reloading part after yielding. The strength degradation rule considers an exponential behavior that is described in the following expression

$$f_x(i) = \beta_a \cdot f_x(i-1) \cdot \left(1 - e^{\beta_b \cdot n \cdot \frac{u_x}{u_y}}\right) \tag{2.7}$$

In Equation (2.7), β_a and β_b are the strength degradation factors and n is the hysteretic excursion number to define the rate of degradation. This model as well as the others is implemented in the software called Utility Software for Data Processing (USDP, 2008). The terms $f_x(i-1)$ and $f_x(i)$ are maximum strength values before and after degradation, respectively. The ratio u_x/u_y is called as the ductility capacity (μ) of the system. In this ratio, u_x is the maximum displacement of the pertaining excursion.

The unloading stiffness after yielding is degraded in accordance with the following rule as in the SD model

$$k_1 = k_0 \cdot \left(\frac{u_x}{u_y} \right)^{\beta_0} \tag{2.8}$$

where k_1, k_0 and β_0 are the unloading stiffness, initial elastic stiffness and stiffness degradation factor, respectively. The parameter β_0 takes values between 0 and 1 as in the case of SD model.

Figure 2.4 illustrates a simple sketch of the SSD model. The envelope curve of this model is not bilinear. The descending part (or post-capping branch) beyond the maximum displacement point denotes a reduction in the strength capacity under large deformations. In this part, once the strength decreases at a constant rate, the system continues to carry additional lateral deformation. At the end of the descending portion, residual displacement part (or residual branch) is reached and the system does not continue to sustain additional deformation.

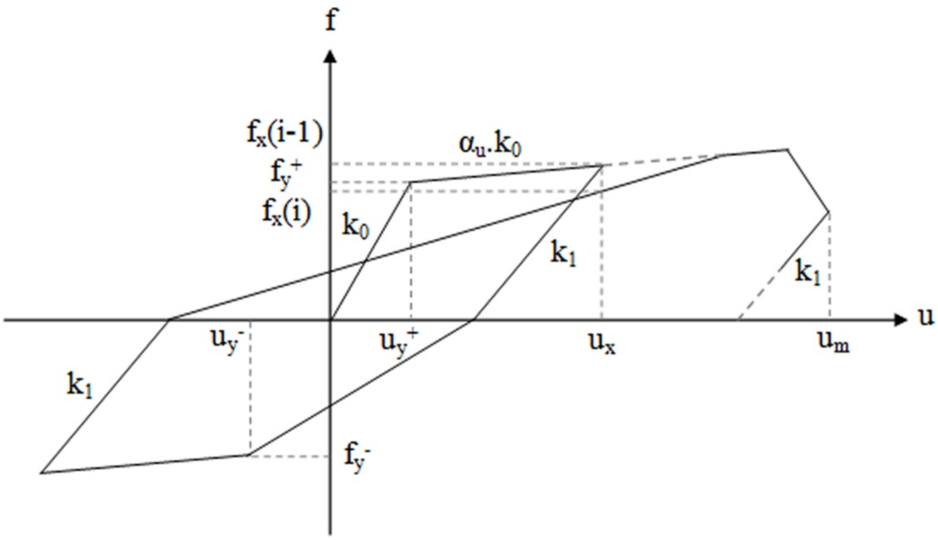

Figure 2.4 Representative force-deformation relationship of SSD Clough hysteretic model.

2.2.5 Calibration of SSD Model

The stiffness and strength degrading hysteretic model is calibrated with force-displacement data obtained from different test results on reinforced concrete (RC) columns (Erberik, 2001; Pujol, 2002; Wight and Sozen, 1973) in order to determine the relevant model parameters used in the analysis. After exploring the column test data, the cyclic strength degradation model parameters (β_a and β_b) are determined from the test results.

While conducting the calibration study, the procedure in Kurtman (2007) is followed. A typical example for the calibration study is presented in Figure 2.5. The gray curve in this figure presents the force-displacement relation from a test specimen (CAH-5) of Erberik (2001). It describes an example case for the moderate level of cyclic strength degradation. The black curve on the same figure represents the hysteretic loops obtained with the model parameters.

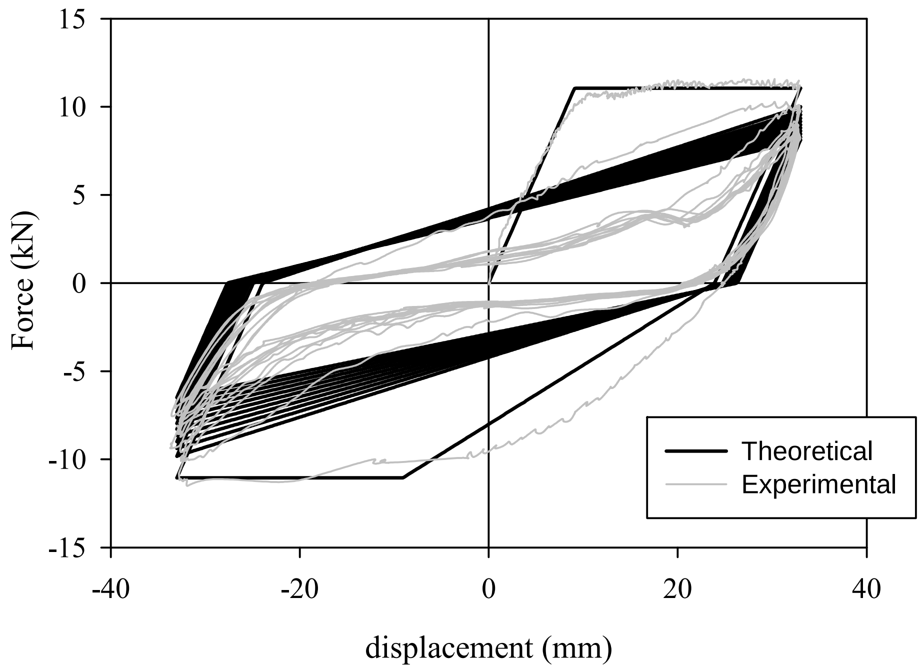

Figure 2.5 Experimental and theoretical force-displacement relationships for a test specimen (CAH-5) of Erberik (2001) for moderate degradation level.

The calibration results for moderate and severe cyclic strength degradation levels are given in Table 2.1. Since the level of cyclic strength degradation is different in positive and negative loading directions with respect to the experimental results, the calibration study is conducted separately for each direction. Table 2.2 lists the average values of the calibration results for a general use in nonlinear response history analysis.

Table 2.1 Calibration results of strength degradation parameters for the considered column test data.

Member ID	**Strength Degradation Level**	**Positive direction of loading**		**Negative direction of loading**	
		β_a	**β_b**	**β_a**	**β_b**
1	Moderate	0.980	0.705	0.960	0.715
2	Moderate	0.990	1.060	0.990	1.180
3	Moderate	0.985	0.845	0.990	0.620
4	Moderate	0.980	1.365	0.990	1.550
5	Moderate	0.975	0.835	0.975	0.655
6	Moderate	0.985	1.500	0.980	0.860
7	Severe	0.910	0.255	0.975	0.795
8	Severe	0.880	0.120	0.920	0.275
9	Severe	0.945	0.250	0.965	0.465
10	Severe	0.885	0.250	0.950	0.990
11	Severe	0.955	0.630	0.950	0.740

Table 2.2 Average values of the strength degradation parameters.

Strength Degradation Level	Positive direction of loading		Negative direction of loading	
	β_a	**β_b**	**β_a**	**β_b**
Moderate	0.983	1.052	0.981	0.930
Severe	0.915	0.301	0.952	0.653

Figure 2.6 presents comparative scatter plots between the calibration results obtained from each test specimen and average values listed in Table 2.2. This plot depicts that when moderate degradation is considered, the average and the individual values for the parameters (β_a and β_b) are close to each other at each direction of loading. However, scatters diverge from each other when severe degradation case is considered.

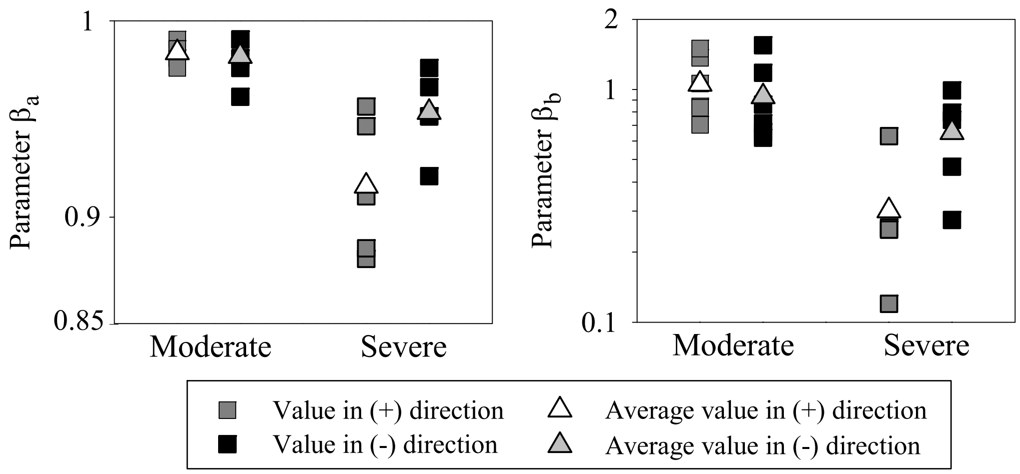

Figure 2.6 Comparisons between the individual calibration results with the average values listed in Table 2.2.

2.2.6 Selection of Model Parameters

Table 2.3 summarizes the hysteretic model parameters considered in the nonlinear response spectrum analysis of this study. During the decision stage of model parameter selection, the recent studies in the literature (Kurtman, 2007; Otani, 1981; Song and Pincheira, 2000) as well as the calibration results of this study are considered. Otani (1981) considers the parameter β_0 between 0 and 0.5 in SD model. In SSD model, once the parameter α_r takes values between 0% and 3%, the parameters α_u, λ and μ are considered as 5%, 10% and 1.25, respectively (Song and Pincheira, 2000). Kurtman (2007) recommends the β_0 value as 0.4 and 0.5 for different stiffness degrading models. The same study gives the parameter α_u as 3% and 1% at different loading directions (positive and negative, respectively) for SSD model (for other SSD model parameters, see Kurtman, 2007). Table 2.3 summarizes the model parameters used in the analysis.

Table 2.3 Summary of the hysteretic models and related model parameters considered in the nonlinear response spectrum analysis.

Model Parameter	ND Bilinear	SD Clough	SSD Clough
α_u	0.03	0.03	0.03
β_0	-	0.5	0.5
β_a	-	-	1.0
β_b	-	-	1.0
α_r	-	-	0.12
λ	-	-	0.10
μ	-	-	4.0

CHAPTER 3

GROUND MOTION

3.1 General

This chapter gives general information about the ground motions used in this study and some brief explanation about the high-pass filtering methodology implemented for the strong-motion data processing. The ground motion records are presented in terms of moment magnitude (M_w), Joyner-Boore (R_{jb}) distance (Joyner and Boore, 1981) and site class. While determining the usable period ranges for inelastic oscillator response, M_w is considered as the only dominant strong-motion parameter. In strong-motion data processing, the set of filter cut-off frequencies, f_c[1], (high-pass filter values) implemented for each record follow uniform distribution and they are randomly generated by using Latin Hypercube Sampling method. The software that is called as Utility Software for Data Processing (USDP) is used for processing the strong-motion data. The procedure explained in Akkar and Bommer (2006) guides this study while determining the set of high-pass filter cut-offs for each record.

[1] Reciprocal of f_c is defined as T_c that defines the high-pass filter values in terms of period.

3.2 Ground-Motion Database

The strong-motion data that comprises of analog and digital records are selected from the recently compiled Turkish strong-motion database[2]. The dataset comprises of dense-to-stiff soil recordings encompassing small to large magnitude events from Turkey. The site classes of the records in the database are classified as NEHRP B, C and D type with V_{S30} (average shear-wave velocity in the upper 30 m soil profile) ranging between 760 m/s < $V_{S30} \leq$ 1500 m/s, 360 m/s < $V_{S30} \leq$ 760 m/s and 180 m/s $\leq V_{S30} \leq$ 360 m/s, respectively (BSSC, 2003). The NEHRP B records whose V_{S30} values are close to the upper limit of the NEHRP C site class definition are considered as NEHRP C site class due to their scarce and uneven distribution in the database. The site class information of a few strong-motion records is represented as N/A in this study since their V_{S30} values do not exist in the database. The moment magnitude (M_w) values of the accelerograms change from 4.0 to 7.6. Since magnitude is a dominating parameter that effects the usable spectral period range (Akkar and Bommer, 2006), the chosen records are subdivided into magnitude clusters as $4 \leq M_w \leq 5$ (digital), $5 < M_w \leq 6$ (analog and digital) and $M_w > 6$ (analog and digital). This way, the effect of high-pass filtering on inelastic spectral displacement is emphasized with the variations of M_w. Table 3.1 gives the number of records in each magnitude bin as a function of site class and record type. Figure 3.1 illustrates the dataset variation in terms of magnitude vs. distance scatter. The database has a distance range of 0 and 200 km. A total of 528 records is used to carry out the statistical analysis of nonlinear oscillator response. The majority of these records are digitally recorded accelerograms.

[2] The database compilation is carried out under the framework of the project entitled "Compilation of Turkish strong-motion network according to the international standards." This collaborative project is supported by the Scientific and Technical Research Council of Turkey.

Table 3.1 The number of ground-motion records that are classified in terms of magnitude (M_w), site class (NEHRP C and D) and recording type (Analog vs. Digital). N/A is the group that comprises of records whose site class information is unknown.

Magnitude-dependent Cluster	NEHRP-C	NEHRP-D	N/A	Σ
$5 < M_w \leq 6$ - Analog	12	6	4	22
$M_w > 6$ - Analog	14	18	2	34
$4 \leq M_w \leq 5$ - Digital	214	138	10	362
$5 < M_w \leq 6$ - Digital	28	20	2	50
$M_w > 6$ - Digital	40	20	-	60

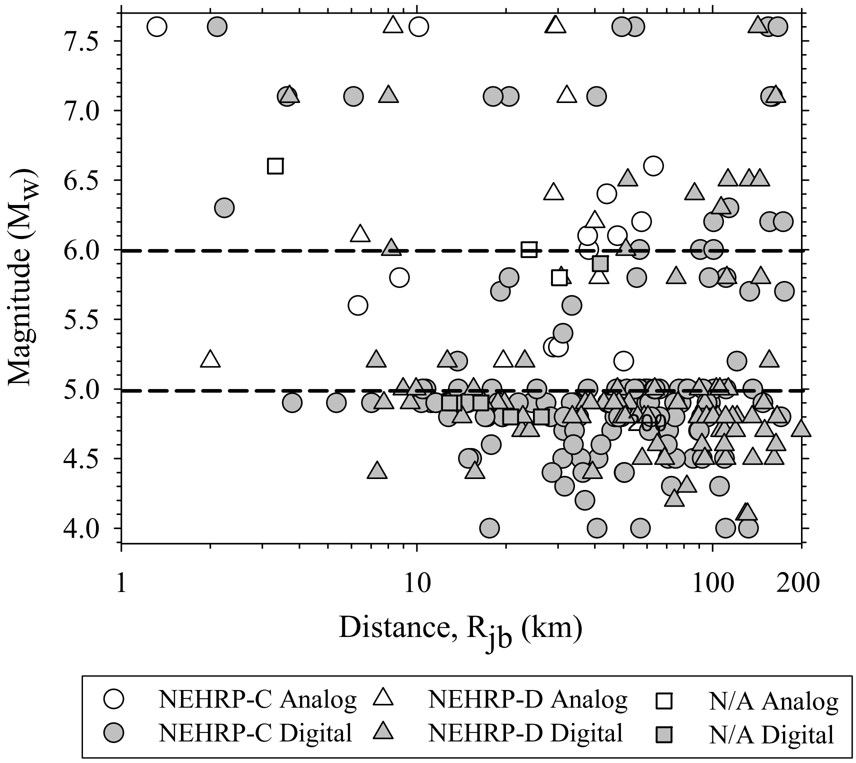

Figure 3.1 Distribution of ground-motion records in terms of moment magnitude (M_w) and distance (R_{jb}). Scatters with different symbols and colors denote different site classes (NEHRP C and D) and recording types (analog and digital).

3.3 Ground-Motion Data Processing Scheme

Each ground-motion record in the dataset is high-pass filtered by 4-pole/4-pole acausal Butterworth filter (USDP, 2008) for a set of randomly generated f_c values. This way, it is attempted to mimic the subjective decisions of the analysts while selecting the high-pass filter cut-off values. Within the scope of this study, the ground-motion records are only high-pass filtered. High-pass filtering aims to remove the long-period noise from the accelerograms that primarily influences the usable spectral period range (Boore and Bommer, 2005; Trifunac and Lee, 1996).

The high-pass filter cut-offs for each record are generated for two different random sets representing the analysts relaxed and severe filtering decisions (details will be discussed later). As stated previously, the generated filter cut-offs follow uniform distribution with upper and lower values bounded by the optimum filter cut-off to minimum and maximum of the magnitude-dependent theoretical source spectrum corner frequency ratio ($f_{c,opt}/f_a$). f_a controls the finite fault size (Atkinson and Silva, 2000) whereas $f_{c,opt}$ values are determined by means of a procedure that considers magnitude-dependent frequency content of strong-motion records (Akkar and Bommer, 2006). The method applies for elastic oscillator response and its main purpose is to determine the most appropriate f_c value that does not distort the low-frequency content (or long-period information) of the accelerogram by excessive filtering. In this study, the use of $f_{c,opt}$ as one of the boundaries is to prevent generating excessive filter cut-offs that would remove a considerable amount of actual ground-motion signal. A record that is high-pass filtered by $f_{c,opt}$ is called as "optimum filtered record" in this study.

The high-pass filter frequency interval [$f_{c,opt}$, f_a] is determined separately for each record in the concerned magnitude-dependent cluster. The minimum and maximum $f_{c,opt}/f_a$ ratios are computed for each cluster and these ratios are listed in Table 3.2. Correspondingly, the minimum and maximum high-pass filtering frequencies ($f_{c,min}$ and $f_{c,max}$, respectively) for each magnitude cluster is calculated by multiplying the minimum and maximum $f_{c,opt}/f_a$ ratio with the f_a value of each record. This way, the limiting filter cut-offs are determined for all of the records in the clusters. This procedure is presented schematically in Figure 3.2.

Table 3.2 The limiting filter cut-off ratios for the magnitude-dependent clusters in the database.

Magnitude-dependent Cluster	$(f_{c,opt}/f_a)_{min}$	$(f_{c,opt}/f_a)_{max}$
$5 < M_w \leq 6$ - Analog	0.50	1.90
$M_w > 6$ - Analog	0.77	3.75
$4 \leq M_w \leq 5$ - Digital	0.08	1.00
$5 < M_w \leq 6$ - Digital	0.14	1.50
$M_w > 6$ - Digital	0.54	2.33

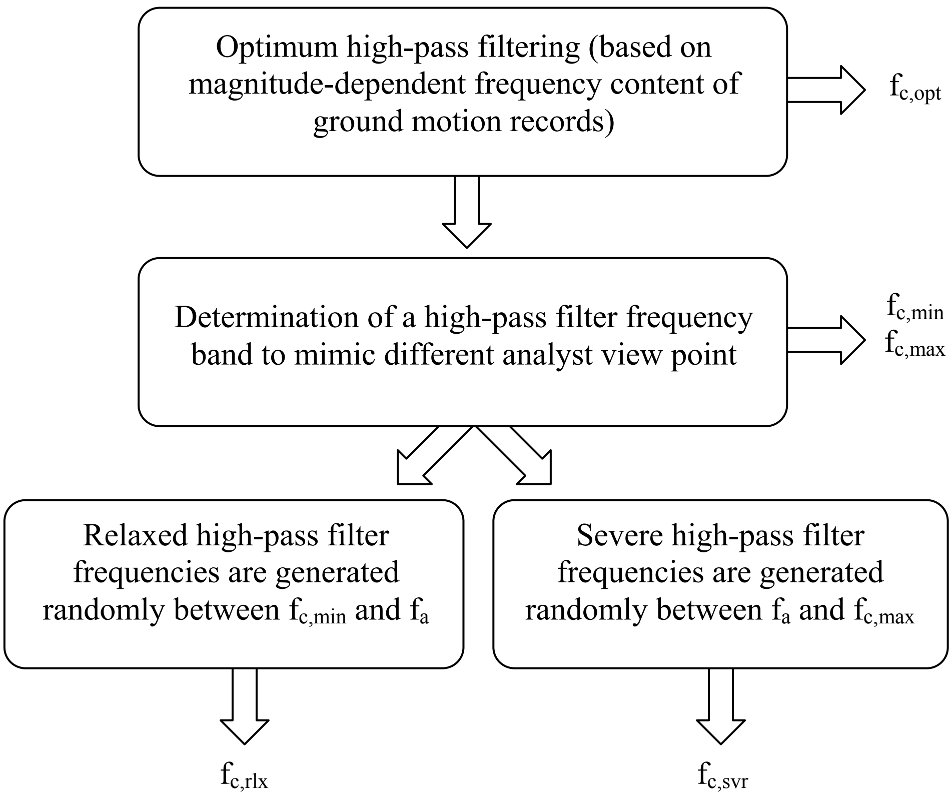

Figure 3.2 Schematic presentation of the procedure for determining the relaxed and severe filter cut-offs.

As it is stated in the previous paragraphs, the high-pass filter cut-offs are generated by considering two different frequency ranges that are termed as “relaxed” and “severe” filtering. The filter frequencies are generated randomly for the relaxed and severe intervals between $f_{c,min}$-f_a and f_a-$f_{c,max}$, respectively. The relaxed filtering represents the non-conservative approach while choosing the high-pass filter cut-offs. The conservative filter cut-off choice in data processing is denoted by severe filtering in this study. The number of f_c values generated for the relaxed and severe filtering is 30 and 40, respectively. The uneven filter numbers is due to the differences in the $f_{c,min}$-f_a and f_a-$f_{c,max}$ bandwidths. In general, the frequency bandwidth of severe filtering is wider with respect to relaxed filtering. This resulted in higher number of severe filter cut-offs to cover the corresponding frequency interval.

In this study, the Latin Hypercube Sampling method (McKay et al., 1979) is used for the random generation of uniformly distributed filter cut-offs. In this approach, the cumulative distribution of the sample is stratified into N equally sized intervals and the data is generated for each interval. This way, the sampling is forced to represent the target probability distribution (Pebesma et al., 2000). A sample case for the generation of cumulative distribution function is shown in Figure 3.3.

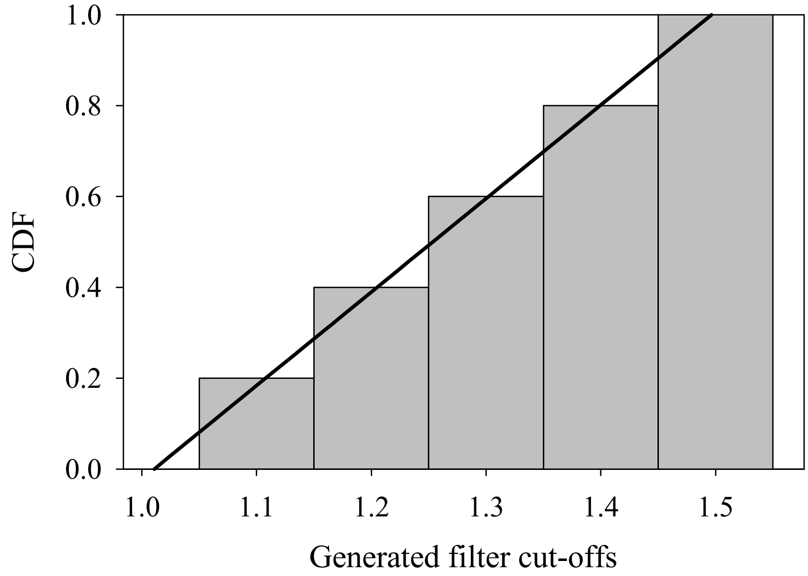

Figure 3.3 Cumulative distribution function of generated filter cut-offs that follows uniform distribution for the cluster of $5 < M_w \leq 6$ digital records.

Figure 3.4 illustrates the above parameters by using the Fourier acceleration spectrum (FAS) of an arbitrary record from the dataset. This illustrative case would simplify the discussions that explain the filtering procedure.

The plots in Figure 3.4 are the Fourier amplitude spectra of a high-pass filtered record with different filter cut-offs. The severe and relaxed filter cut-offs are represented in different color schemes. The FAS curves show how the relaxed and severe filtering values affect the lower-end frequency content of a chosen record. The straight line on the left hand side of the figure describes the f^2 gradient; the theoretical decay rate of low-frequency components in an accelerogram. Conversely, the FAS components with more gradual decay with respect to f^2 gradient may suggest the existence of long-period (or low-frequency) noise. It is depicted from this figure that the relaxed filter cut-offs remove lesser low-frequency components. For some relaxed filtering cases the long-period noise still seems to exist as their FAS curves are above the f^2 gradient at the low-frequency end. As it is expected, the FAS of all severe filtering cases show faster decay with respect to the f^2 gradient. Some of the severe filter cut-offs might have removed a significant portion of the actual long-period components of the record as their low-frequency components display a very fast decay rate with respect to the gradient of f^2.

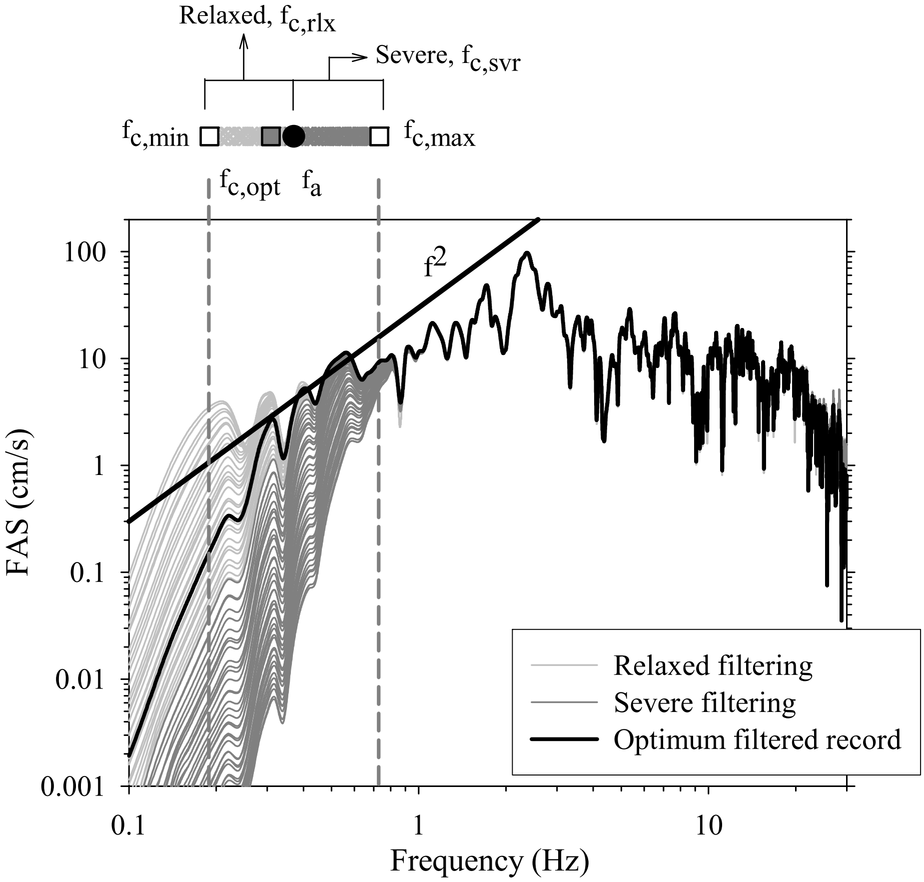

Figure 3.4 FAS of filtered accelerograms and explanation of generated filter cut-off bandwidths for Dursunbey record (18/07/1979 – Balıkesir Earthquake – Dursunbey Station – North-South component – M_w=5.3 – Analog record). The black curve, the optimum filtered record, is the FAS of the record that is filtered according to the procedure of Akkar and Bommer (2006). FAS of relaxed and severe filtered records are denoted as gray and dark gray curves, respectively. The f^2 gradient is fitted by eye shows consistent with the single-corner source theory. f^2 guides us about the decaying rate at long periods.

CHAPTER 4

DETERMINATION OF USABLE PERIOD RANGES FOR INELASTIC OSCILLATOR RESPONSE

4.1 General

In this chapter, the reliable period-bands for which the influence of high-pass filtering is minimum on nonlinear deformation response of SDOF systems is described. The uncertainty associated with the filter cut-off decisions of analysts that affect the inelastic deformation demands of SDOF systems is investigated in the first part. Statistical analyses are performed using the hysteretic models described in Chapter 2 to address the variations in inelastic spectral and residual displacements (SD_{IE} and SD_R, respectively) due to different high-pass filter decisions. The observations on these statistics guide this study to reach its main objective. Thereafter, the methodology for period-dependent probability distributions to quantify the level of reliability in SD_{IE} is explained by illustrative sketches. The degree of nonlinear behavior in SDOF response is described by varying the normalized yield strength (R, yield strength of the oscillator normalized by the elastic strength to maintain the same system in the linear range) and displacement ductility (μ, maximum displacement normalized by the yield displacement) levels. The level of high-pass filter cut-off influence is investigated by considering the record quality (analog vs. digital), earthquake magnitude, level of inelasticity and degradation during the hysteretic excursions. Note that the variations in hysteretic model parameters that control the nonlinear oscillator response are not fully covered while studying the uncertainty of high-pass filtering in nonlinear deformation demands. Thus, the findings of this study are limited to the chosen model parameters. One can extend the observations presented here by systematically varying these model parameters for a complete assessment of high-pass filtering influence on nonlinear SDOF deformations.

4.2 Uncertainty in Nonlinear SDOF Deformation Demands Caused by High-pass Filtering

In this section, observations on the contributions of magnitude, inelasticity level, recording quality and μ vs. R difference to the uncertainties in SD_{IE} and SD_R that stem from the random selection of T_c are presented.

Figure 4.1 shows the scatter plots of some selected cases to emphasize the significance of magnitude, inelasticity level, μ and R difference as well as analog vs. digital record quality on the reliability of nonlinear oscillator deformations that is affected by the variations in high-pass filter values. The plots are computed from the ND, SD and SSD hysteretic models to cover non-degrading to severely degrading hysteretic behavior. The scatters in Figure 4.1.a indicate that the dispersion in nonlinear deformation demands is larger for small magnitude events. The increase in vibration period (left panel vs. right panel) also increases the sensitivity of nonlinear deformation demands due to the variations in T_c. The significance of inelasticity level on nonlinear deformation uncertainty is emphasized in Figure 4.1.b. As the level of inelasticity increases from R=2 to R=6, the dispersion in SD_R increases for the source-to-site distance range considered here. In the light of nonlinear response of oscillators, this observation is expected as higher inelasticity level would result in longer period shifts causing the prominence of high-pass filter cut-offs. As depicted in Figure 4.1.c constant ductility (left panel) and constant strength (right panel) spectra would be equally influenced from variations in high-pass filter cut-offs.

The influence of hysteretic behavior on the uncertainty of nonlinear deformations stemming from random filter cut-offs is displayed in Figures 4.2.a, 4.2.b and 4.2.c that describe the variations of SD_R for random filter cut-offs for ND, SD and SSD hysteretic behavior, respectively. The scatters clearly show that increase in the level of degradation provokes the uncertainty in nonlinear oscillator deformations. As already discussed in Figure 4.1, the smaller magnitudes result in larger uncertainty in the nonlinear deformations.

Note that the recording quality (analog vs. digital) is important for reducing the uncertainty in nonlinear deformations due to high-pass filtering. The dispersion pertaining to analog records is higher with respect to those of digital accelerograms for all cases presented in Figures 4.1 and 4.2.

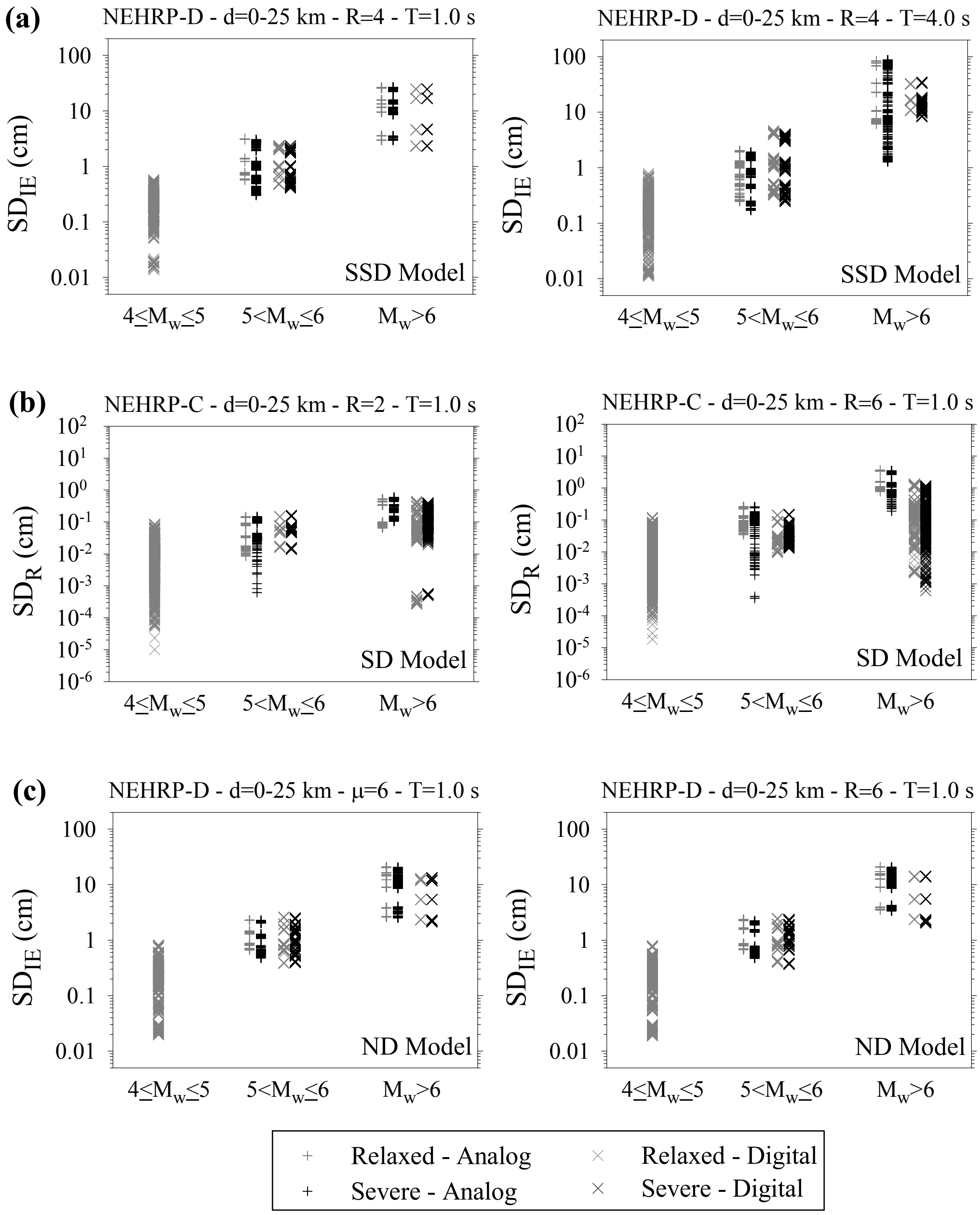

Figure 4.1 Selected cases from different site class to emphasize the influence of (a) magnitude, (b) inelasticity level and (c) μ vs. R difference on the dispersive behavior of nonlinear oscillator demands due to high-pass filter cut-offs.

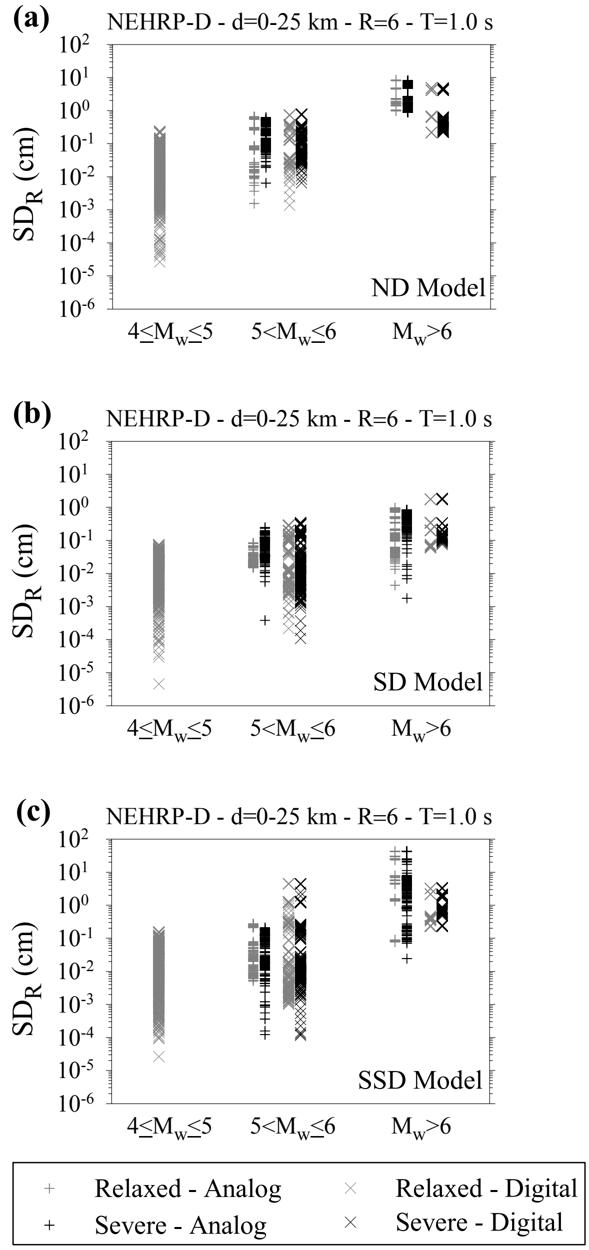

Figure 4.2 Selected cases to highlight the influence of hysteretic degradation on the dispersive behavior of nonlinear oscillator demands due to high-pass filter cut-offs

4.3 Fitting a Probability Distribution on High-Pass Filtered Spectral Displacements

Identification of a probability distribution function on high-pass filtered spectral displacements would be ideal for describing reliable spectral period ranges where the influence of filtering is minimum. A well determined probability distribution would enable one to study the period-dependent behavior of standard deviation (dispersion) for each record under the set of randomly generated high-pass filter cut-offs. Studying the variations in standard deviation through ANOVA for each magnitude cluster would describe the limiting spectral period beyond which the reliability of spectrum is questionable due to high-pass filtering.

In order to see whether the high-pass filtered spectral data (i.e. SD_E and SD_{IE}) fit a well-known distribution, each low-cut filtered record with a set of randomly generated filter cut-offs is examined separately at each spectral period. Lognormal distribution is chosen as the target probability distribution due to its wide range of use in the applications of engineering and strong-motion seismology. [Note: The choice of this distribution alone can be considered as a serious restriction and it can be extended to other probability distributions in a follow up study.] Figure 4.3 shows an illustrative sketch of histograms and corresponding lognormal probability density function plots for elastic spectral displacement (SD_E) of an arbitrary record in the database for some selected periods. The cases resemble the "severe" filter cut-off criterion. Figure 4.4 displays the same cases in terms of cumulative probability density functions associated with the application of Kolmogorov-Simirnov (K-S) goodness-of-fit tests at 5% significance level to verify the applicability of the assumed probability distribution (Ang and Tang, 1975). For the given case study, although the lognormal distribution is verified at T=1.5 s, the K-S test results reject the suitability of lognormal distribution for the rest of the spectral periods. The K-S test is applied to the entire database (SD_E and SD_{IE}) and percentages of distributions failed to fit lognormal distribution for each cluster are summarized in Table 4.1. The lognormal distribution assumption seems to hold for many cases. However, when the entire hypothesis test results are of concern, the existence of rejected null hypothesis cases led this study to disregard the assumption of lognormality in the spectral data variation. The lack of lognormal distribution may stem from the insufficient number of filter cut-off values used in the relaxed or severe high-pass filtering. It can also be the insufficiency of the methodology implemented while generating the filter cut-off values. Thus, the usable spectral period ranges where the high-pass filtering influence is minimum are determined by considering the probability distributions of spectral ordinates specified to each vibration period and for each record in the database. This procedure is described in the next section.

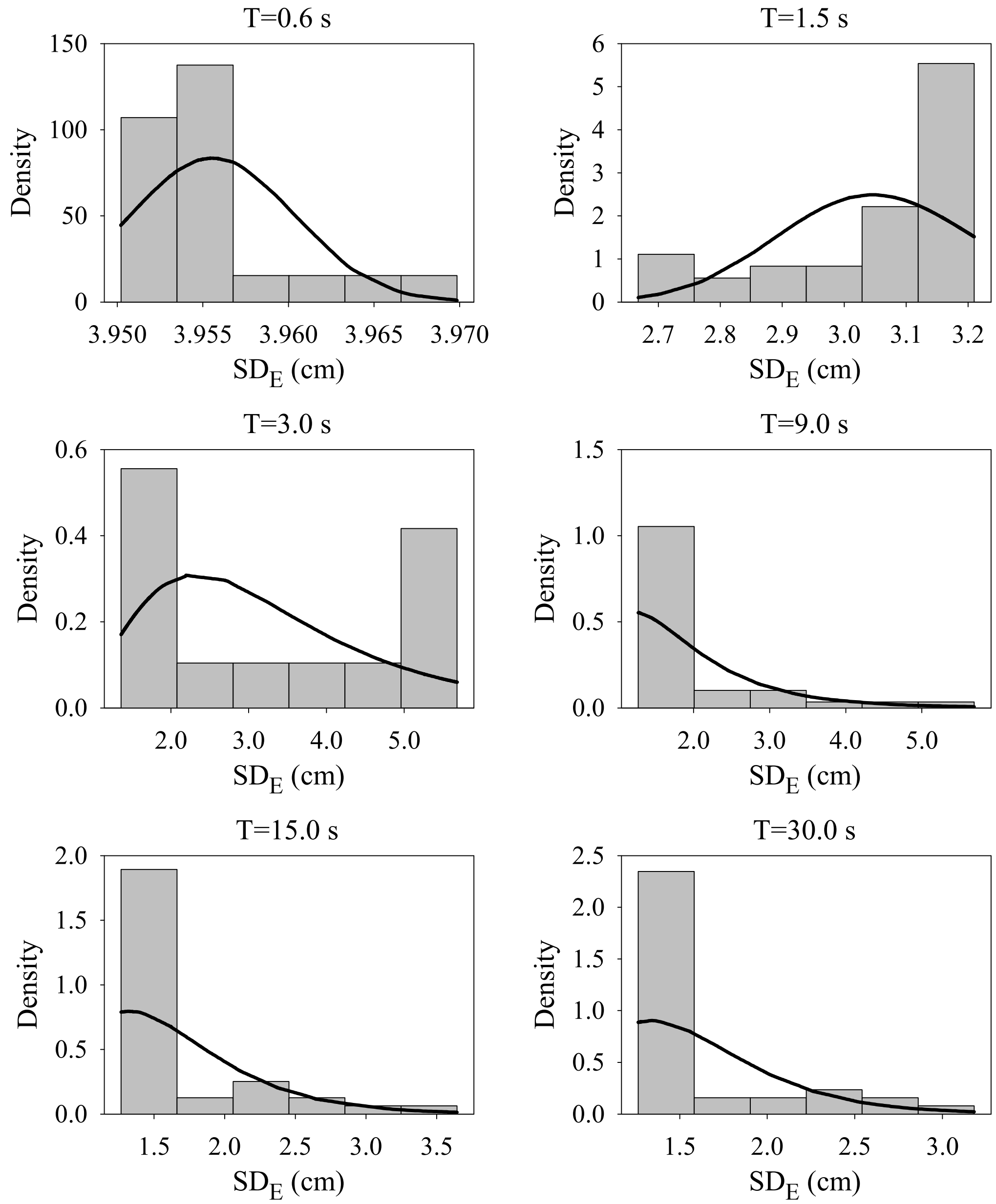

Figure 4.3 Histogram and lognormal probability density function plots of SD$_E$ for an arbitrary record at different periods.

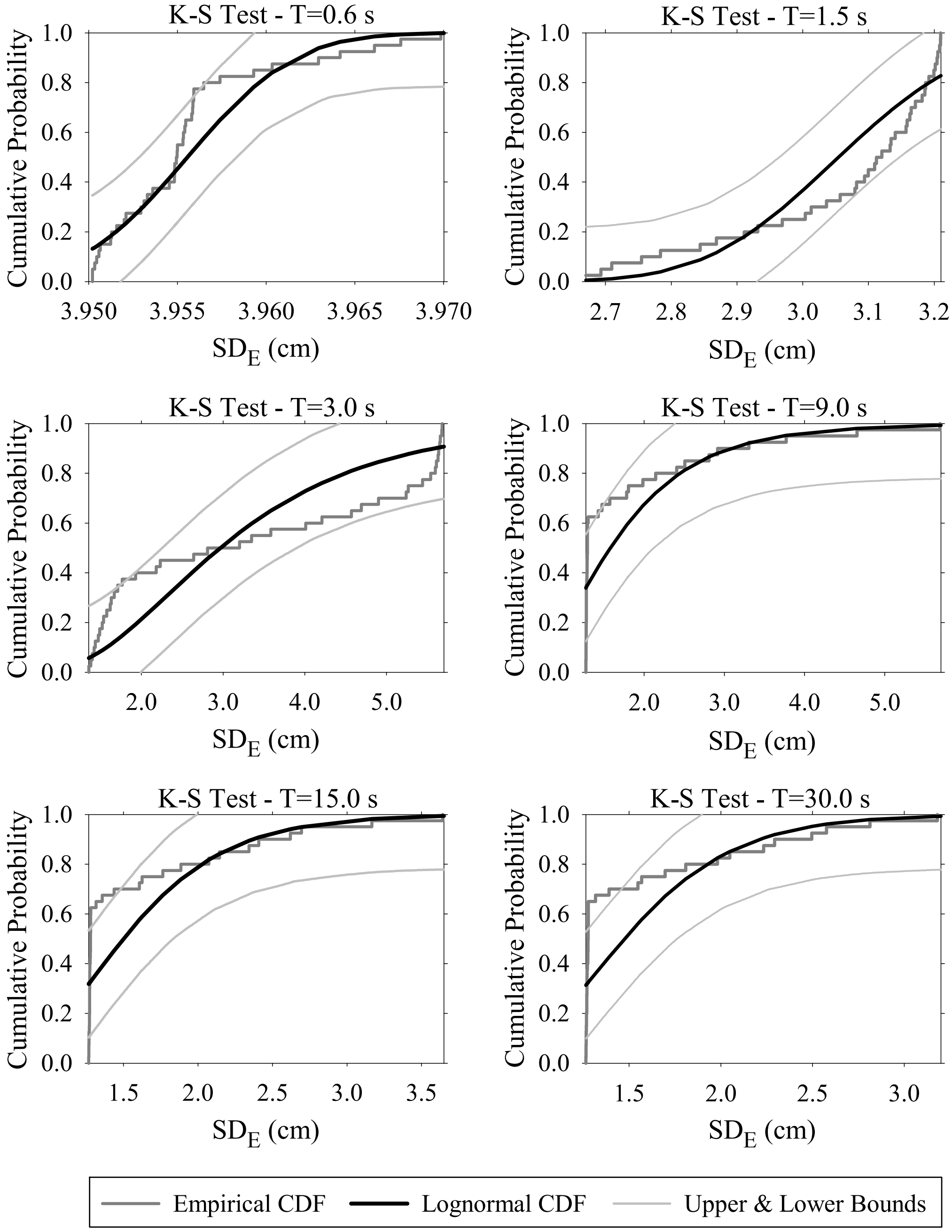

Figure 4.4 Empirical and lognormal (theoretical) cumulative distribution functions associated with the Kolmogorov-Smirnov (K-S) goodness-of-fit tests for the cases presented in Figure 4.3.

Table 4.1 Percentages of probability distributions that failed to fit the lognormal distribution.

	Relaxed Filtering					**Severe Filtering**			
	Analog		**Digital**			**Analog**		**Digital**	
	$5 < M_w \leq 6$	**$M_w > 6$**	**$4 \leq M_w \leq 5$**	**$5 < M_w \leq 6$**	**$M_w > 6$**	**$5 < M_w \leq 6$**	**$M_w > 6$**	**$5 < M_w \leq 6$**	**$M_w > 6$**
Elastic	11	3	36	49	7	6	23	7	15
ND - μ=2	11	11	33	47	16	14	34	15	33
ND - μ=4	11	6	34	48	15	13	39	17	32
ND - μ=6	10	7	31	42	13	18	40	17	28
ND - R=2	8	6	34	47	9	12	30	11	24
ND - R=4	10	3	32	46	10	13	30	15	25
ND - R=6	11	4	30	47	9	16	31	15	22
SD - μ=2	11	5	34	42	10	8	27	12	22
SD - μ=4	11	6	32	42	10	9	29	10	25
SD - μ=6	12	7	31	43	11	9	30	11	24
SD - R=2	9	3	35	42	7	9	22	10	19
SD - R=4	11	4	33	42	7	7	26	10	19
SD - R=6	11	4	32	42	8	8	23	9	18
SSD - μ=2	13	7	34	42	18	10	29	14	27
SSD - μ=4	13	8	32	43	17	10	28	15	26
SSD - μ=6	15	12	31	42	18	12	33	14	28
SSD - R=2	13	3	35	42	9	13	25	14	21
SSD - R=4	12	5	33	42	13	11	24	13	20
SSD - R=6	14	7	31	42	12	11	25	12	22

4.4 Spectral Period Ranges for the Minimum Influence of High-Pass Filtering

As discussed briefly in the previous section, the level of reliability in SD_{IE} is specified by the period-dependent probability distributions of spectral points that result from the implementation of pre-determined T_c values of each record in the database. Given a constant ductility or normalized strength level, let $\mu_{SD_{IE}}$ be the average spectrum of all nonlinear spectral curves of an accelerogram due to the implementation of pre-determined high-pass filter cut-offs (see Figure 4.6). For a given vibration period, the probability of spectral points falling into an interval $\mu_{SD_{IE}} \mp \chi\mu_{SD_{IE}}$ where the fractional factor χ takes a value less than 1 is calculated. Note that when the calculated probability attains a high value, it is an indication of almost all spectral points falling within the interval defined by $\mu_{SD_{IE}} \mp \chi\mu_{SD_{IE}}$. This concept is presented in Figure 4.5.

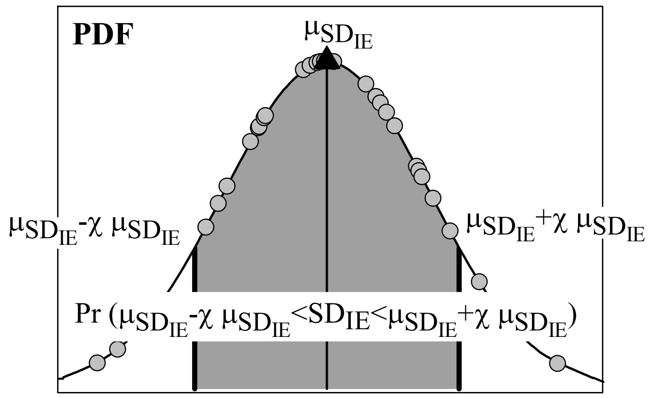

Figure 4.5 Illustration of the probability distribution of SD_{IE} values about $\mu_{SD_{IE}}$ for a given vibration period. The gray shaded region is the probability of spectral points falling into an interval $\mu_{SD_{IE}} \mp \chi\mu_{SD_{IE}}$.

When this methodology is repeated for a large range of vibration periods, one can obtain the probability curves for each $\mu_{SD_{IE}} \mp \chi\mu_{SD_{IE}}$ interval. The case presented in Figure 4.6 (SD hysteretic model), shows the illustrative sketches to determine the probabilities at the selected periods (T=0.6 s and T=3.0 s) that are presented in Figure 4.7. The typical set of such probability curves is displayed in Figure 4.8 for the same case. The fraction χ is chosen as 0.05, 0.1, 0.15 and 0.2 for all vibration periods and these constants are also kept the same for the entire probability calculations in this study.

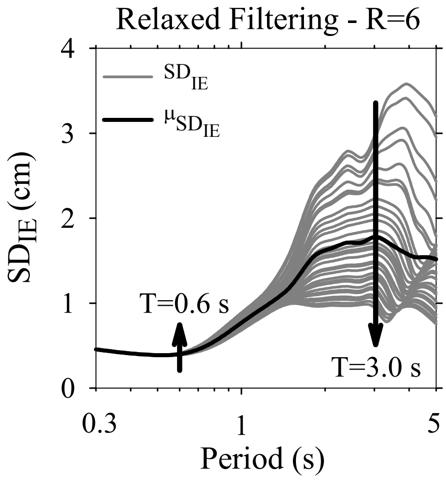

Figure 4.6 Stiffness degrading (SD) nonlinear constant strength (R=6) displacement spectra of the record whose high-pass filter cut-offs are determined through the methodology illustrated in Figure 3.4. The SD_{IE} curves are due to the implementation of relaxed filter cut-offs to the concerned accelerogram. The black solid line is the mean variation of all SD_{IE} curves ($\mu_{SD_{IE}}$). As discussed in Figure 4.1.a, the dispersion in SD_{IE} (described by the scatter about $\mu_{SD_{IE}}$) increases with increasing vibration period. (Compare the divergence of spectral curves about $\mu_{SD_{IE}}$ at T=0.6 s and T=3.0 s). This behavior suggests a decrease in the reliability of SD_{IE} after a certain vibration period. The reason for the decreased reliability (or increased uncertainty) in SD_{IE} towards longer vibration periods is the pronounced interaction between the filter cut-offs and nonlinear oscillator response that is magnified further with different high-pass filter cut-offs.

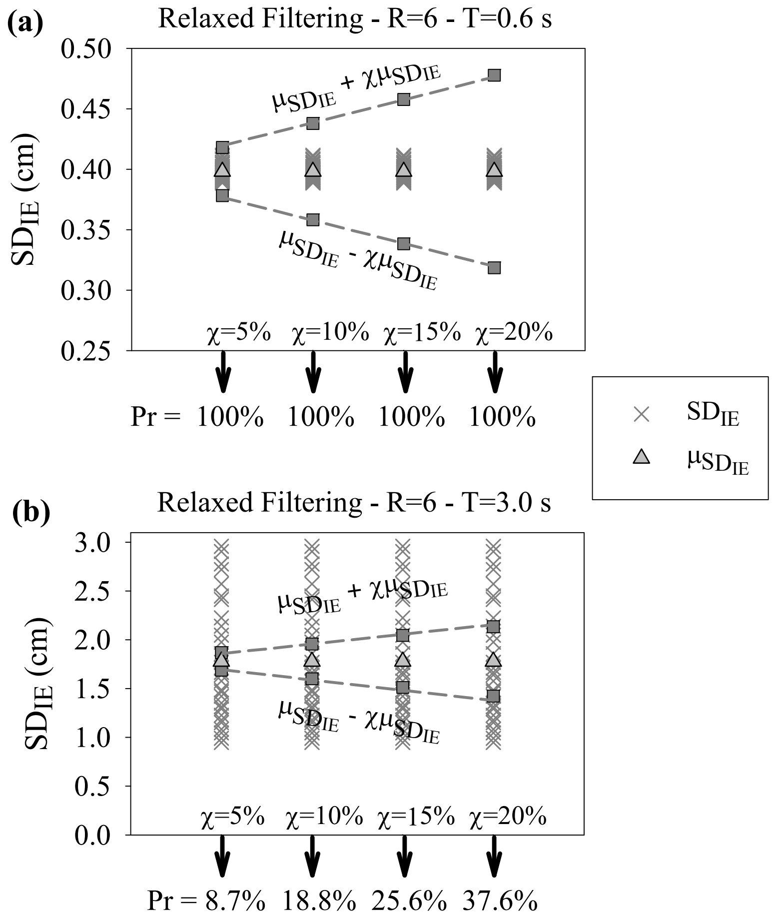

Figure 4.7 Calculation of the probabilities of different χ by applying the method demonstrated in Figure 4.5. Probability values of different χ are computed for the SD case presented in Figure 4.6 at vibration periods of (a) T=0.6 s and (b) T=3.0 s. SD_{IE} scatters and $\mu_{SD_{IE}}$ are denoted as gray crosses and triangles, respectively. Gray squares show the $\mu_{SD_{IE}} \mp \chi\mu_{SD_{IE}}$ interval.

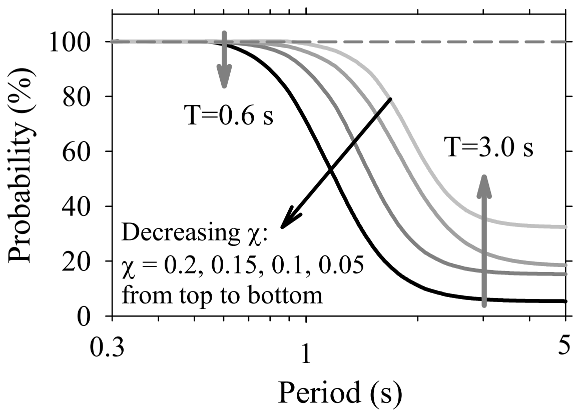

Figure 4.8 Probability curves of different χ for the case presented in Figure 4.6. They are computed by applying the described probability concept in Figures 4.5 and 4.7 for a large range of periods.

When the dispersion at T=0.6 s and T=3.0 s (Figure 4.6) is compared with the probability curves in Figure 4.8, one realizes that higher dispersion in T=3.0 s is associated with the decaying portion of probabilities at any χ level. Such decay in the probability curves would suggest low levels of reliability for SD_{IE}. Thus for this particular case it can be speculated that high-pass filtering interferes with the nonlinear oscillator response for T > 1.5 s (where the decay in the probability curves is steep), and use of SD_{IE} at vibration periods longer than T = 1.5 s might result in erroneous conclusions on the nonlinear deformation demands. Note that use of larger χ results in a more gradual decay in the probability curves (compare χ=0.2 and χ=0.05 curves). However, their gradients are approximately the same revealing a similar assessment about the range of spectral periods where high-pass filtering starts dominating the nonlinear oscillator response.

The procedure described above accounts for the dispersion due to uncertainty in high-pass filtering by a fraction proportional to $\mu_{SD_{IE}}$. The alternative to this approach is the direct use of standard deviation, σ, about $\mu_{SD_{IE}}$. In other words, one can replace the interval definition $\mu_{SD_{IE}} \mp \chi\mu_{SD_{IE}}$ with $\mu_{SD_{IE}} \mp \kappa\sigma$ while describing the probabilities presented in Figures 4.5 and 4.7. This alternative approach is presented in Figure 4.9 using the same record and vibration periods as in Figure 4.6. The κ values are selected as 0.2, 0.4, 0.6, 1.0 and 2.0 for describing alternative intervals for probability calculations. When the variations in intervals are compared between Figures 4.7 and 4.9 one can immediately realize that the $\kappa\sigma$ approach results in wider intervals as the oscillator response shifts to longer periods (i.e. T = 3.0 s) where the dispersion is more prominent due to negative effects of low-cut filtering on spectral ordinates. Wider intervals are expected in this approach particularly for dispersion dominant situations because σ is directly related to dispersion (i.e. higher the dispersion larger the σ and this results in wider intervals for probability calculations). The resulting probability plots for $\mu_{SD_{IE}} \mp \kappa\sigma$ approach is presented in Figure 4.10 that suggests a period-independent probability variation that can be explained by the sensitivity of intervals to σ that, in turn, effects the probability computations. Based on these discussions the probabilities that define the usable period ranges where low-cut filtering influence is minimum are calculated by using the $\mu_{SD_{IE}} \mp \chi\mu_{SD_{IE}}$ intervals.

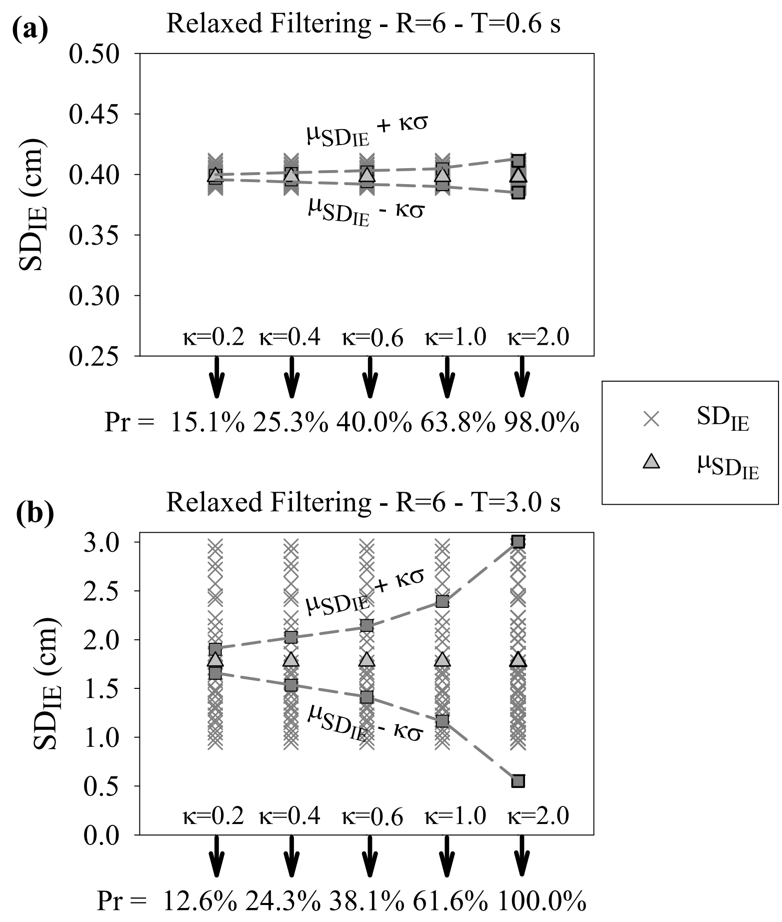

Figure 4.9 Calculation of the probabilities for different $\mu_{SD_{IE}} \mp \kappa\sigma$ intervals by applying the method presented in Figure 4.5. Probabilites are calculated for the same cases as demonstrated in Figure 4.6: (a) T=0.6 s and (b) T=3.0 s. SD_{IE} scatters and $\mu_{SD_{IE}}$ are denoted as gray crosses and triangles, respectively. Gray squares show the $\mu_{SD_{IE}} \mp \kappa\sigma$ interval.

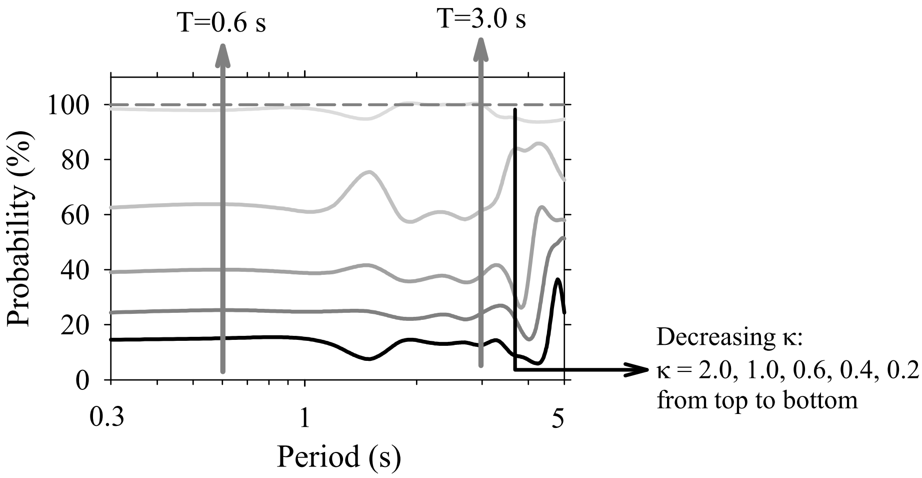

Figure 4.10 Probability curves of different κ for the case presented in Figure 4.6. They are computed by applying the described probability concept in Figures 4.5 and 4.9 for a wide range of periods.

Figure 4.11 that also uses stiffness degrading hysteretic model indicates the significance of severe filtering on inelastic displacement response spectra. When SD_{IE} curves in Figures 4.6 (relaxed filtering) and 4.11 (severe filtering) are compared, it is observed that the dispersion in the severe filtering case commences much earlier than the relaxed counterparts. While the influence of filter cut-offs on SD_{IE} curves that are obtained from relaxed filtering (Figure 4.6) commences at 1.5 s, this effect is observed at about 0.9 s in severe filtering. It is also depicted from Figure 4.11 that the dispersive behavior of SD_{IE} is more prominent in the severe high-pass filtering case since those filter cut-offs would remove relatively larger amounts of long-period components hence accentuate the filter cut-off influence more on the nonlinear oscillator response.

For severe filtering case (Figure 4.11), schematic illustrations of determining the probability values at T=0.6 s and T=3.0 s by applying the concept displayed in Figure 4.5 are shown in Figure 4.12. Probability curves of this case that are obtained for a wider period interval are presented in Figure 4.13. When plots in Figures 4.7 and 4.12 or Figures 4.8 and 4.13, respectively are compared, the increased dispersion on nonlinear spectral displacements due to the use of severe filtering is clearly observed.

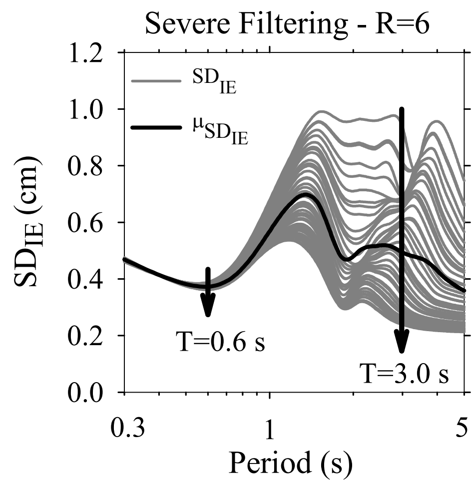

Figure 4.11 Same record presented in Figure 4.6 filtered by severe filtering criterion. Relatively larger variations in the SD_{IE} with respect to those in Figure 4.6 are due to the implementation of severe filter cut-offs.

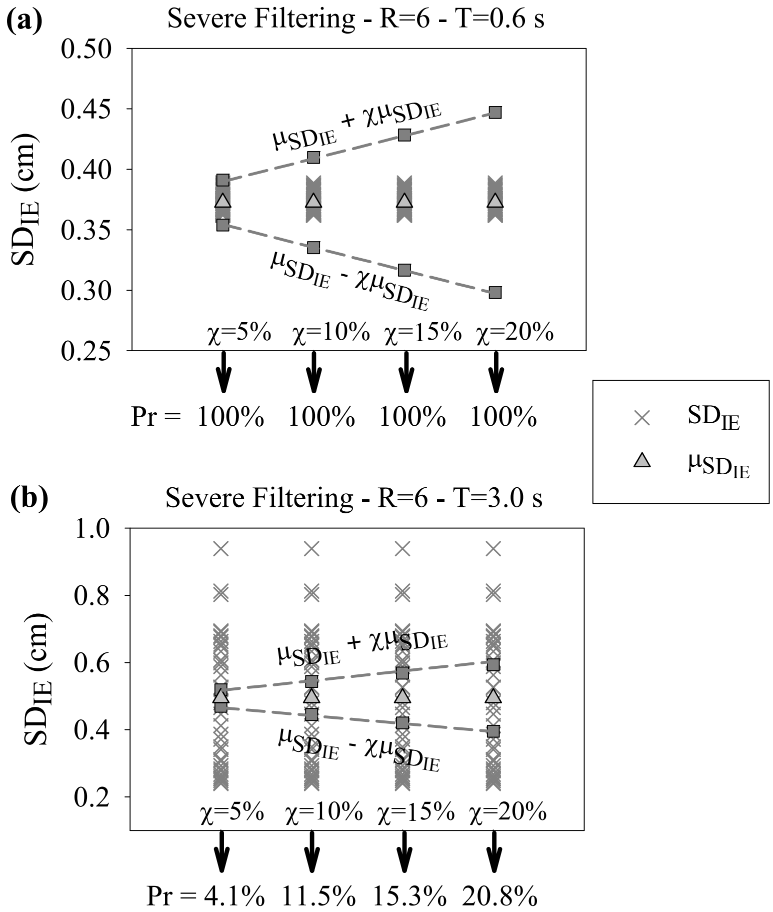

Figure 4.12 Calculation of the probabilities of different χ by applying the method demonstrated in Figure 4.5 for severe filtering. Probability values of different χ are computed for the case presented in Figure 4.11 at vibration periods of (a) T=0.6 s and (b) T=3.0 s. Definitions in this figure are the same as those in Figure 4.7.

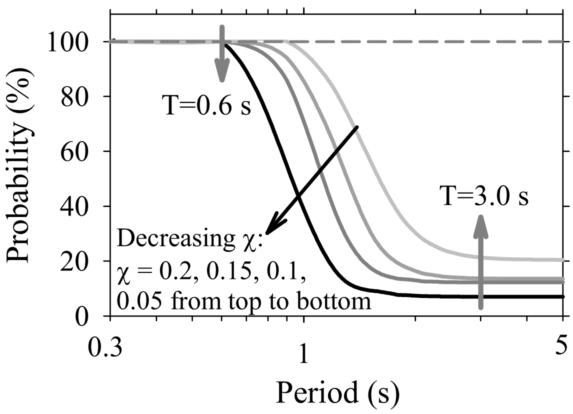

Figure 4.13 Probability curves of different χ for the case presented in Figure 4.11. They are computed by applying the probability concept presented in Figures 4.5 and 4.12 for a large range of periods.

Tables 4.2 to 4.4 list the usable spectral periods determined from the mean probability curves of ND, SD and SSD hysteretic models, respectively that are computed by the application of above concept to each magnitude cluster considered in this study. The periods are determined for analog and digital records. Confined to the rationale in the presented methodology, the reliability of SD_{IE} will not be affected by the chosen high-pass filter cut-off within the spectral bands bounded by these periods. The spectral period ranges are based on a probability of $\Pr(\mu_{SD_{IE}} - \chi\mu_{SD_{IE}} < SD_{IE} < \mu_{SD_{IE}} + \chi\mu_{SD_{IE}}) =$ 80 percent for χ=0.05. The choice of this probability level was an arbitrary decision. However, for most cases, the decay in the probability curves becomes steep in the vicinity of this probability level giving an indication for the significant interference between high-pass filtering and nonlinear oscillator response. Consequence of this argument was to choose this probability level in the methodology. A usable spectral period range for small magnitude ($4 \leq M_w \leq 5$) analog records cannot be recommended due to the insufficient data within this magnitude interval.

4.5 Proposed Usable Period Ranges in Terms of Inelasticity Level and Hysteretic Model

The usable period ranges suggested in this study are verified by comparing the usable period ranges of elastic oscillator response derived from this study with the results of similar investigations from the literature (Abrahamson and Silva, 1997; Akkar and Bommer, 2006). The comparisons are presented in Figure 4.14. Despite of its slightly conservative usable period ranges, the scatters in this figure suggest a fairly good agreement between the recommendations of this study and those suggested by previous studies in particular for the relaxed filtering criterion. This observation may be an indication of the stability of the proposed methodology.

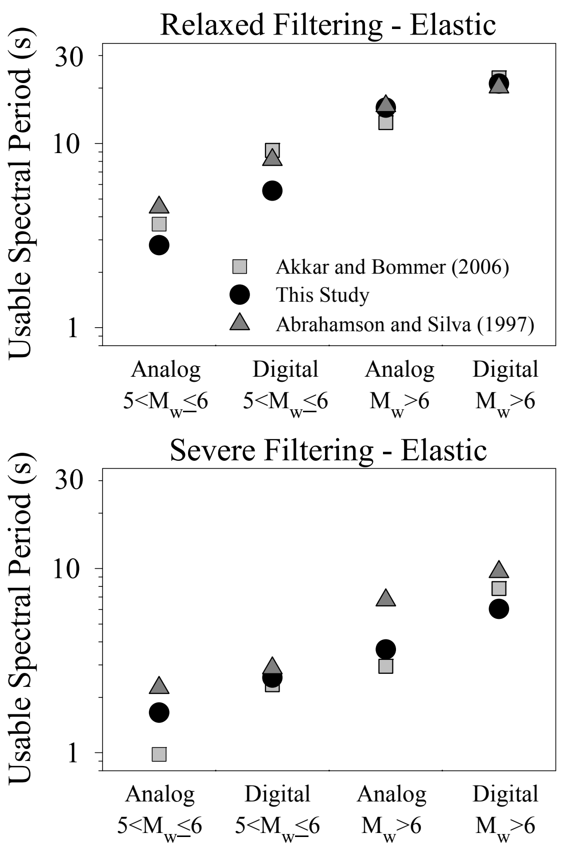

Figure 4.14 Usable spectral periods of this study for elastic response and their comparisons with other recommendations in the literature.

The usable period ranges for ND, SD and SSD hysteretic behavior are listed in Tables 4.2 to 4.4 that are computed from the probabilistic methodology discussed in the previous sections of this chapter and Chapter 3. As indicated previously the suggested usable period values are determined for χ=0.05. The tables list these spectral ranges for relaxed and severe filtering criteria and also present the elastic usable ranges as discussed above for comparison purposes. The discrepancy between the suggested usable spectral periods of elastic and nonlinear oscillator responses once again emphasizes the significance of high-pass filter cut-off influence on nonlinear SDOF deformations. As presented in Figure 4.15 the usable period ranges generally decrease with the increase in the degradation level.

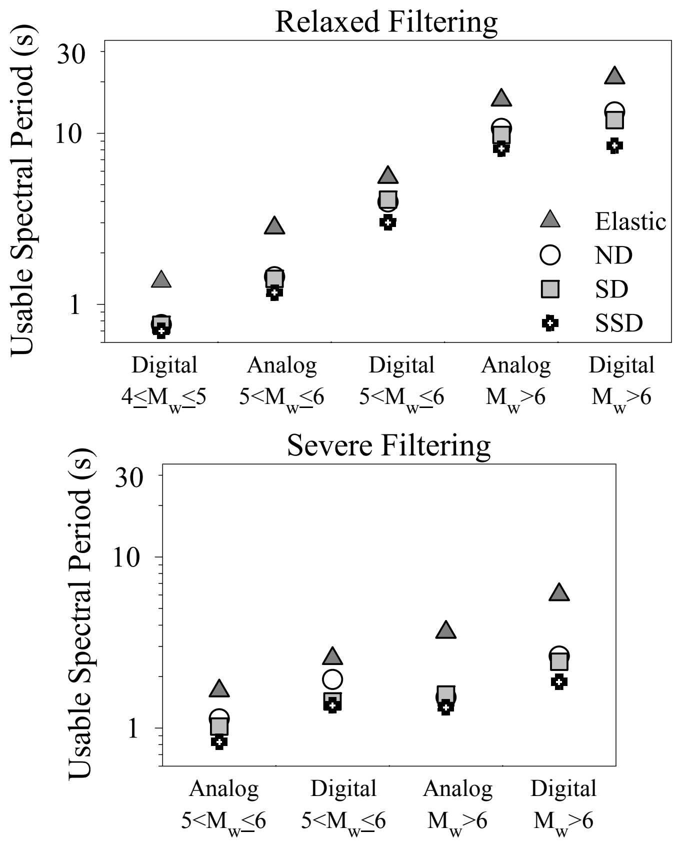

Figure 4.15 Illustration of elastic and non-degrading to severely degrading inelastic usable period ranges for relaxed and severe filtering. The inelastic usable periods are presented for μ=6.

Figure 4.16 is another version of Figure 4.15 and displays the usable period ranges of analog and digital records only for $5<M_w\leq6$ magnitude cluster in order to emphasize the influence of relaxed and severe filtering criteria on analog and digital records. The influence of severe filtering is much more pronounced in analog records and it increases as the level of degradation increases.

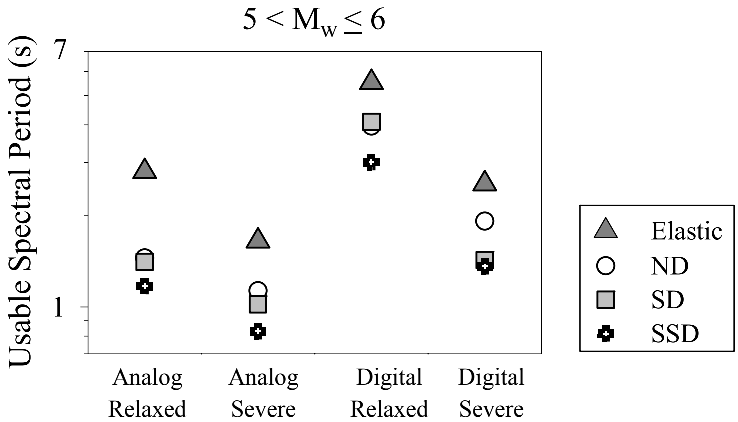

Figure 4.16 Illustration of the same case in Figure 4.15 for $5 < M_w \leq 6$ magnitude cluster. The inelastic usable periods are presented for μ=6.

Table 4.2 Proposed vibration periods for SD_E and constant ductility and strength SD_{IE} obtained from ND Bilinear model for analog and digital records when relaxed and severe filtering criteria are applied. (SD_E vibration periods are given in the first row for comparison purposes)

	Relaxed Filtering					**Severe Filtering**			
	Analog		**Digital**			**Analog**		**Digital**	
	$5 < M_w \leq 6$	**$M_w > 6$**	**$4 \leq M_w \leq 5$**	**$5 < M_w \leq 6$**	**$M_w > 6$**	**$5 < M_w \leq 6$**	**$M_w > 6$**	**$5 < M_w \leq 6$**	**$M_w > 6$**
Elastic	2.80	15.61	1.36	5.52	21.06	1.65	3.63	2.55	6.02
μ=2	2.07	12.56	1.14	5.45	16.89	1.41	2.83	2.31	4.14
μ=4	1.88	12.11	0.92	4.65	15.06	1.16	2.01	1.88	2.90
μ=6	1.45	10.67	0.76	3.96	13.32	1.13	1.51	1.92	2.63
R=2	2.08	13.29	1.17	4.98	17.76	1.33	2.55	2.27	4.13
R=4	2.13	12.21	0.97	4.35	14.70	1.31	1.69	1.81	2.54
R=6	1.90	10.75	0.84	3.98	13.58	1.14	1.42	1.62	2.16

Table 4.3 Proposed vibration periods for SD_E and constant ductility and strength SD_{IE} obtained from SD Clough model for analog and digital records when relaxed and severe filtering criteria are applied. (SD_E vibration periods are given in the first row for comparison purposes)

	Relaxed Filtering					**Severe Filtering**			
	Analog		**Digital**			**Analog**		**Digital**	
	$5 < M_w \leq 6$	**$M_w > 6$**	**$4 \leq M_w \leq 5$**	**$5 < M_w \leq 6$**	**$M_w > 6$**	**$5 < M_w \leq 6$**	**$M_w > 6$**	**$5 < M_w \leq 6$**	**$M_w > 6$**
Elastic	2.80	15.61	1.36	5.52	21.06	1.65	3.63	2.55	6.02
μ=2	2.12	13.94	1.09	4.90	16.65	1.23	3.02	2.13	3.93
μ=4	1.78	11.37	0.88	4.40	12.08	1.11	2.25	1.80	2.80
μ=6	1.41	9.77	0.76	4.09	11.94	1.02	1.57	1.43	2.44
R=2	2.33	14.16	1.19	4.96	18.31	1.30	2.59	2.21	3.96
R=4	1.92	11.68	0.98	4.52	15.72	1.11	1.91	1.83	2.58
R=6	1.58	10.96	0.86	3.86	15.23	1.02	1.34	1.66	1.84

Table 4.4 Proposed vibration periods for SD_E and constant ductility and strength SD_{IE} obtained from SSD Clough model for analog and digital records when relaxed and severe filtering criteria are applied. (SD_E vibration periods are given in the first row for comparison purposes)

	Relaxed Filtering					**Severe Filtering**			
	Analog		**Digital**			**Analog**		**Digital**	
	$5 < M_w \leq 6$	**$M_w > 6$**	**$4 \leq M_w \leq 5$**	**$5 < M_w \leq 6$**	**$M_w > 6$**	**$5 < M_w \leq 6$**	**$M_w > 6$**	**$5 < M_w \leq 6$**	**$M_w > 6$**
Elastic	2.80	15.61	1.36	5.52	21.06	1.65	3.63	2.55	6.02
μ=2	1.96	11.78	1.05	4.48	17.34	1.10	2.13	2.02	2.56
μ=4	1.53	10.01	0.79	3.77	10.75	1.02	1.72	1.71	2.22
μ=6	1.17	8.12	0.70	3.01	8.48	0.83	1.32	1.36	1.86
R=2	2.30	13.45	1.13	4.73	14.47	1.24	2.36	2.09	2.64
R=4	1.65	10.30	0.91	4.14	11.02	1.04	1.25	1.75	2.54
R=6	1.51	8.52	0.79	3.29	11.20	0.99	1.06	1.43	1.97

4.6 Application of the Proposed Usable Periods to Strong-Motion Databases

The usable period ranges determined in this study are implemented to the pan-European strong motion database of Akkar and Bommer (2007b). This way one can understand the decrease in database resolution (i.e. Magnitude vs. R_{jb} distribution) with increase in vibration period. This type of information is practically important for deriving ground-motion prediction equations. The database originally contains a total of 532 accelerograms from 131 earthquakes with a magnitude range of 5.0 and 7.6. The relevant information about the databank is given in Akkar and Bommer (2007b).

Figure 4.17 shows the magnitude vs. distance scatters at vibration periods varying between T=0.5 s to T=5.0 s for elastic response. The relaxed usable period range criterion suggested in this study is implemented. The plots depict the decrease in data scatter with increasing vibration period. This is because the records outside the range of suggested usable period drop out automatically in the computation of predicted model regression coefficients. The data seems to decrease severely after T=3.0 s. Figures 4.18 to 4.20 repeat the same investigation for nonlinear oscillator response. The decrease in data number is more prominent with increasing level of inelasticity (consider Figures 4.18 and 4.20 whose inelasticity levels are R=2 and R=6, respectively). These scatter plots clearly show that an inelastic spectral displacement GMPE that is based on the criteria set in this study will be considered reliable for $T \leq 2.5$ s. Figure 4.21 describes the same information in the scatter plots of Figures 4.17 to 4.20 by displaying the variation as a continuous function of vibration period. As stated in the above sentences, the data number decreases considerably for $T \geq 2.5$ s. Thus while deriving inelastic spectral displacement GMPEs for this database, one should consider the period limitation as 2.5 s.

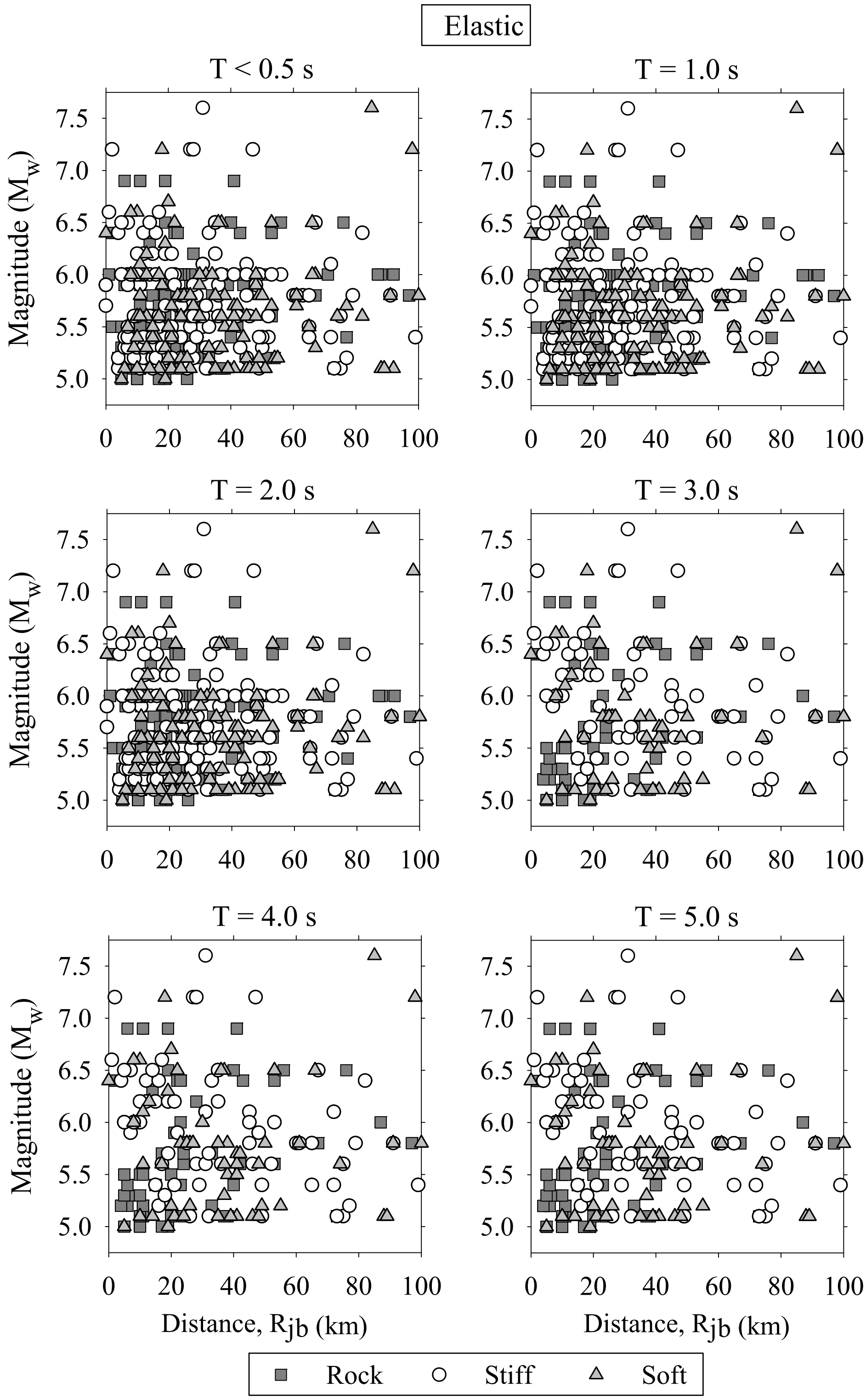

Figure 4.17 Magnitude-distance-site class distribution of databank at different periods for elastic case.

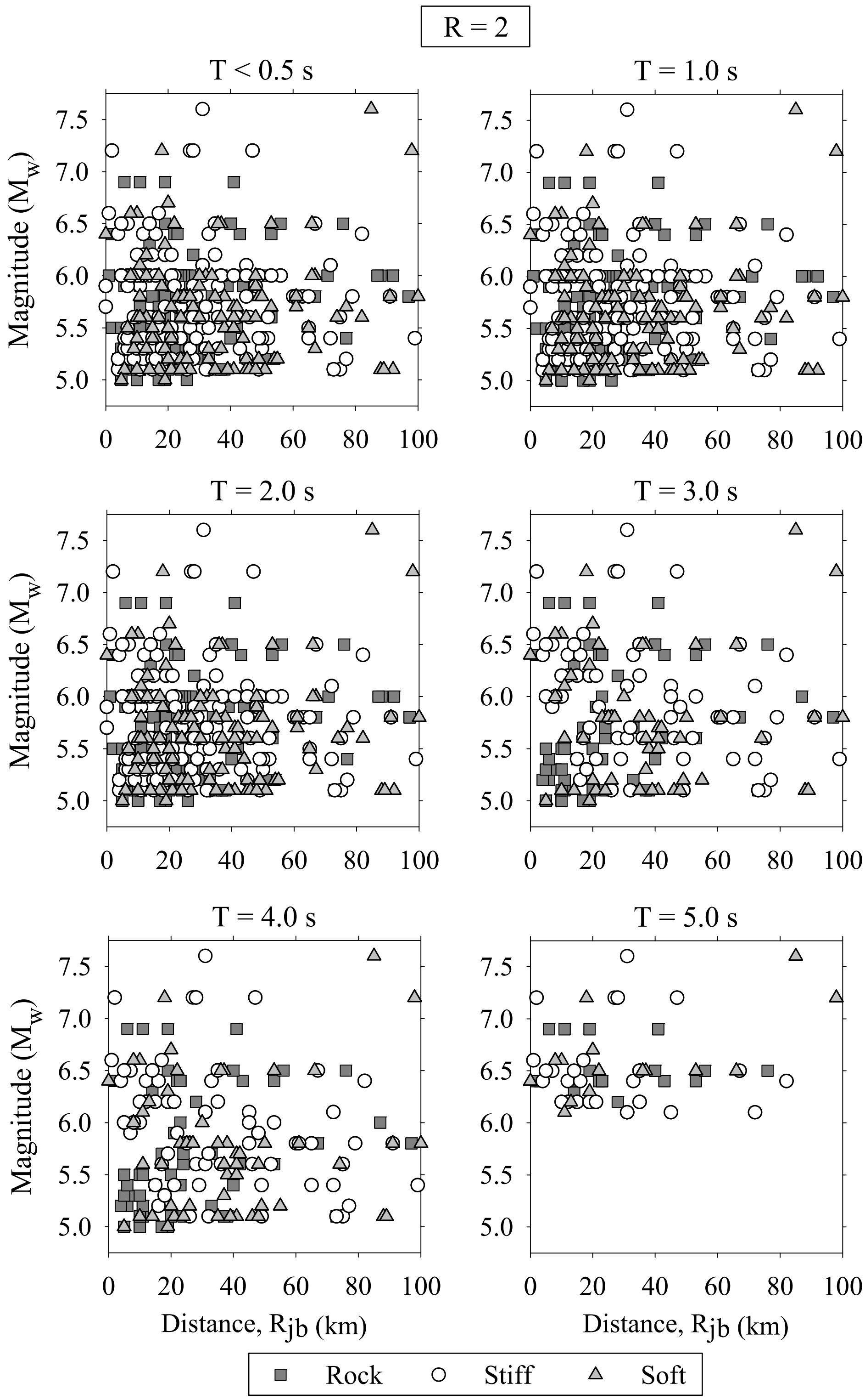

Figure 4.18 Magnitude-distance-site class distribution of databank at different periods for inelastic case (R=2).

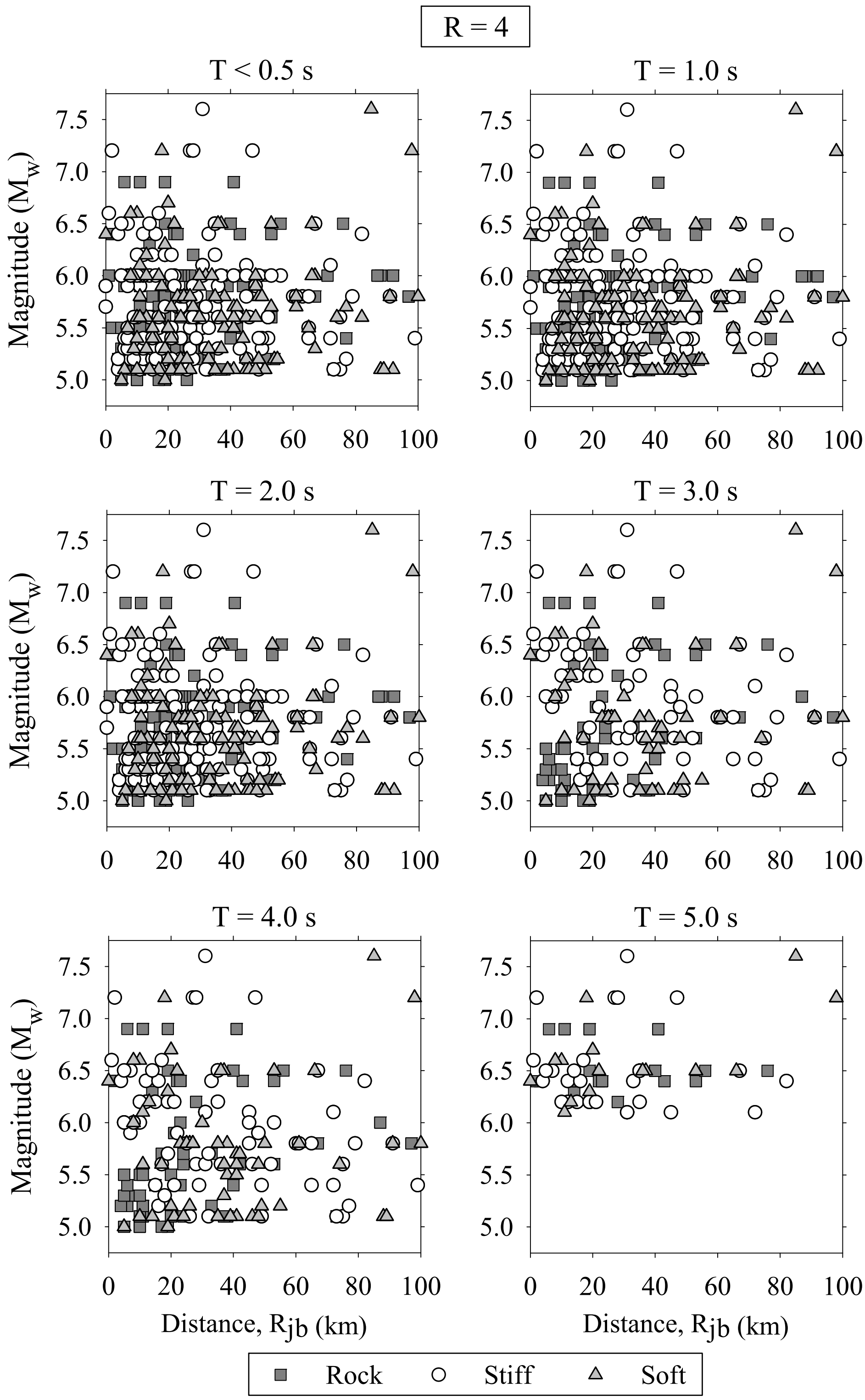

Figure 4.19 Magnitude-distance-site class distribution of databank at different periods for inelastic case (R=4).

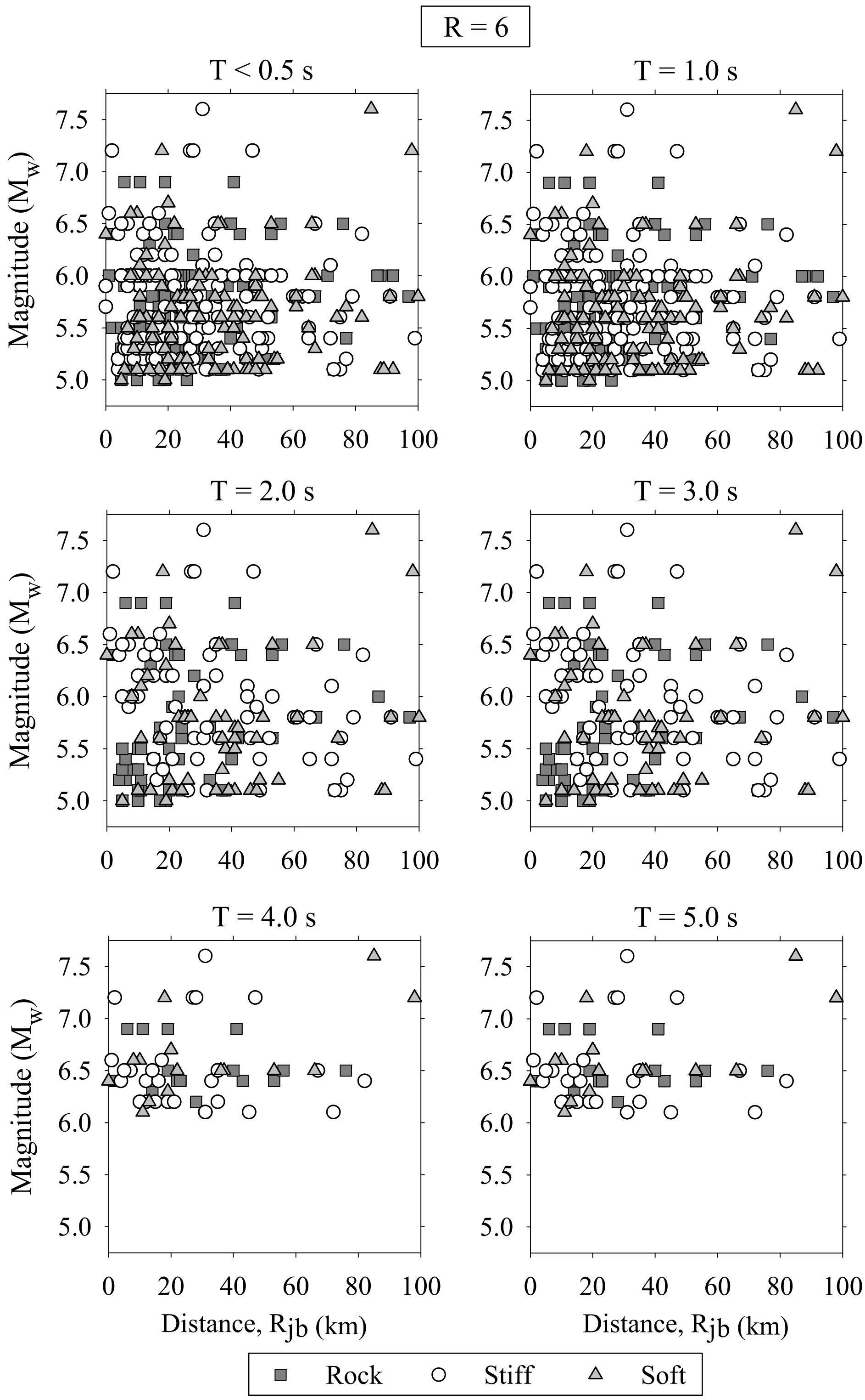

Figure 4.20 Magnitude-distance-site class distribution of databank at different periods for inelastic case (R=6).

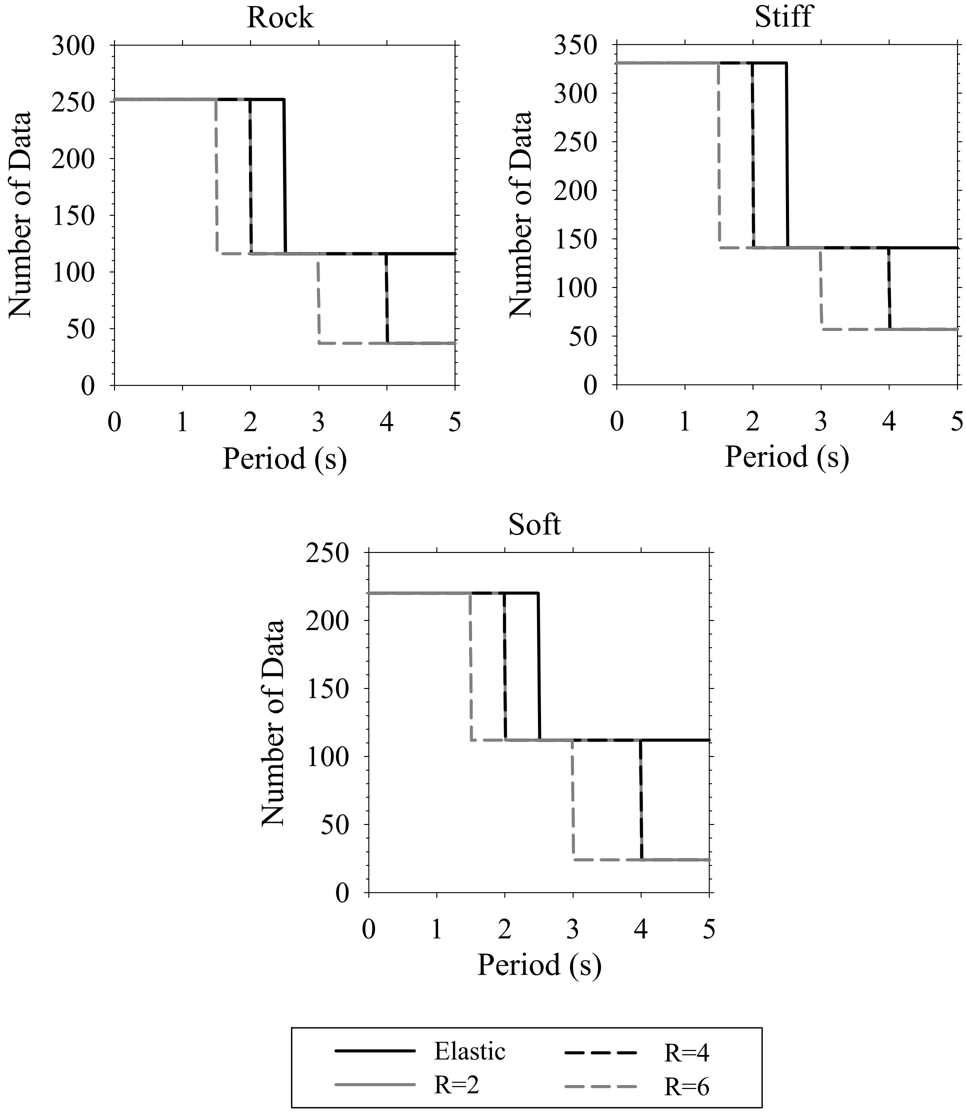

Figure 4.21 Period-dependent variation of European ground-motion database for reliable linear and nonlinear spectral displacements considering the relaxed filtering criterion presented in this study.

CHAPTER 5

SUMMARY AND CONCLUSIONS

5.1 Summary

In this study, the influence of high-pass filtering on nonlinear oscillator response is investigated to derive a usable spectral period range in which filtering effects are minimal. The nonlinear behavior of SDOF systems are represented by hysteretic models that reflect no-degradation to severe degradation levels. Modified version of Clough and Johnston (1966) model is used to represent degrading model. Non-degrading hysteretic behavior is presented by bilinear model. The strong-motion database used in the nonlinear response spectrum analysis is also briefly explained in terms of magnitude (M_w), site class (NEHRP C and D) and recording type (analog vs. digital).

While removing the long-period noise of accelerograms, the randomly generated filter cut-offs (T_c) following uniform distribution are implemented to each record in the database. Latin Hypercube Sampling method is used for generating the data. The generated data is considered as two different random sets that are called as "relaxed" and "severe" representing different analysts' decisions. The uncertainty due to high-pass filter cut-off decisions of analysts is explored to reach the main objective of this study. The analysis show that the level of uncertainty is influenced by earthquake magnitude, recording quality (analog vs. digital), inelasticity level (different R or μ values) and degradation during the hysteretic excursions. In uncertainty analysis, inelastic spectral and residual displacements (SD_{IE} and SD_R, respectively) are considered to examine the dispersion.

Finally, the usable spectral period ranges are derived by using the methodology based on period-dependent probability distributions. In order to verify the performance of proposed methodology, the usable period ranges for elastic SDOF systems are also derived and compared with the studies in the literature (Abrahamson and Silva, 1997; Akkar and Bommer, 2006). The inelastic period ranges for non-degrading (ND), stiffness degrading (SD) and stiffness and strength degrading (SSD) hysteretic behavior are determined.

5.2 Conclusions

The most important findings of this study are summarized below:

- The variations in high-pass filter cut-offs that are used for removing the long-period noise of accelerograms introduces significant amount of uncertainty to the nonlinear deformation demands.

- The level of uncertainty depends primarily on the variations in magnitude, recording quality (analog vs. digital), level of inelasticity (different levels of μ and R) and degradation level during hysteretic excursions.

- The dispersion in nonlinear deformation demands is larger for small magnitude events. The increase in level of inelasticity and degradation increases the uncertainty.

- The increase in vibration period decreases the reliability of inelastic displacement response due to the pronounced interaction between the high-pass filter cut-offs and nonlinear oscillator response that is magnified further with variations in T_c.

- The variations in high-pass filter cut-off influence constant ductility and constant strength spectra equally.

- The dispersion pertaining to analog records is higher with respect to those of digital accelerograms.

- When the effect of relaxed and severe filtering is of concern, the SD_{IE} resulting from relaxed filtering criteria commences consistently at longer periods with respect to the SD_{IE} obtained from the severe filtering counterparts. The dispersion in nonlinear oscillator deformations due to the application of severe filter cut-offs is more prominent.

- In order to verify the methodology proposed in this study, the usable period ranges of elastic oscillator response are also determined and compared with the findings of similar studies (Abrahamson and Silva, 1997; Akkar and Bommer, 2006). The comparisons indicate that the suggested methodology is compatible with the other investigations despite relatively conservative usable period ranges of this study.

- The usable spectral period ranges are derived for inelastic oscillator responses that are represented by ND, SD and SSD hysteretic models. It is depicted from the results that the usable period ranges generally decrease with increasing level of degradation.

- The reliability of inelastic spectral displacements within the spectral bands bounded by the proposed usable periods is almost not affected by the chosen high-pass filter cut-off.

- Confined to the ground-motion dataset used in this study, the proposed inelastic usable spectral period ranges can form a basis for deriving rational

GMPEs of nonlinear spectral displacements with the least interference of high-pass filter cut-offs.

- The usable periods suggested in this study would be important for structural engineers to understand the limitations of high-pass filtered records that are implemented in the nonlinear time history analysis of long-period structural systems.

REFERENCES

Abrahamson, N. A. and Silva W. J. (1997). Empirical response spectral attenuation relations for shallow crustal eartqaukes, *Seismological Reserach Letters*, Vol. 68, 94-127.

Akkar, S. and Bommer, J. J., (2006). Influence of long-period filter cut-off on elastic spectral displacements, *Earthquake Engineering and Structural Dynamics*, Vol. 35, 1145-1165.

Akkar, S. and Ozen, O., (2006). Influence of low-cut filtering on SDOF linear/nonlinear deformation demands, *8th US National Conference on Earthquake Engineering*, San Francisco, USA, Paper No. 8NCEE-580.

Akkar, S. and Bommer, J. J., (2007b). Prediction of elastic displacement response spectra in Europe and the Middle East, *Earthquake Engineering and Structural Dynamics*, Vol. 36, 1275-1301.

Akkar, S. and Boore, D. M., (2009). On baseline corrections and uncertainty in response spectra for baseline variations commonly encountered in digital accelerograph records, *Bulletin of the Seismological Society of America*, Vol. 99, 1671-1690.

Ang, A. H-S. and Tang, W. H., (1975). *Probability Concepts in Engineering Planning and Design, Volume I: Basic Principles,* John Wiley, New York.

Atkinson, G. M. and Silva, W., (2000). Stochastic modeling of California ground motions, *Bulletin of the Seismological Society of America*, Vol. 90, 255–274.

Bazzurro, P., Sjoberg, B., Luco, N., Silva, W. J. and Darragh R. E., (2005). Effects of strong motion processing procedures on time histories, elastic and inelastic spectra, *COSMOS Publication No. CP-2005/02*.

Boore, D. M. and Akkar, S., (2003). Effect of causal and acausal filters on elatsic and inealstic response spectra, *Earthquake Engineering and Structural Dynamics*, Vol. 32, 1729-1748.

Boore, D. M. and Bommer, J. J., (2005). Processing of strong-motion accelerograms: needs, options and consequences, *Soil Dynamics and Earthquake Engineering*; Vol. 25, 93–115.

BSSC (Building Seismic Safety Council), (2003). *The 2003 NEHRP recommended provisions for new buildings and other structures. Part 1: Provisions (FEMA 450)*, Federal Emergency Management Agency, Washington, DC.

Clough, R. W. and Johnston, S. B., (1966). Effect of stiffness degradation on earthquake ductility requirements, *2nd Japan National Conference on Earthquake Engineering*, 227-232.

Erberik, M. A., (2001). *Energy based seismic assessment of degrading systems*, Ph.D. Thesis, Civil Engineering Department, Middle East Technical University, Ankara.

Joyner, W. B. and Boore, D. M., (1981). Peak horizontal acceleration and velocity from strong motion records including records from the 1979 Imperial Valley, California, earthquake, *Bulletin of Seismological Society of America*, Vol. 71, 2011-2038.

Kawashima, K., MacRae, G. A., Hoshikuma, J. and Nagaya, K., (1998). Residual displacement response spectrum, *Journal of Structural Engineering ASCE,* Vol. 124, 523-530.

Kurtman, B., (2007). *A detailed analysis for evaluation of the degradation characteristics of simple structural systems*, M. Sc. Thesis, Civil Engineering Department, Middle East Technical University, Ankara.

Mahin, S. A. and Bertero, V. V., (1976). Nonlinear seismic response of a coupled wall system, *Journal of Structural Engineering ASCE*, Vol.102 (ST9), 1759-1780.

McKay, M. D., Conover, W. J. and Beckman, R. J., (1979). A comparison of three methods for selection values of input variables in the analysis of output from a computer code, *Technometrics*, Vol. 2, 239-245.

Otani, S., (1981). Hysteresis models of reinforced concrete for earthquake response analysis, *Journal of Faculty of Engineering, University of Tokyo*, Vol. 36, No. 2, 407-441.

Pebesma, E. J., Heuvelink, G. B. M. and Kros, J., (2000). Error assessment in a soil acidification modeling study: efficiency issues and change of support, *Proceedings of the 4th International Symposium on Spatial Accuracy Assessment in Natural Resources and Environmental Sciences*, Delft University Press, 521-528.

Pujol, S., (2002). *Drift Capacity of Reinforced Concrete Columns Subjected to Displacement Reversals*, Ph.D. Thesis, Purdue University, West Lafayette, Indiana.

Song, J. K. and Pincheira, J. A., (2000). Spectral displacement demands of stiffness- and strength-degrading systems, *Earthquake Spectra*, Vol.16, No. 4, 817-851.

Tothong, P. and Cornell, C. A., (2006). An empirical ground-motion attenuation relation for inelastic spectral displacement, *Bulletin of the Seismological Society of America*. doi: 10.1785/0120060018.

Trifunac, M. D. and Lee, V. W., (1996). Peak Surface Strains During Strong Earthquake Motion, *International Journal of Soil Dynamics and Earthquake Engineering*, Vol. 15, 311-319.

Utility Software for Data Processing (USDP), (2008). Department of Civil Engineering, Middle East Technical University, Ankara, Turkey, available on Internet at http://www.usdp.org/download.htm, last visited on June 2009.

Wight, J. K. and Sozen, M. A., (1973). *Shear strength decay in reinforced concrete columns subjected to large deflection reversals*. Structural Research Series No. 403, Civil Engineering Studies, University of Illinois, Urbana-Champaign.

APPENDIX A

SCATTER PLOTS OF INELASTIC SPECTRAL DISPLACEMENTS

Scatter plots of inelastic spectral displacements are illustrated for different site classes (NEHRP C and D), levels of inelasticity and distance intervals at T=1.0 s and T=4.0 s. The distance intervals of d=0-25 km and 25-50 km are only shown due to scarce and uneven data distribution for distances greater than 50 km.

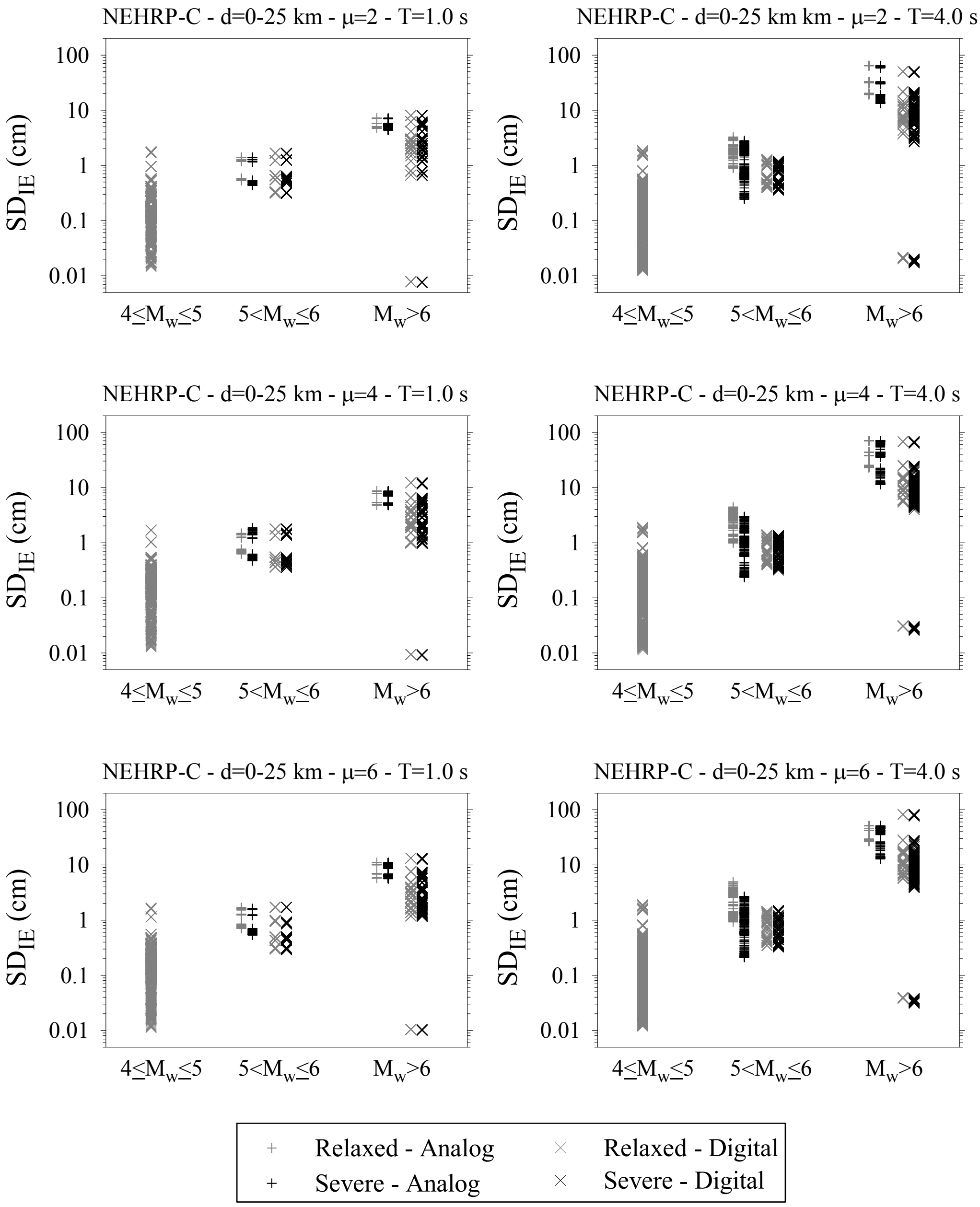

Figure A.1 Scatter plots of inelastic spectral displacements for ND model.

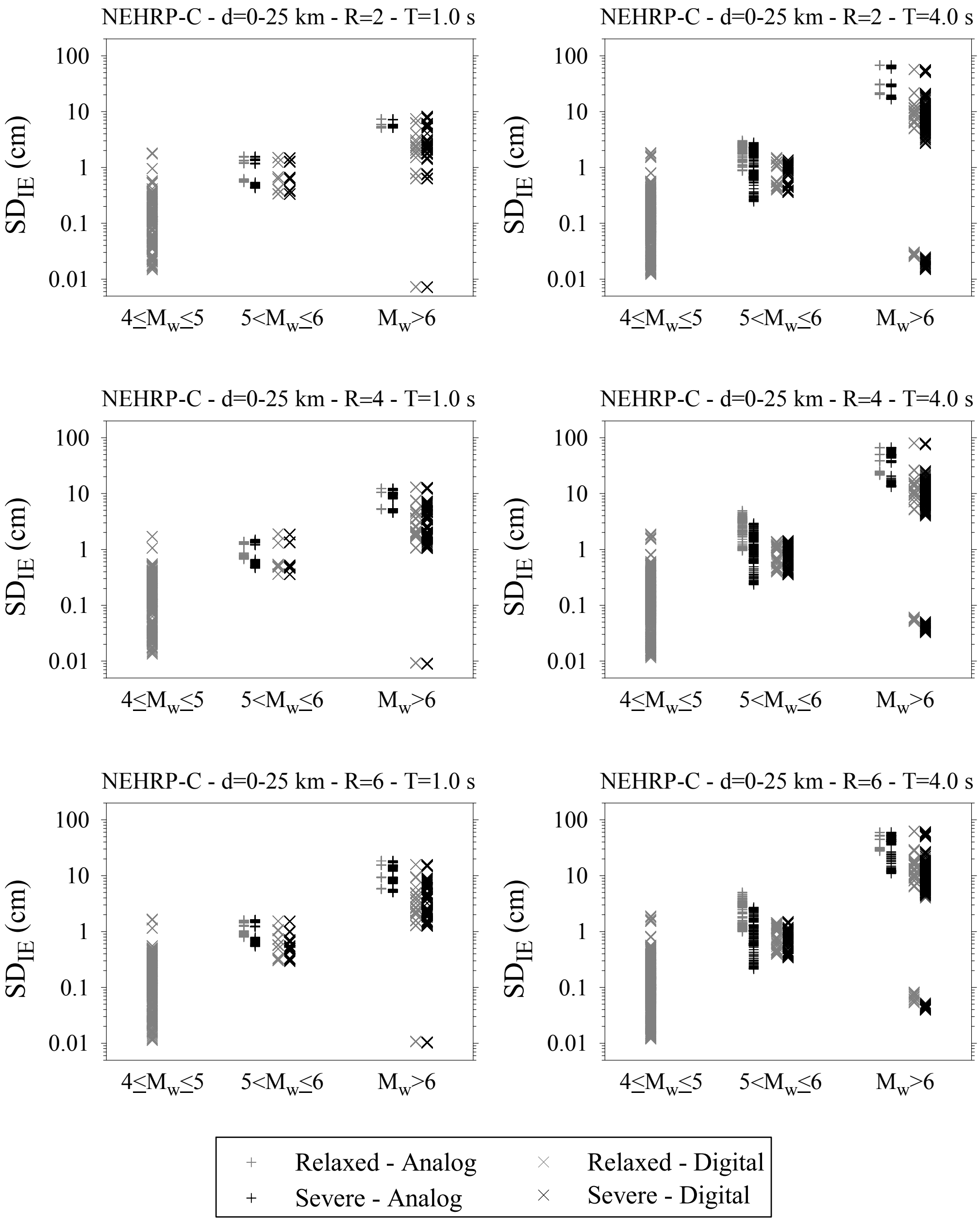

Figure A.2 Scatter plots of inelastic spectral displacements for ND model.

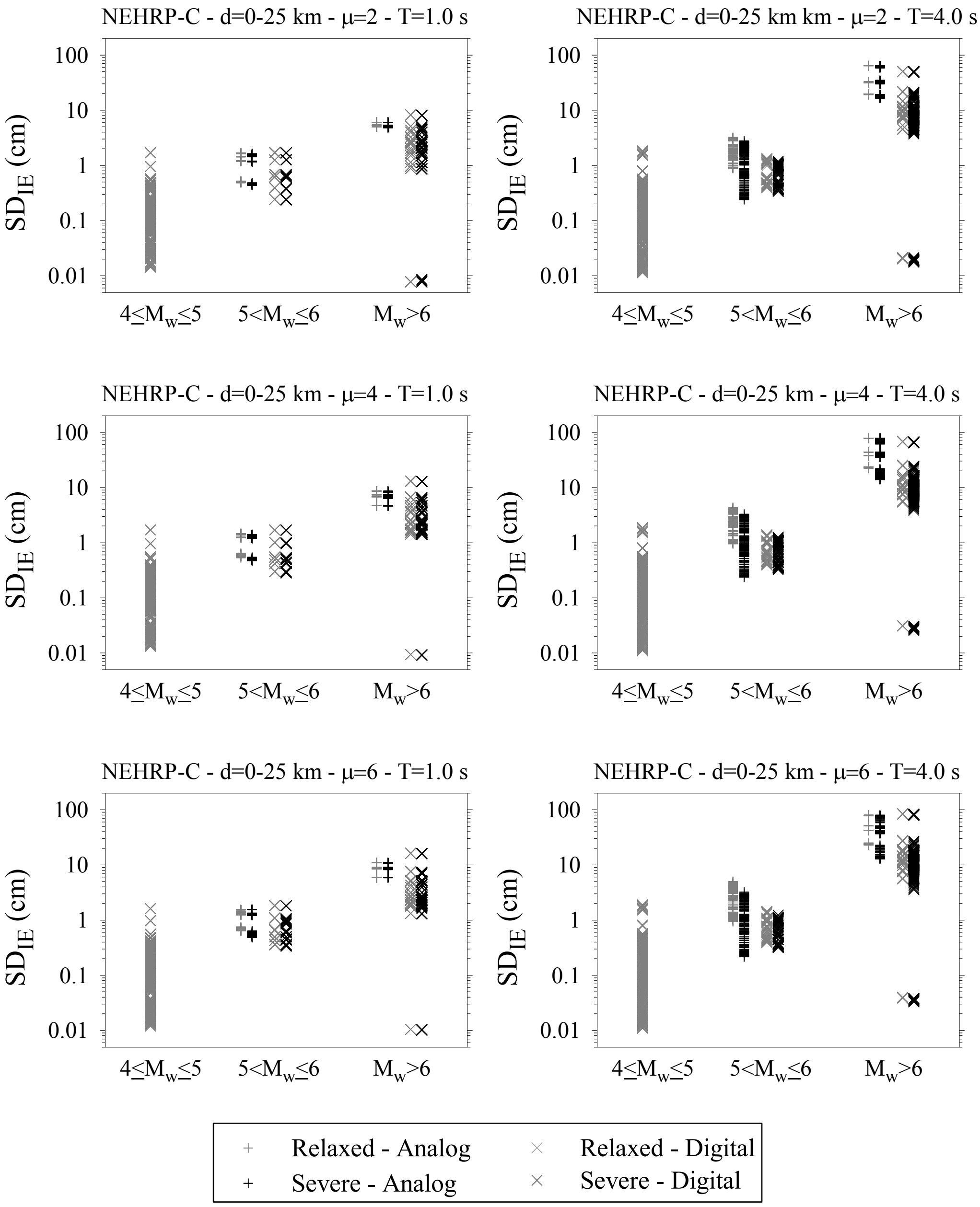

Figure A.3 Scatter plots of inelastic spectral displacements for SD model.

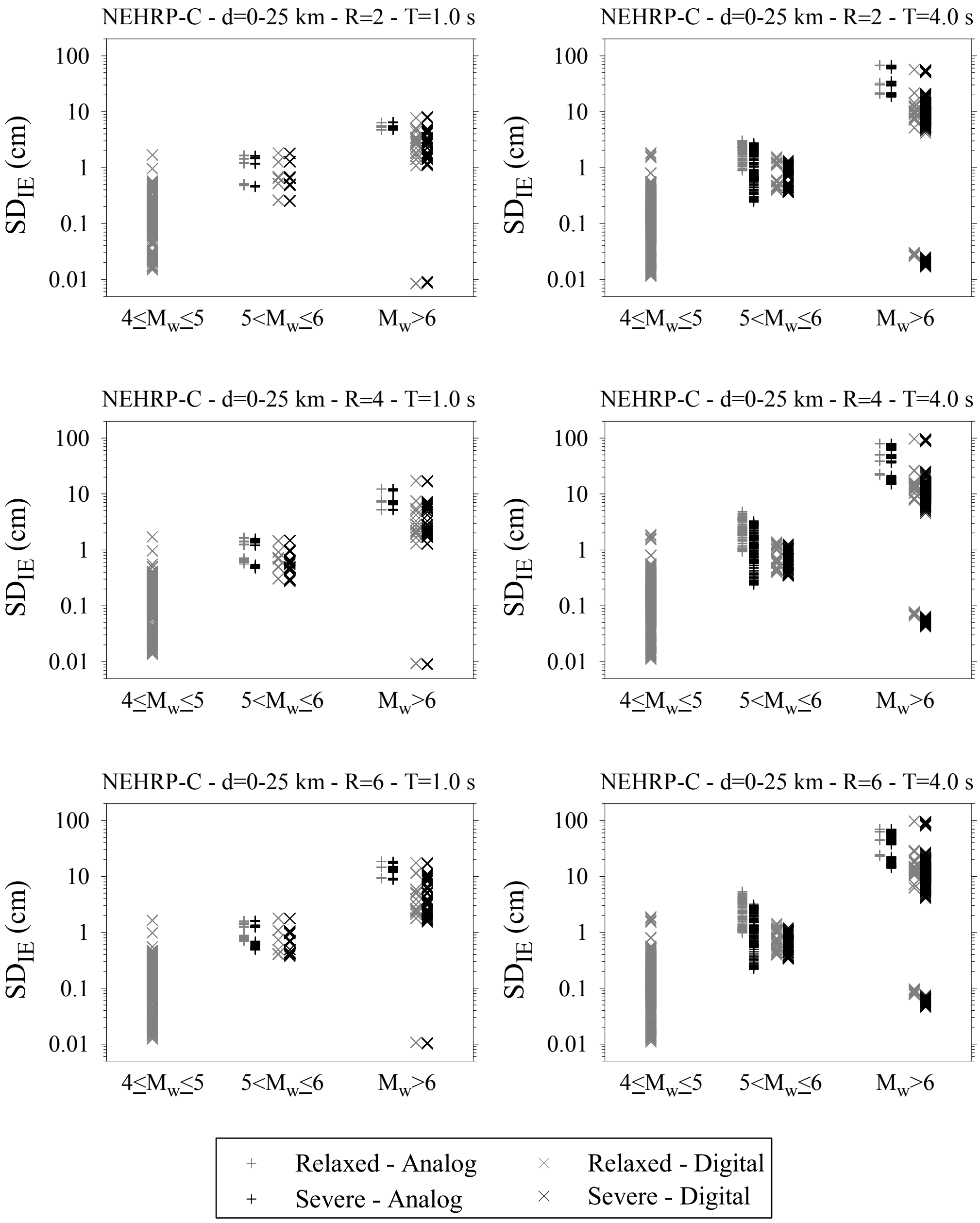

Figure A.4 Scatter plots of inelastic spectral displacements for SD model.

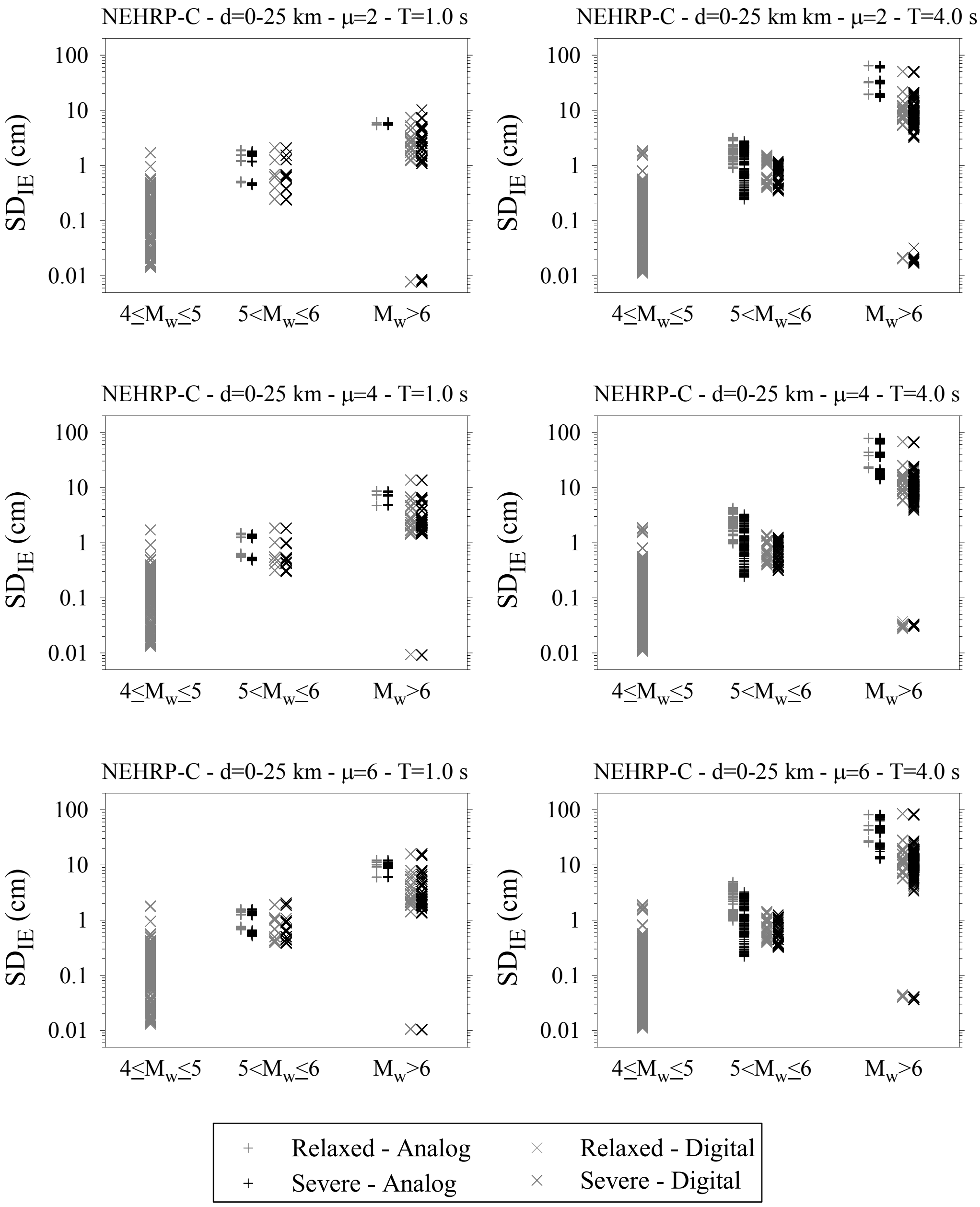

Figure A.5 Scatter plots of inelastic spectral displacements for SSD model.

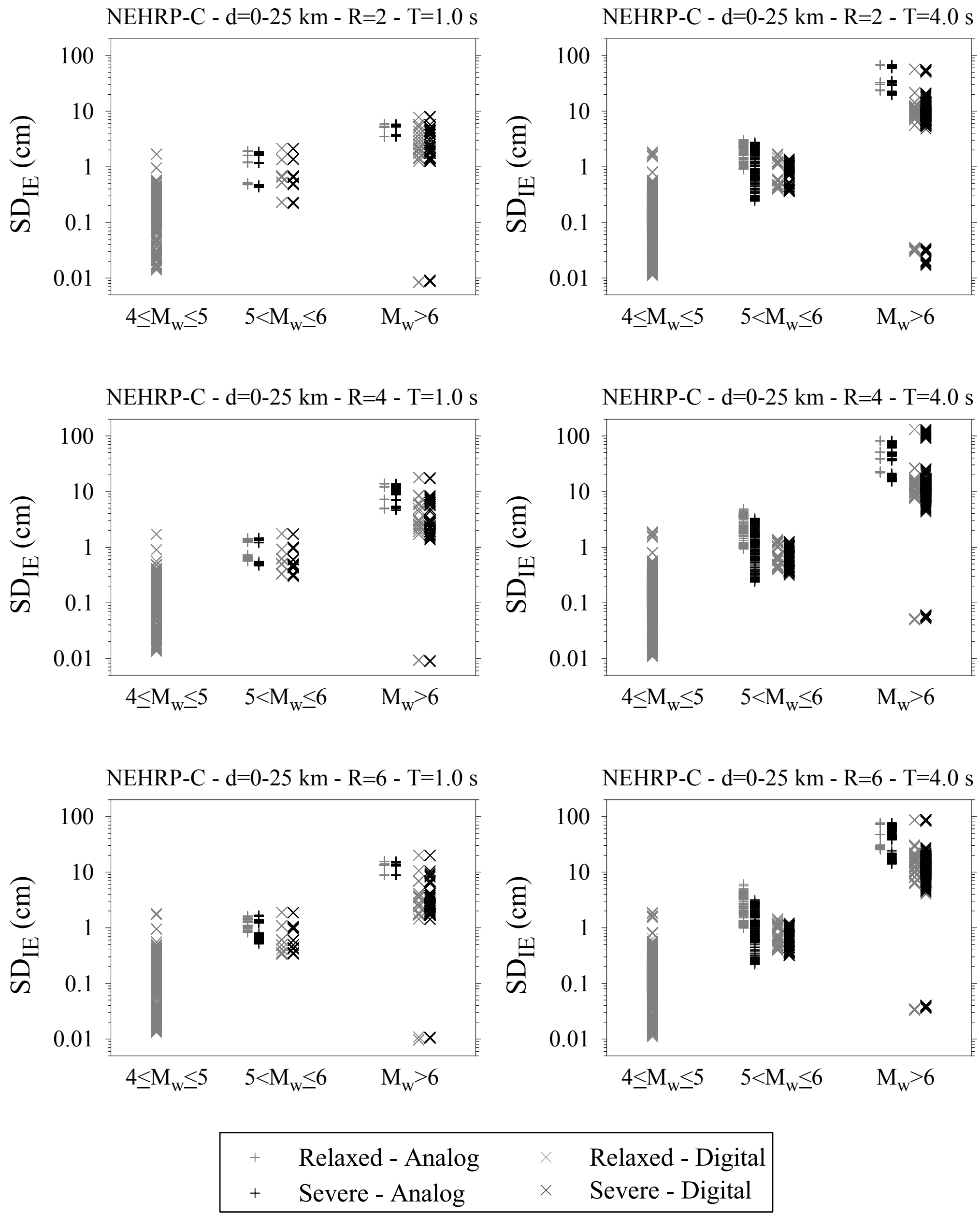

Figure A.6 Scatter plots of inelastic spectral displacements for SSD model.

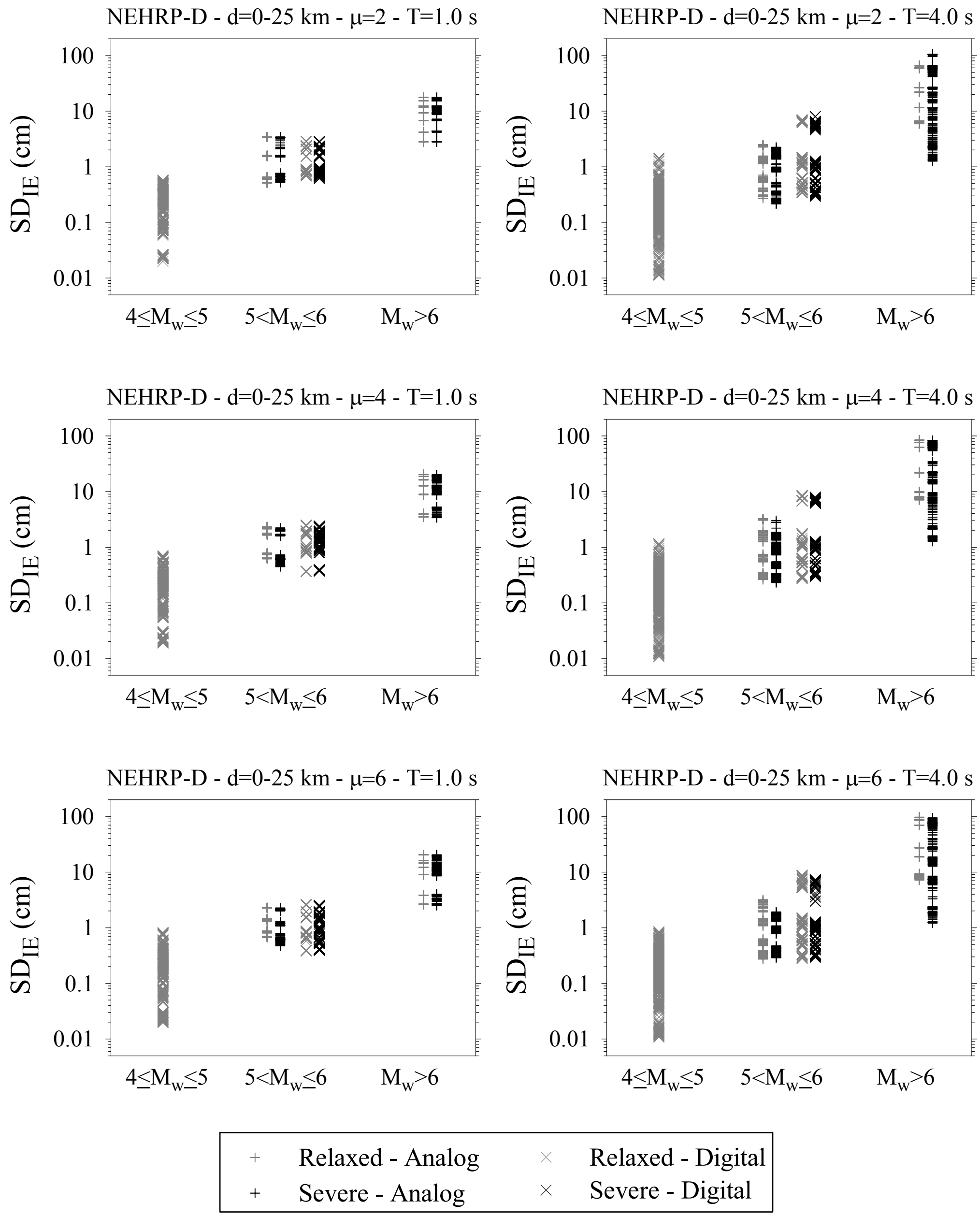

Figure A.7 Scatter plots of inelastic spectral displacements for ND model.

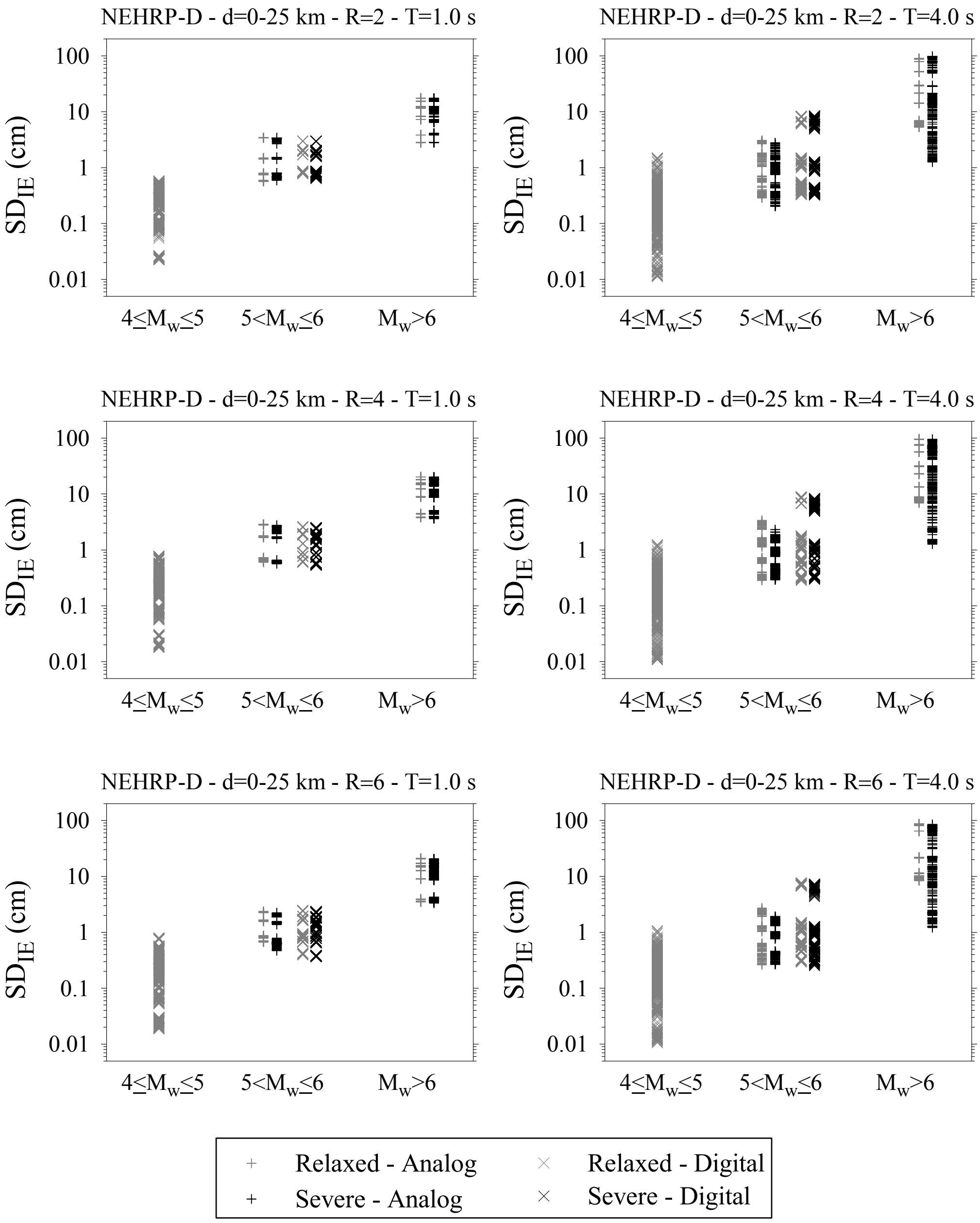

Figure A.8 Scatter plots of inelastic spectral displacements for ND model.

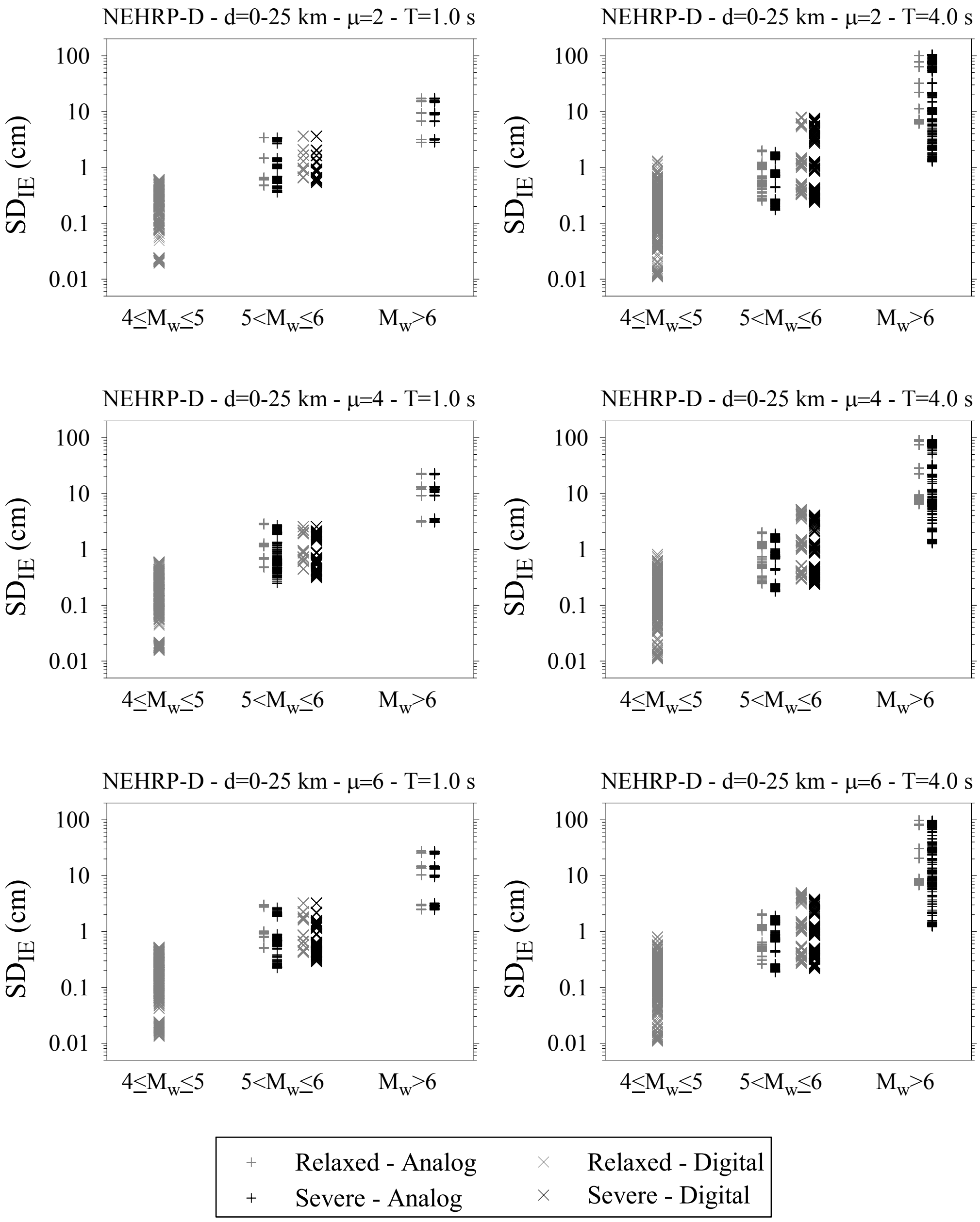

Figure A.9 Scatter plots of inelastic spectral displacements for SD model.

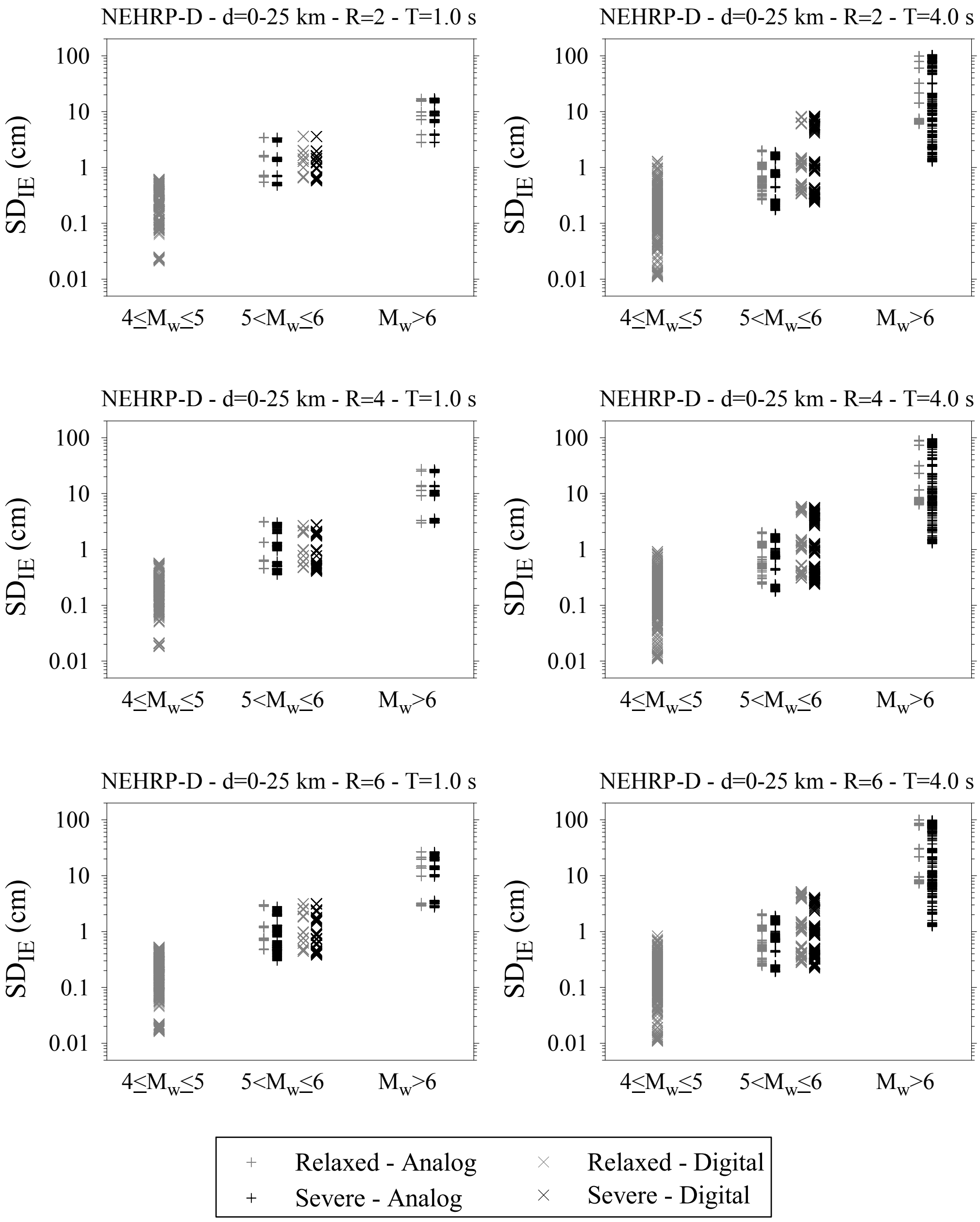

Figure A.10 Scatter plots of inelastic spectral displacements for SD model.

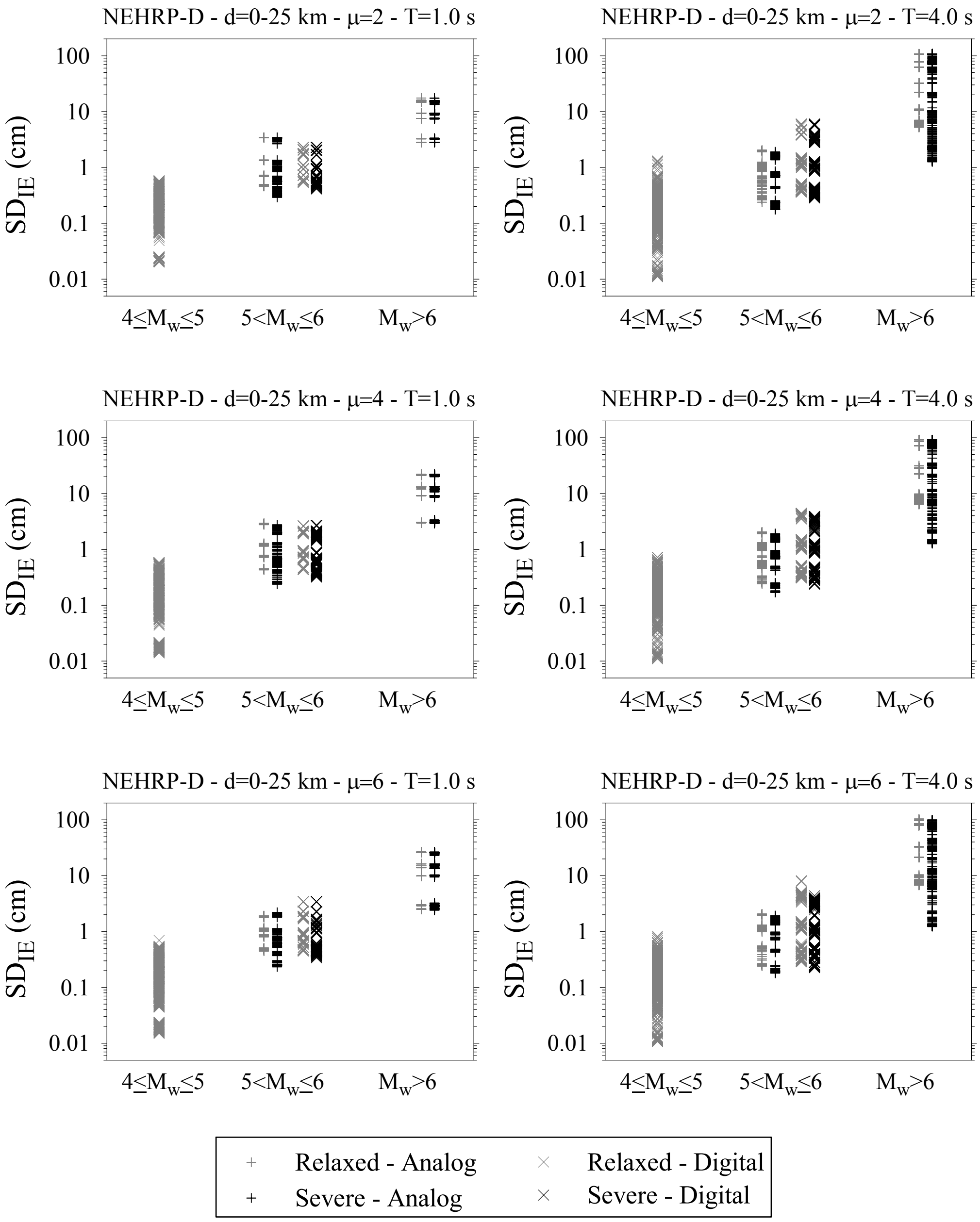

Figure A.11 Scatter plots of inelastic spectral displacements for SSD model.

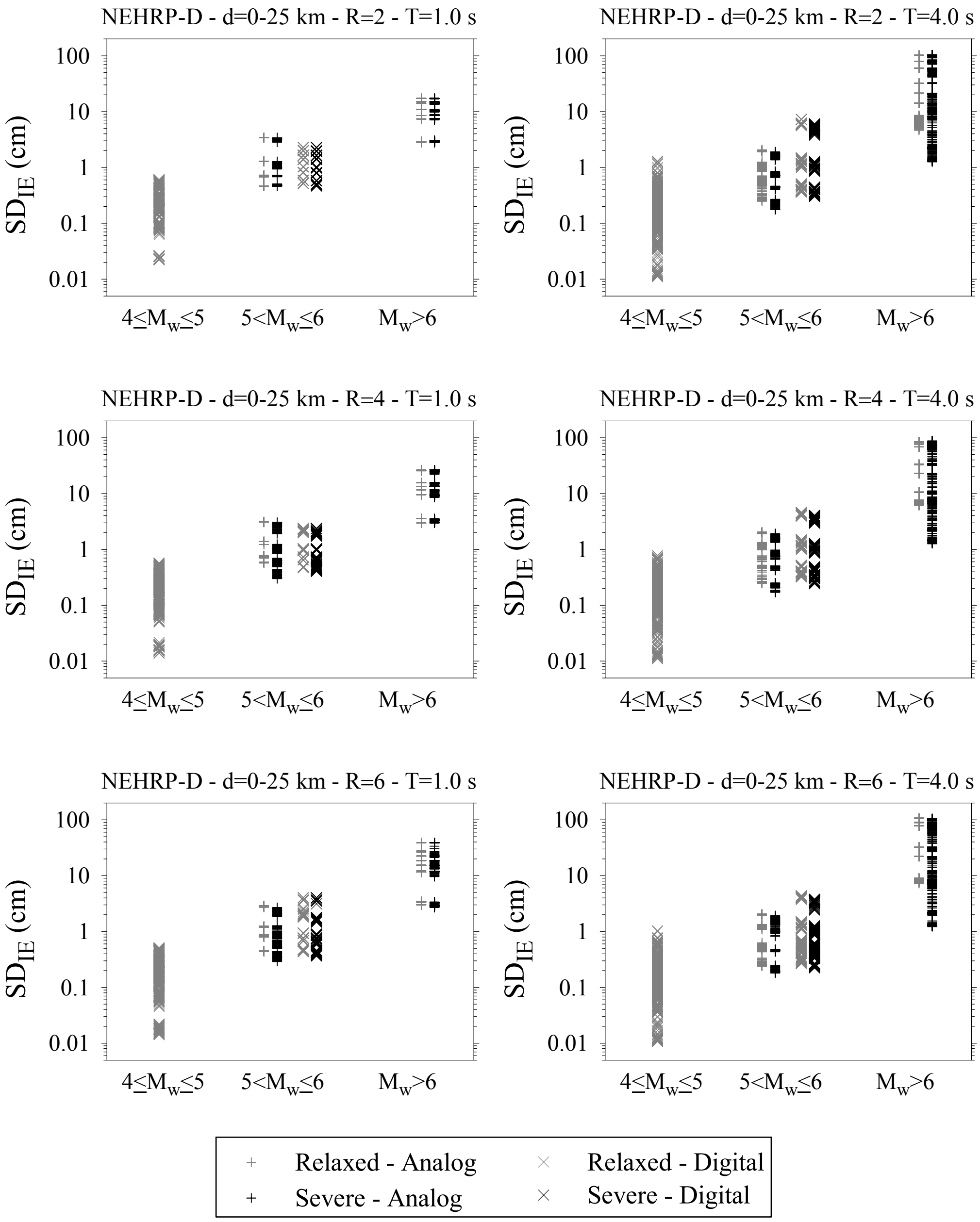

Figure A.12 Scatter plots of inelastic spectral displacements for SSD model.

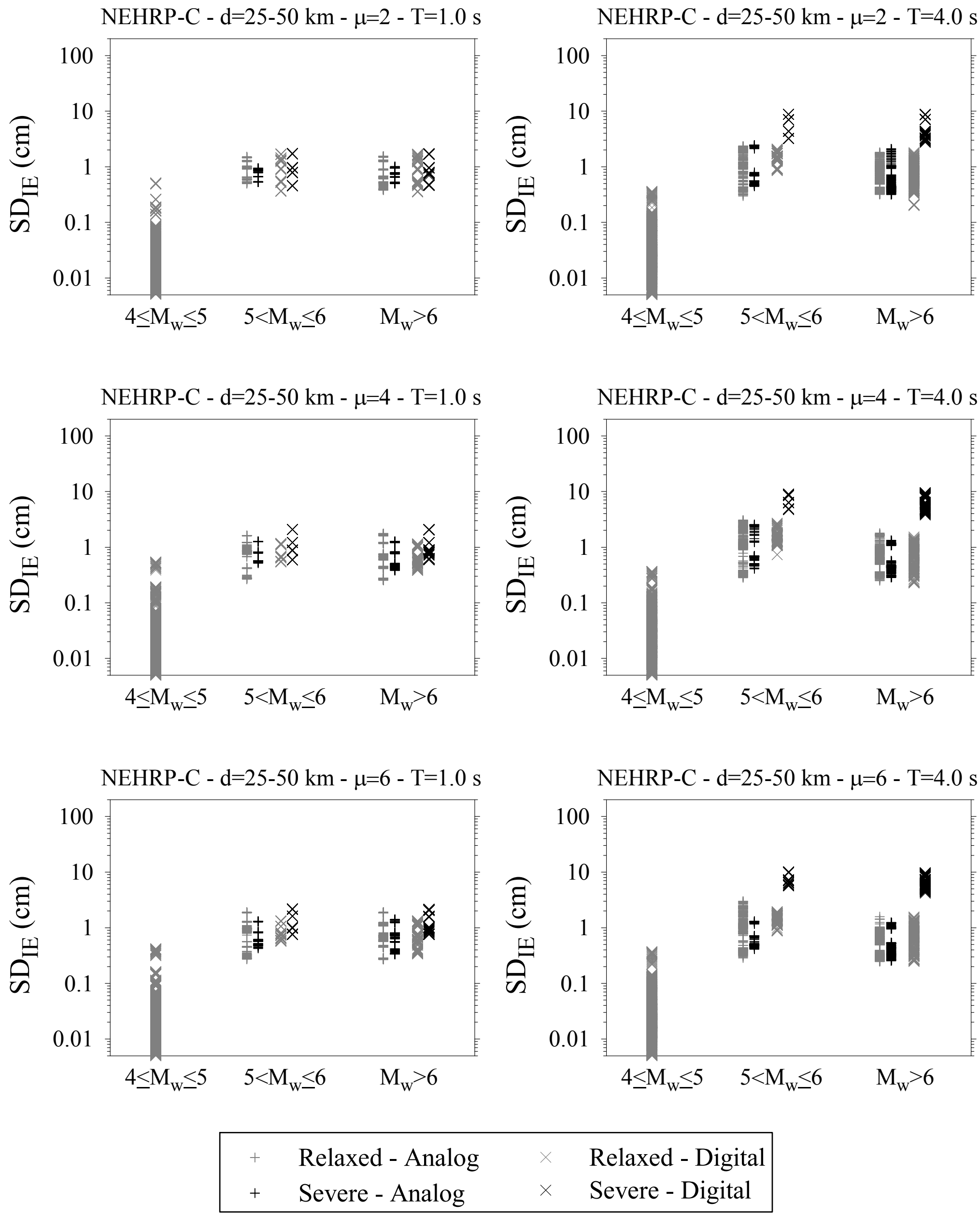

Figure A.13 Scatter plots of inelastic spectral displacements for ND model.

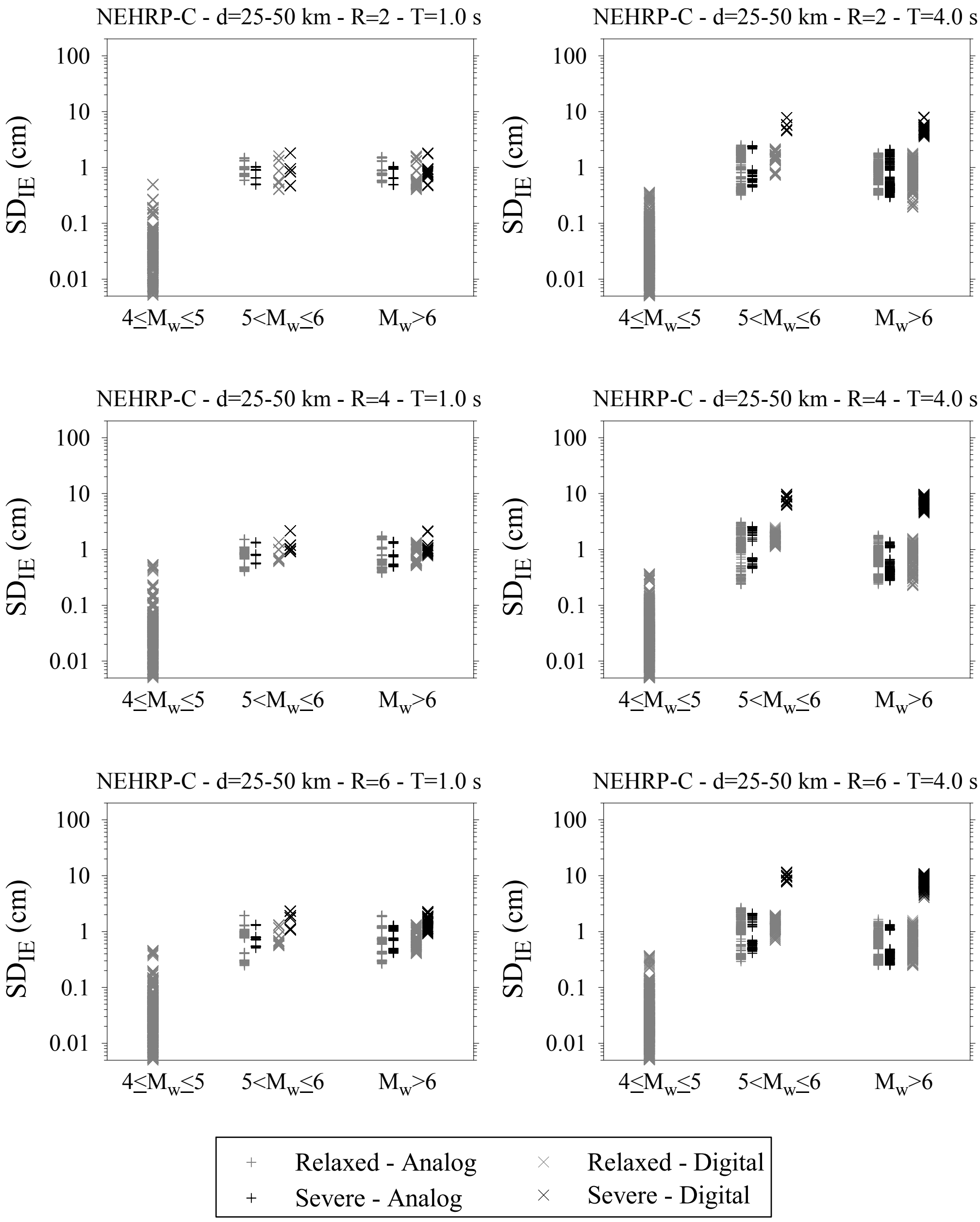

Figure A.14 Scatter plots of inelastic spectral displacements for ND model.

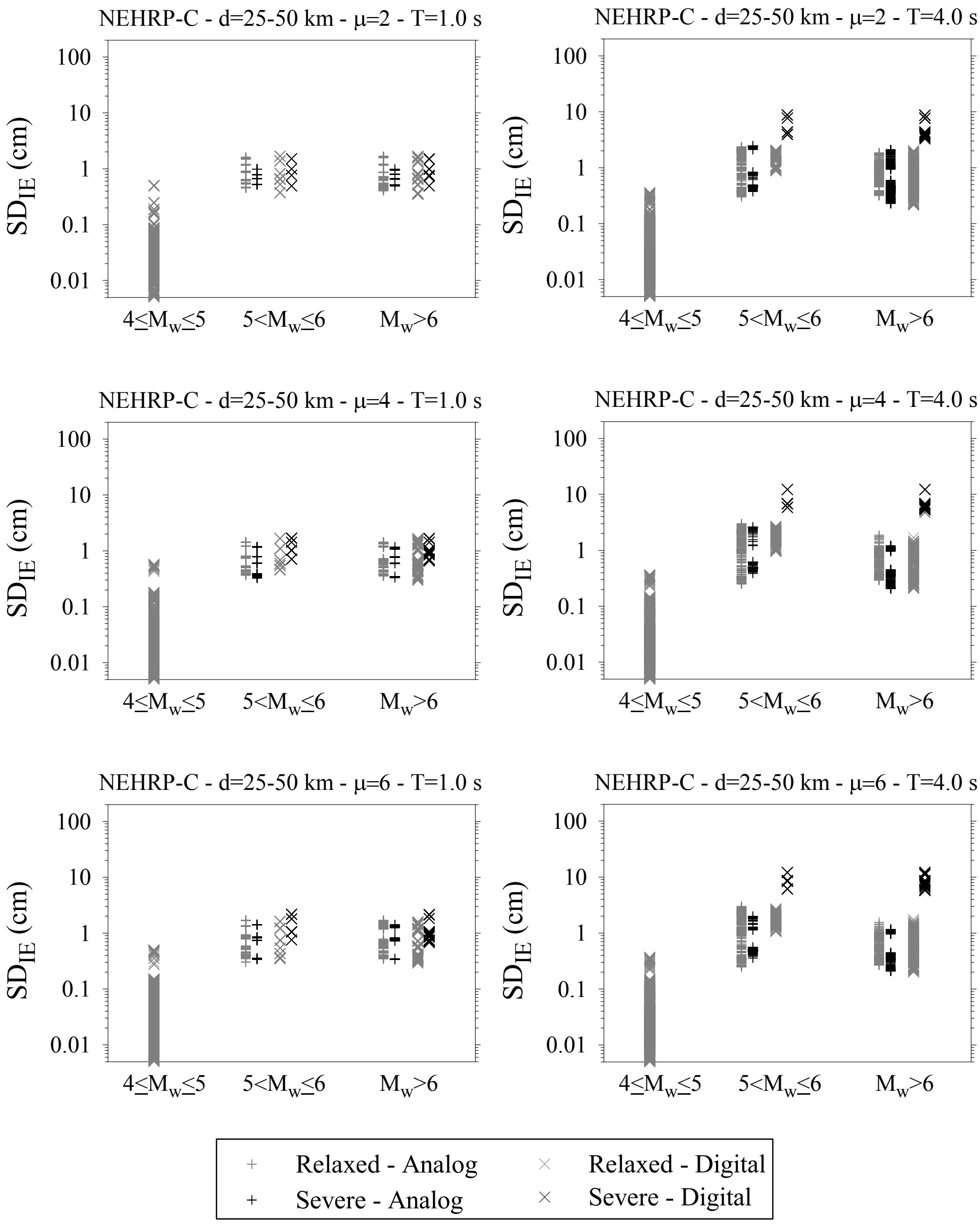

Figure A.15 Scatter plots of inelastic spectral displacements for SD model.

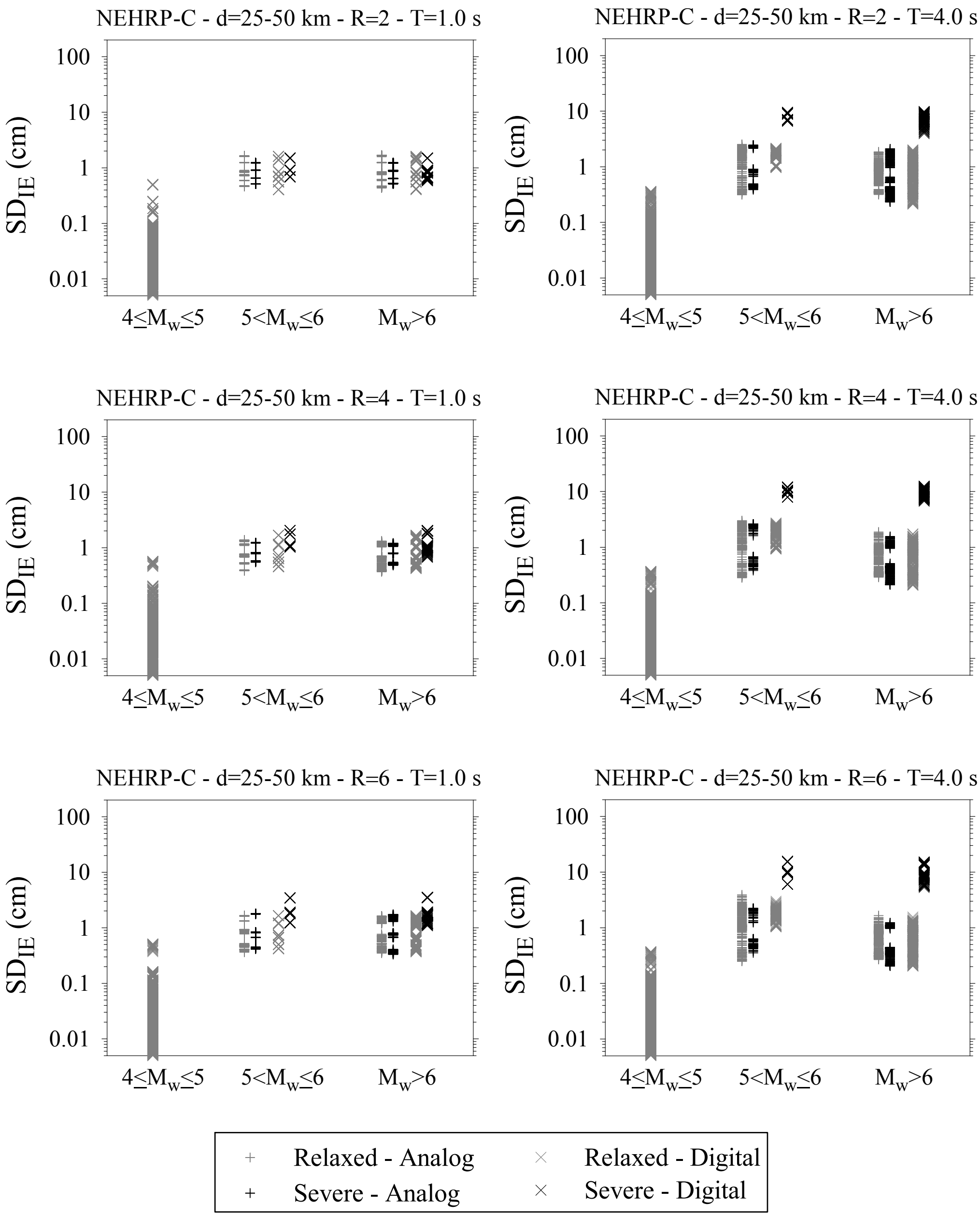

Figure A.16 Scatter plots of inelastic spectral displacements for SD model.

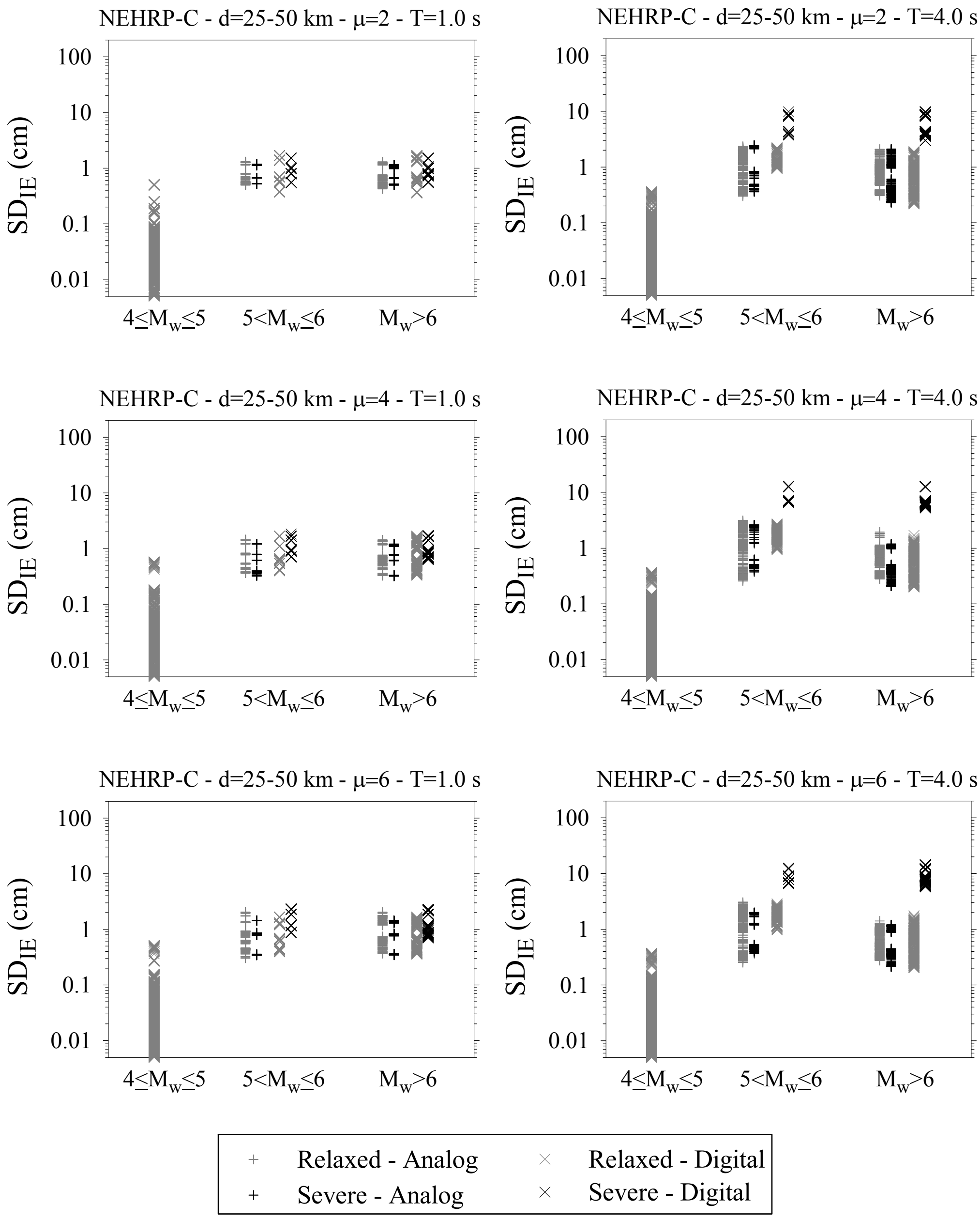

Figure A.17 Scatter plots of inelastic spectral displacements for SSD model.

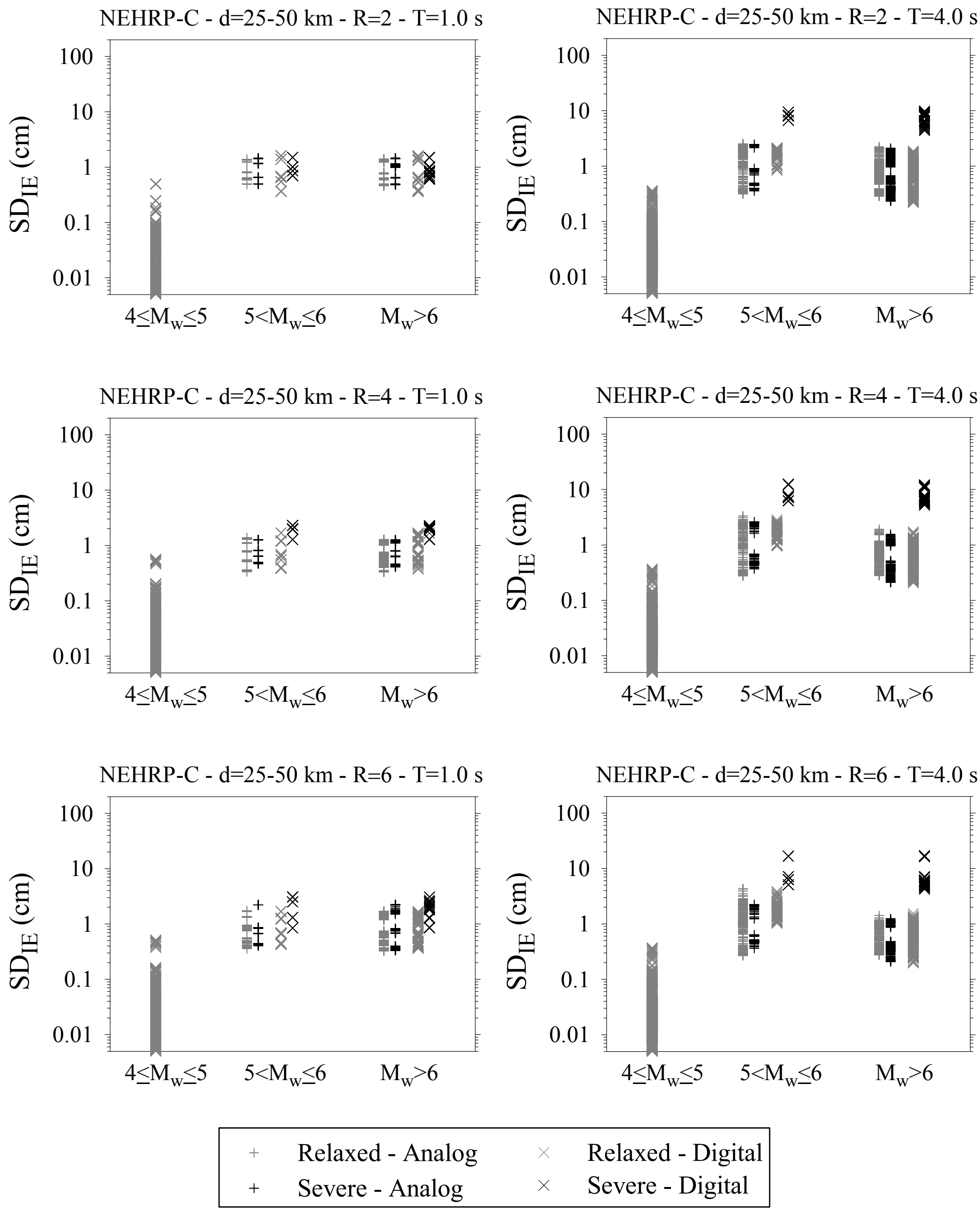

Figure A.18 Scatter plots of inelastic spectral displacements for SSD model.

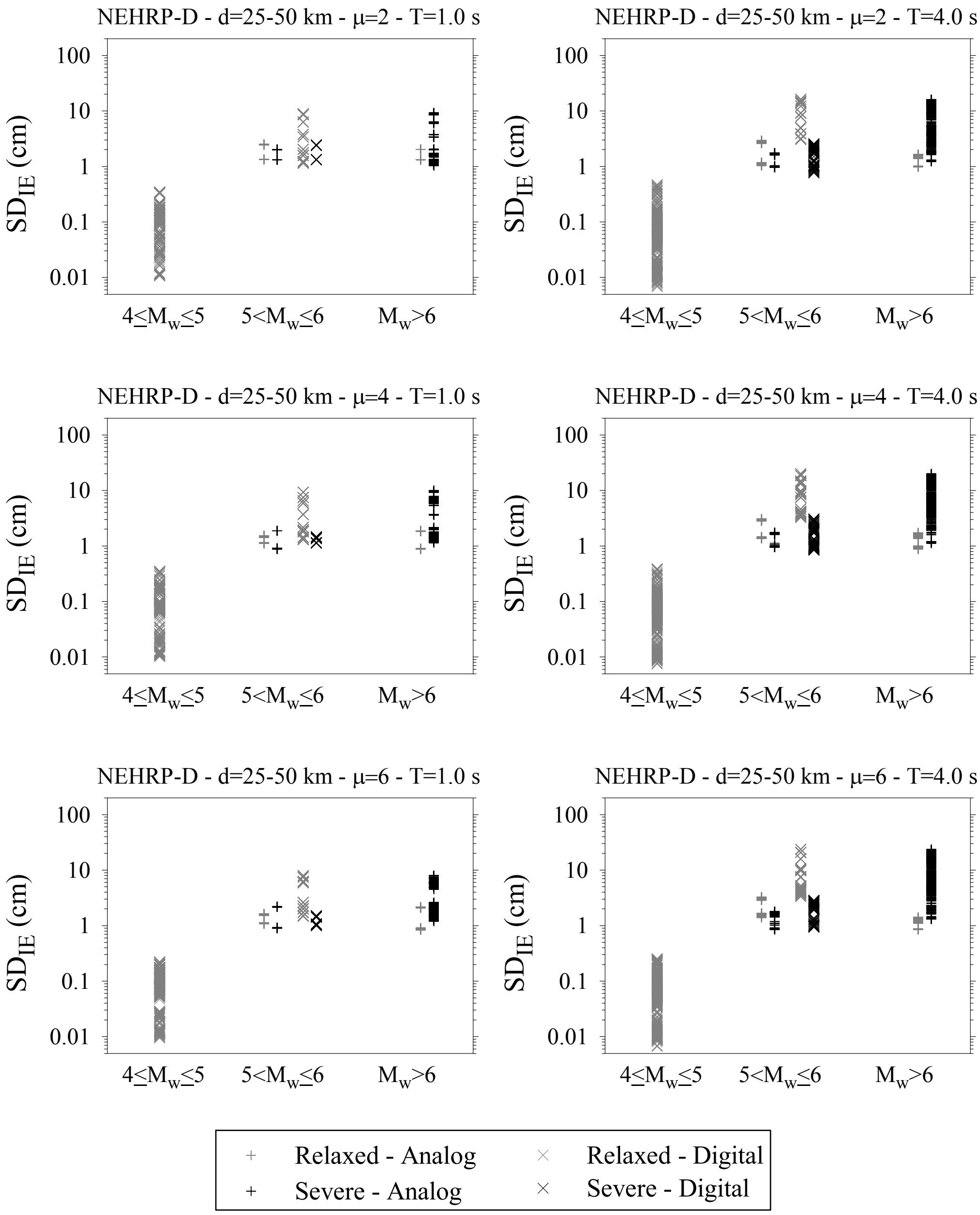

Figure A.19 Scatter plots of inelastic spectral displacements for ND model.

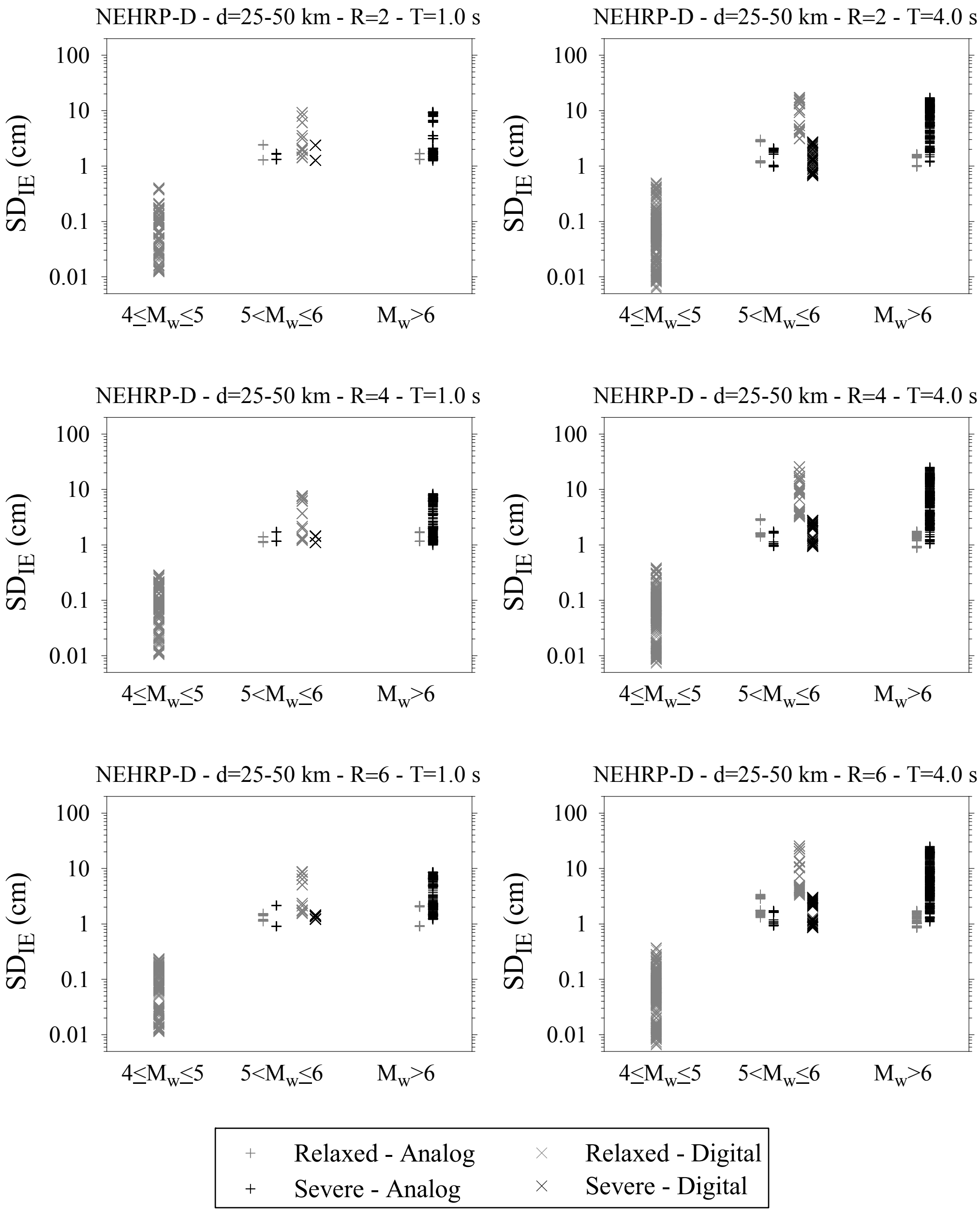

Figure A.20 Scatter plots of inelastic spectral displacements for ND model.

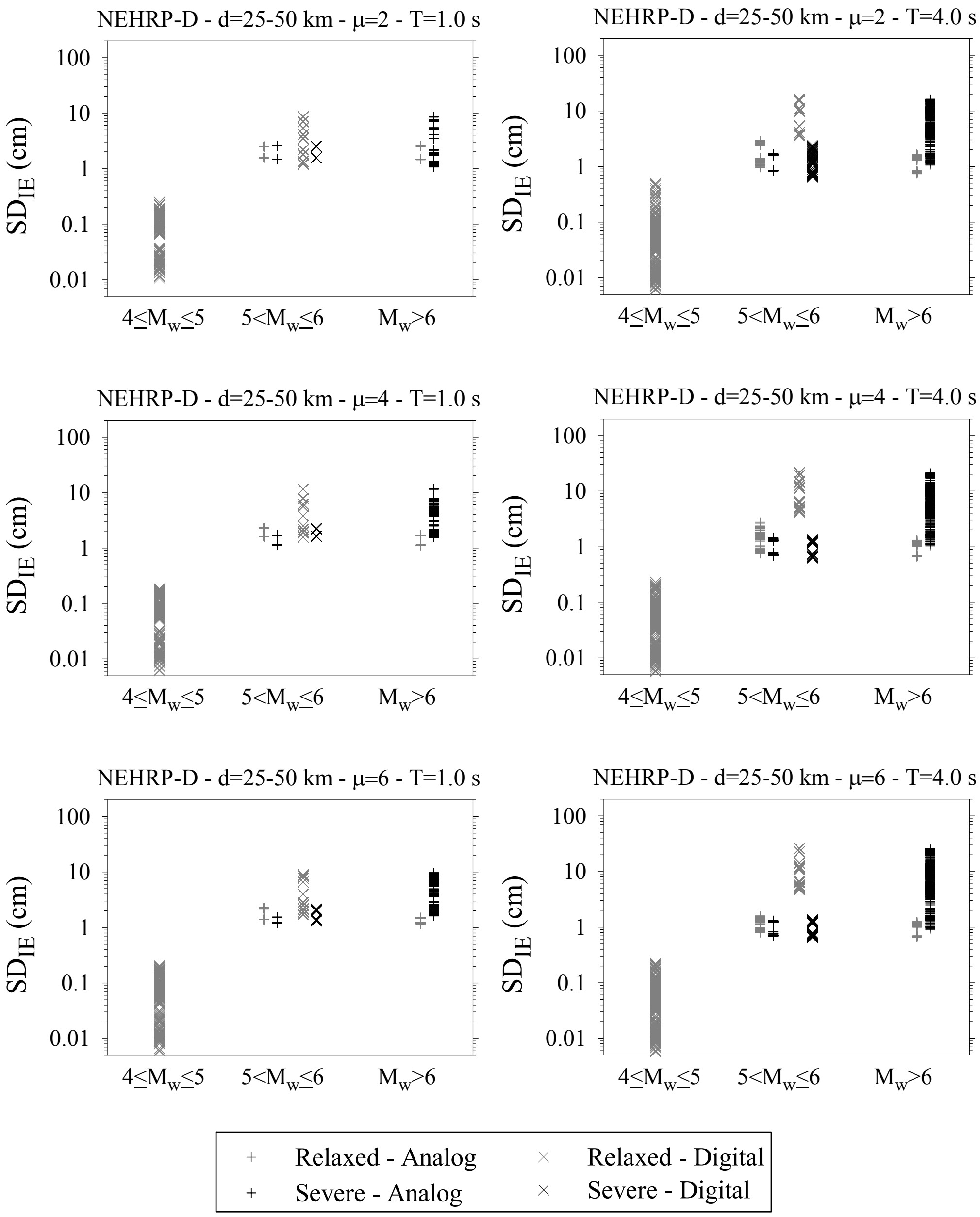

Figure A.21 Scatter plots of inelastic spectral displacements for SD model.

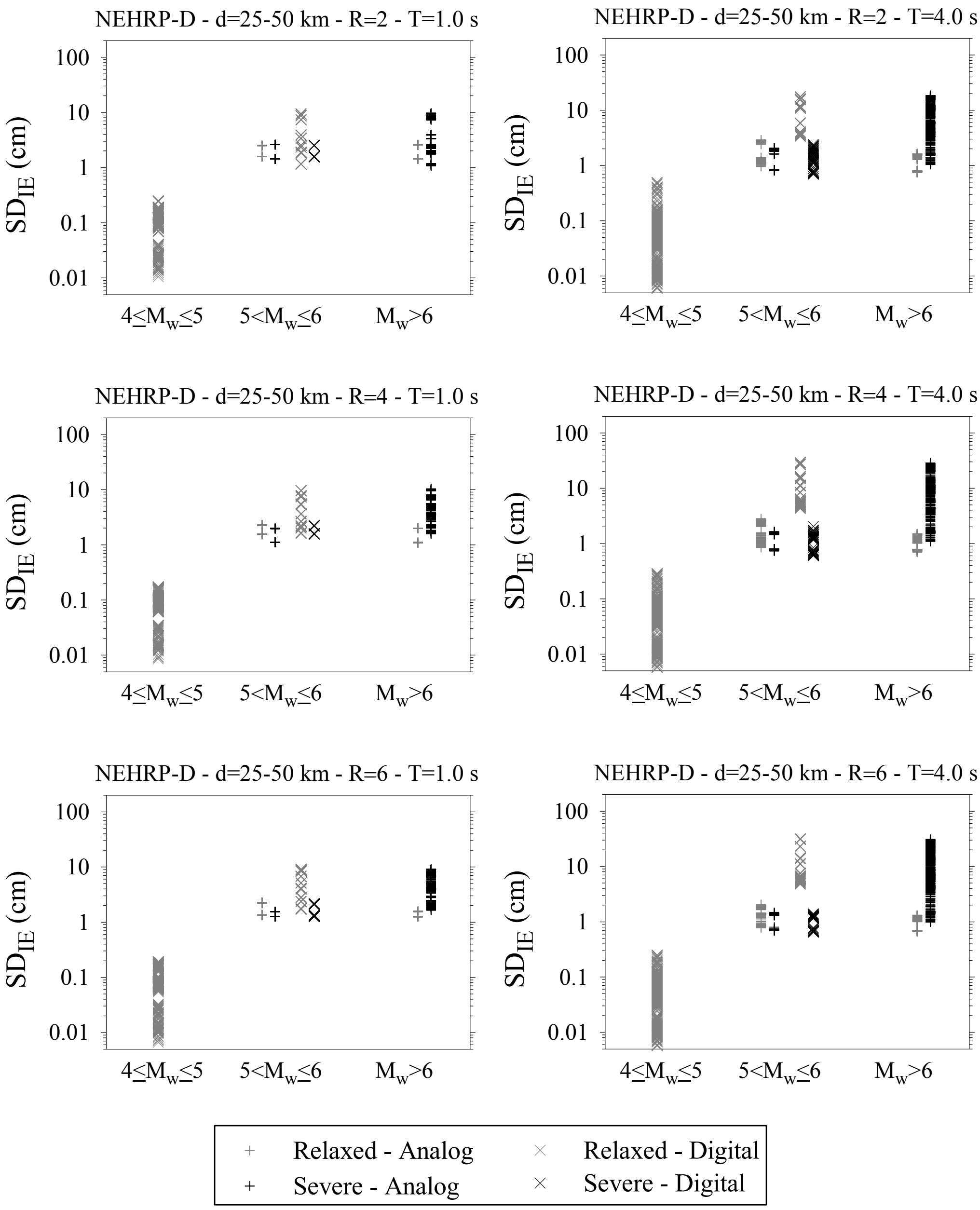

Figure A.22 Scatter plots of inelastic spectral displacements for SD model.

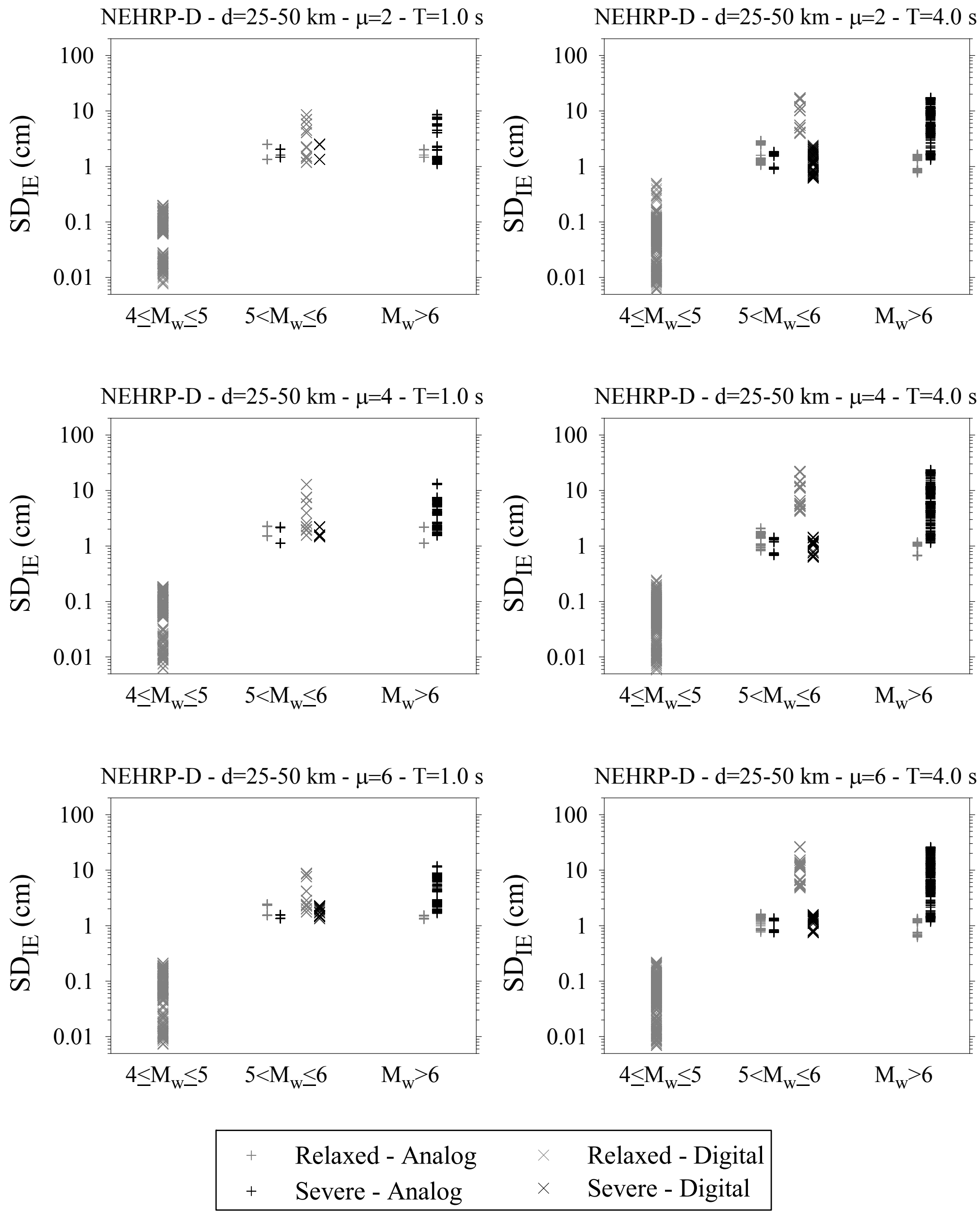

Figure A.23 Scatter plots of inelastic spectral displacements for SSD model.

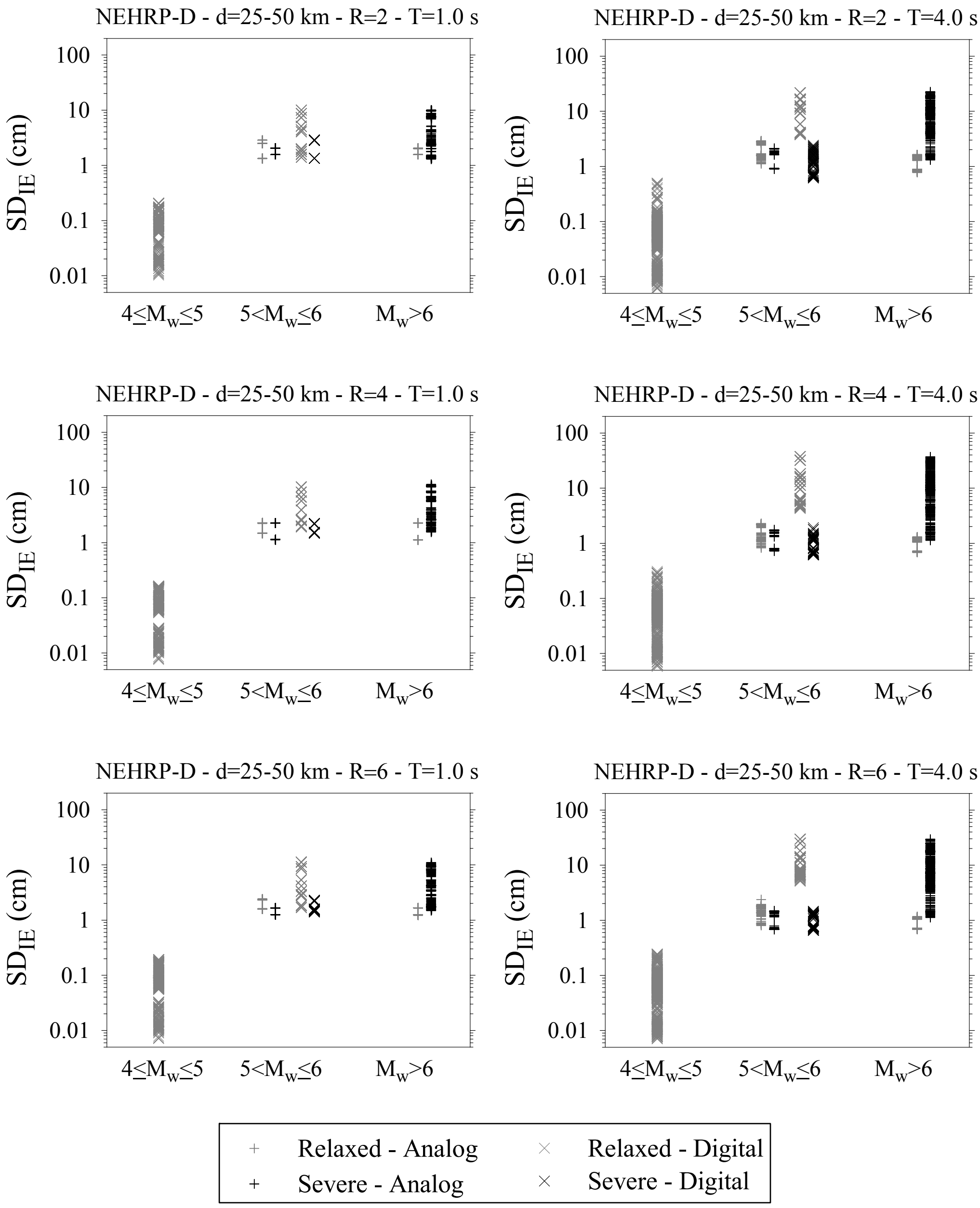

Figure A.24 Scatter plots of inelastic spectral displacements for SSD model.

APPENDIX B

SCATTER PLOTS OF RESIDUAL DISPLACEMENTS

Scatter plots of residual displacements are illustrated for different site classes (NEHRP C and D), levels of inelasticity and distance intervals at T=1.0 s and T=4.0 s. The distance intervals of d=0-25 km and 25-50 km are only shown due to scarce and uneven data distribution for distances greater than 50 km.

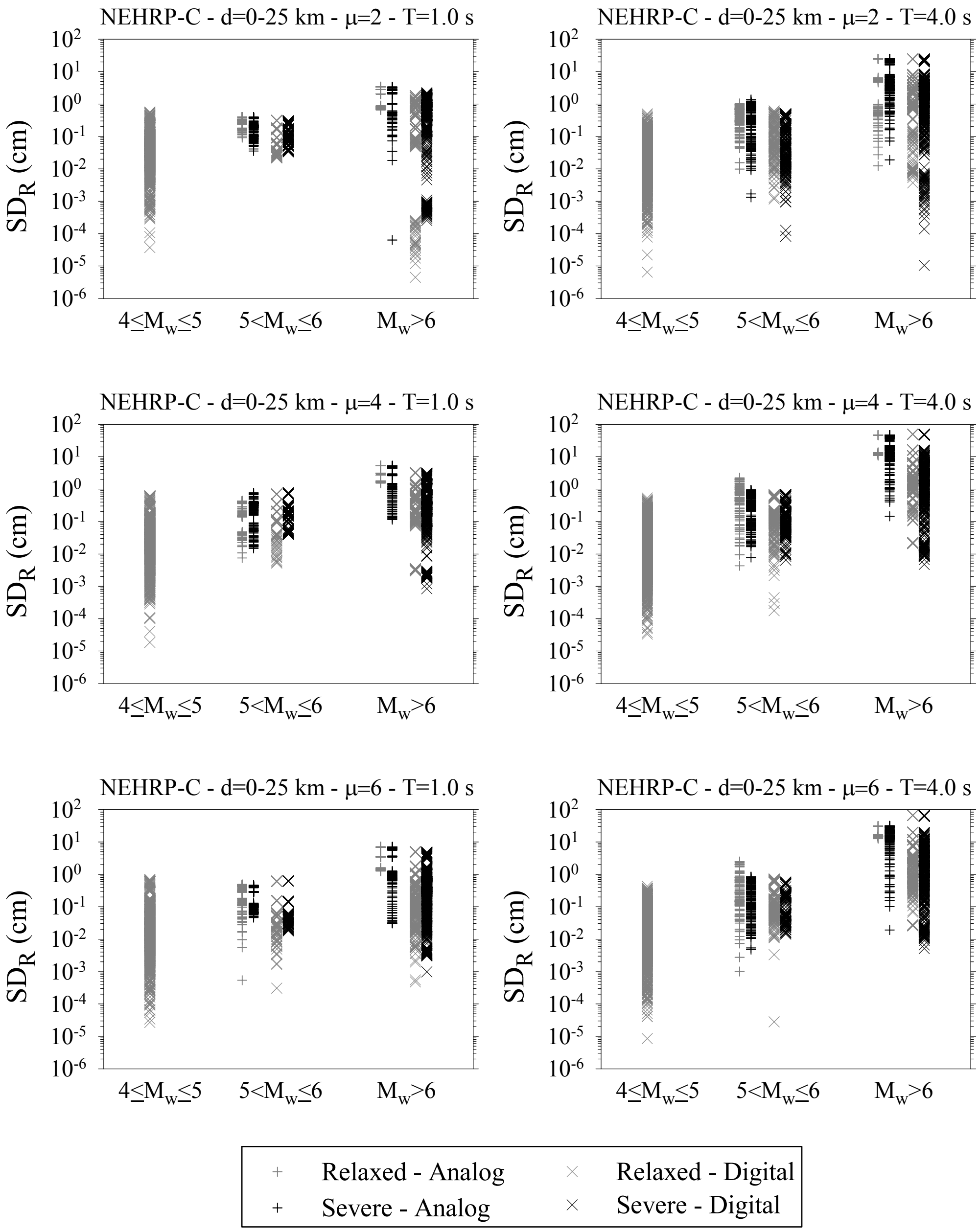

Figure B.1 Scatter plots of residual displacements for ND model.

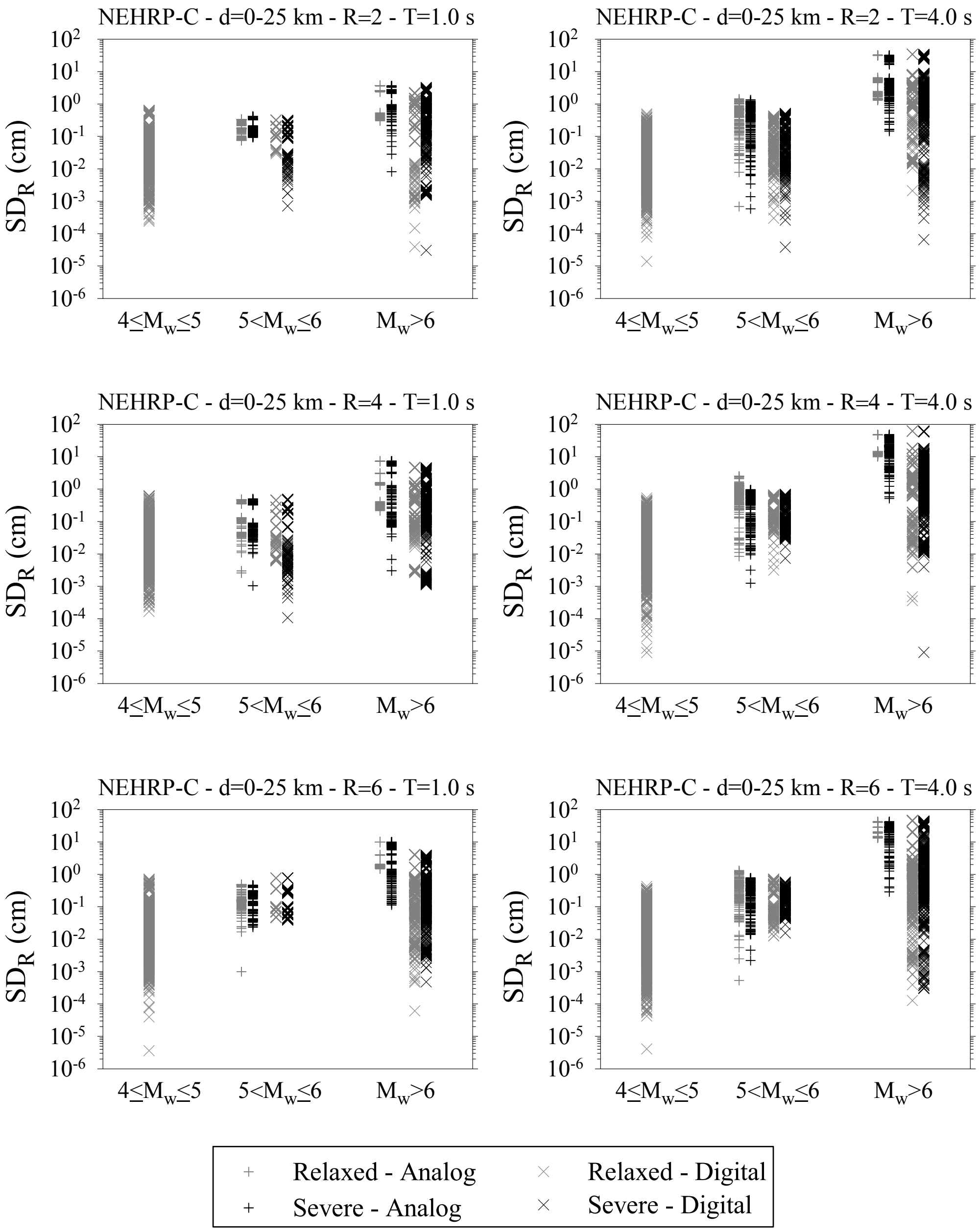

Figure B.2 Scatter plots of residual displacements for ND model.

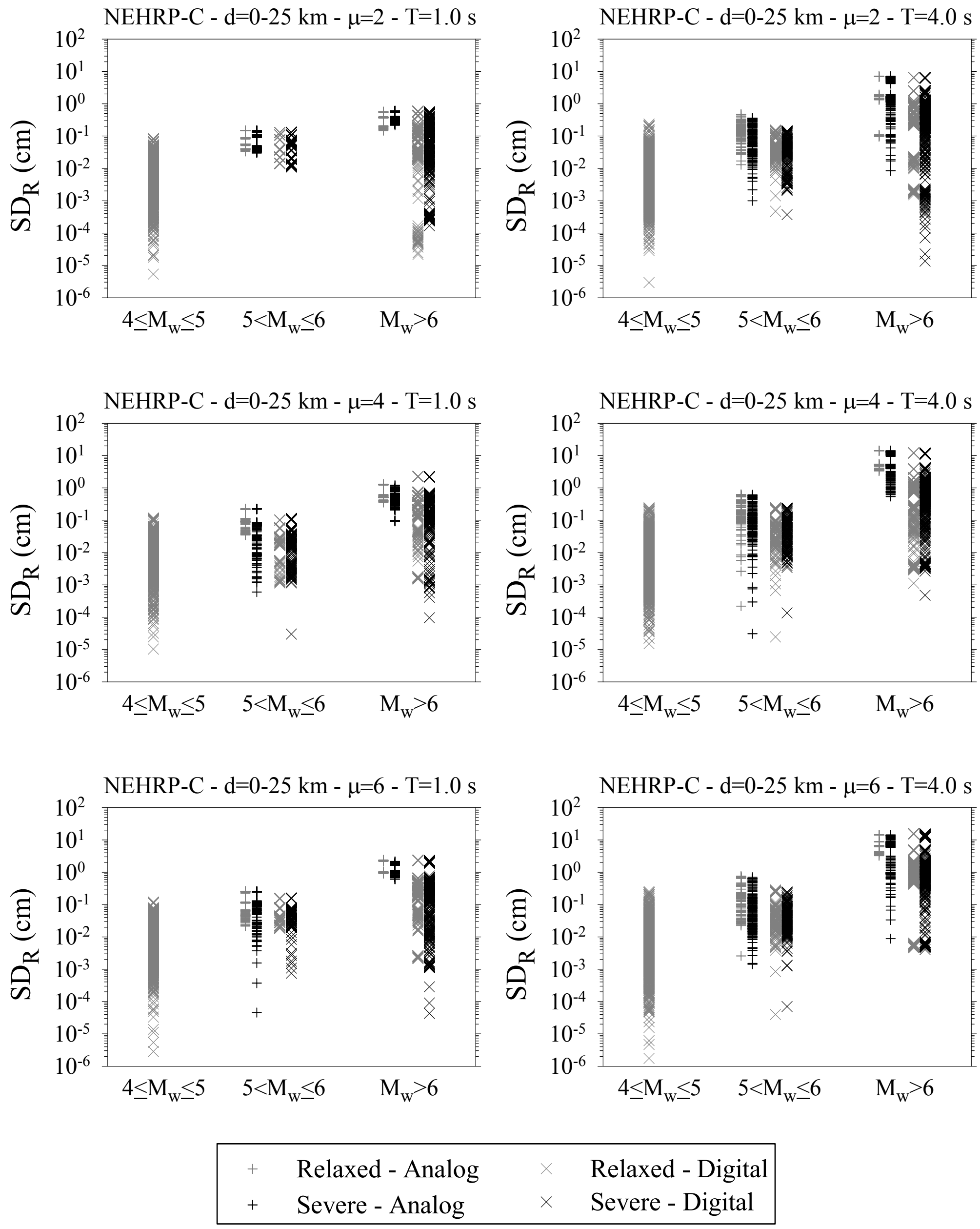

Figure B.3 Scatter plots of residual displacements for SD model.

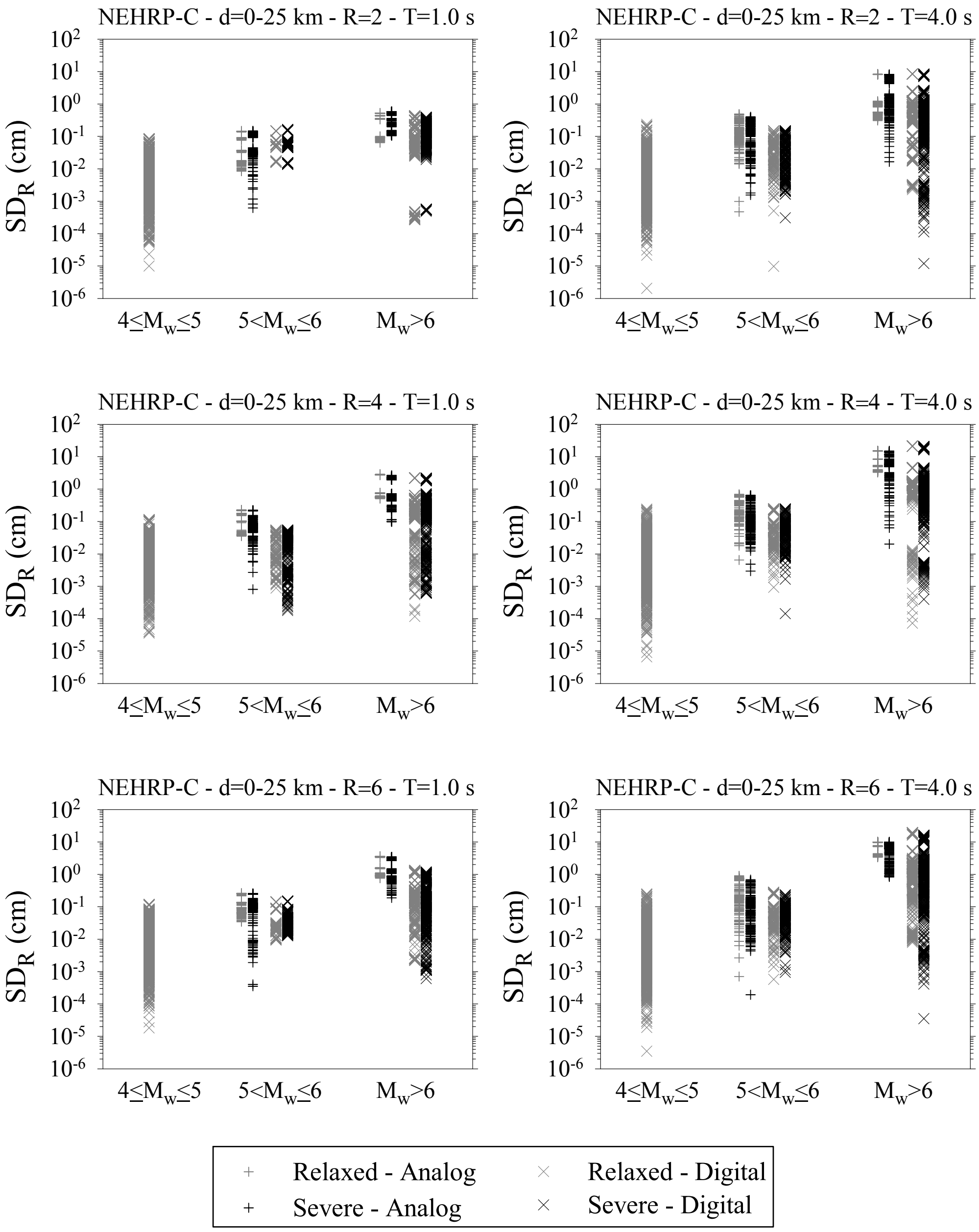

Figure B.4 Scatter plots of residual displacements for SD model.

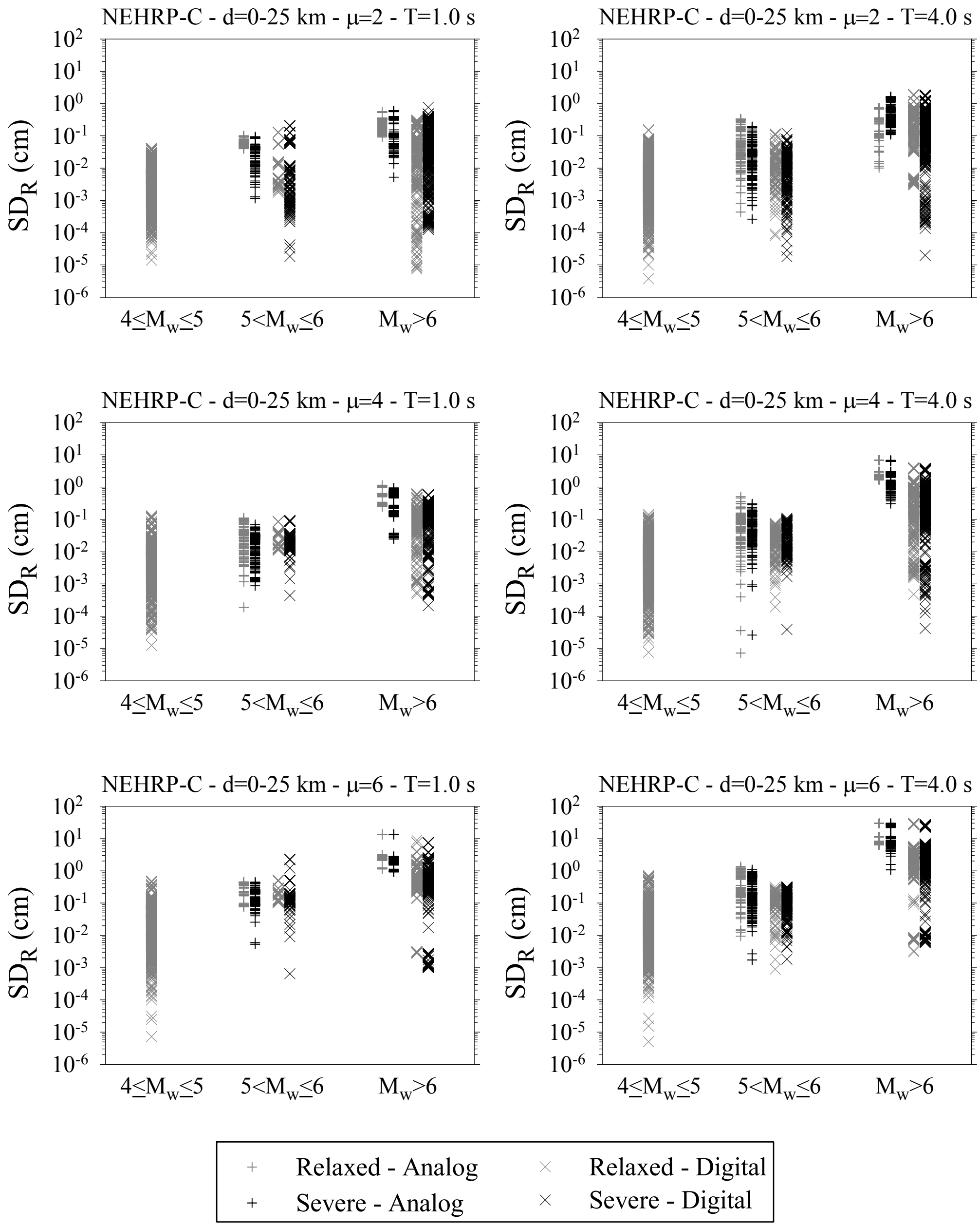

Figure B.5 Scatter plots of residual displacements for SSD model.

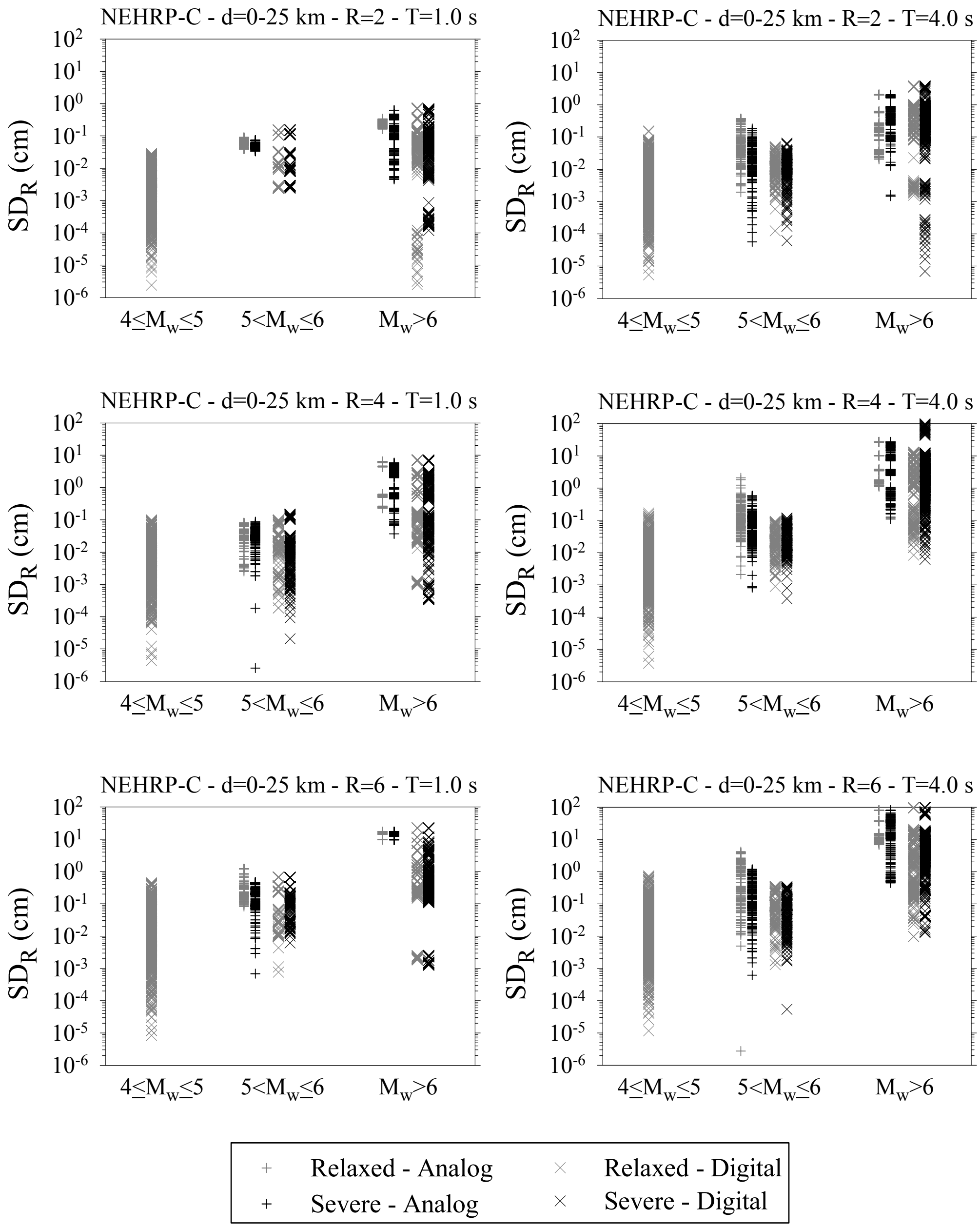

Figure B.6 Scatter plots of residual displacements for SSD model.

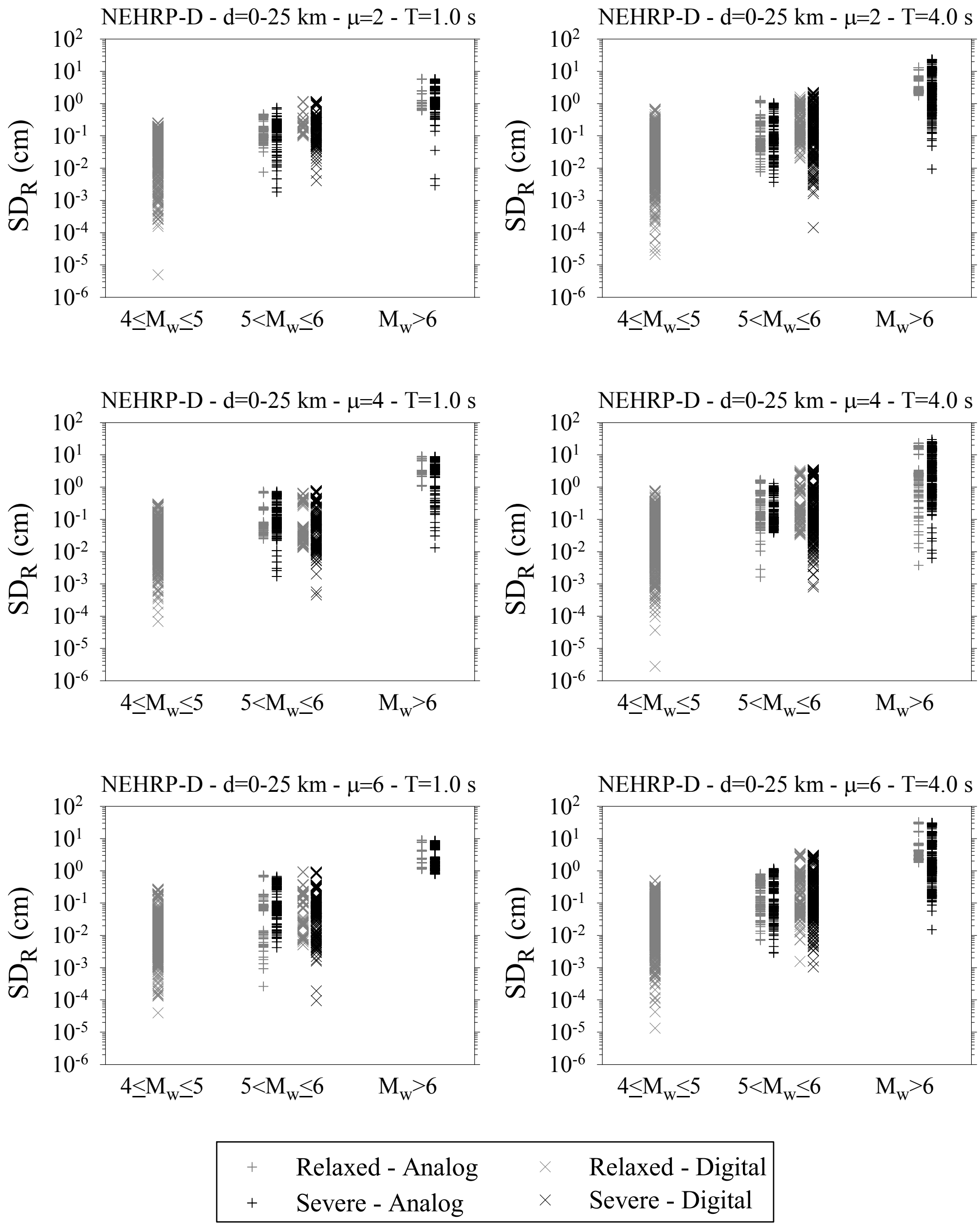

Figure B.7 Scatter plots of residual displacements for ND model.

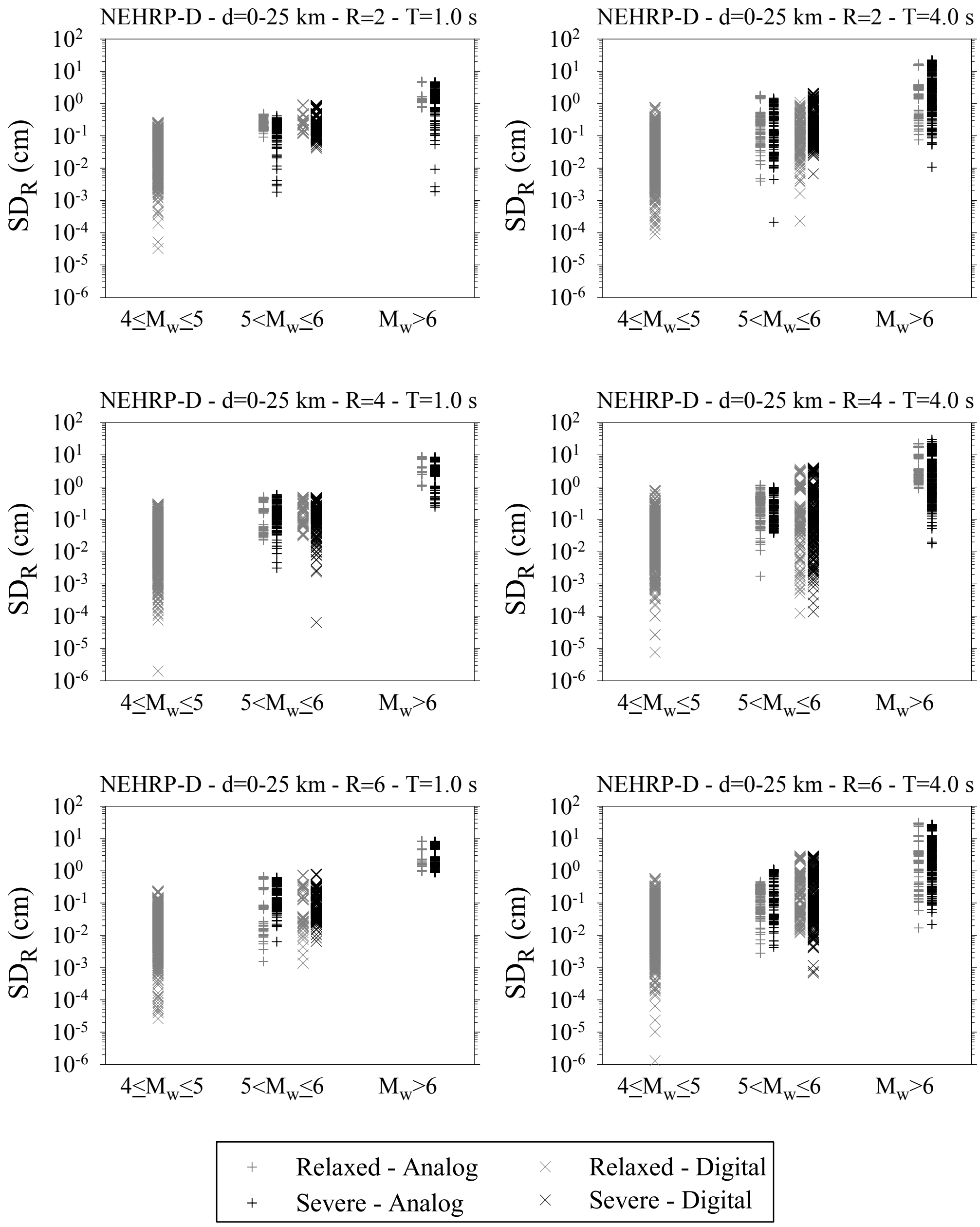

Figure B.8 Scatter plots of residual displacements for ND model.

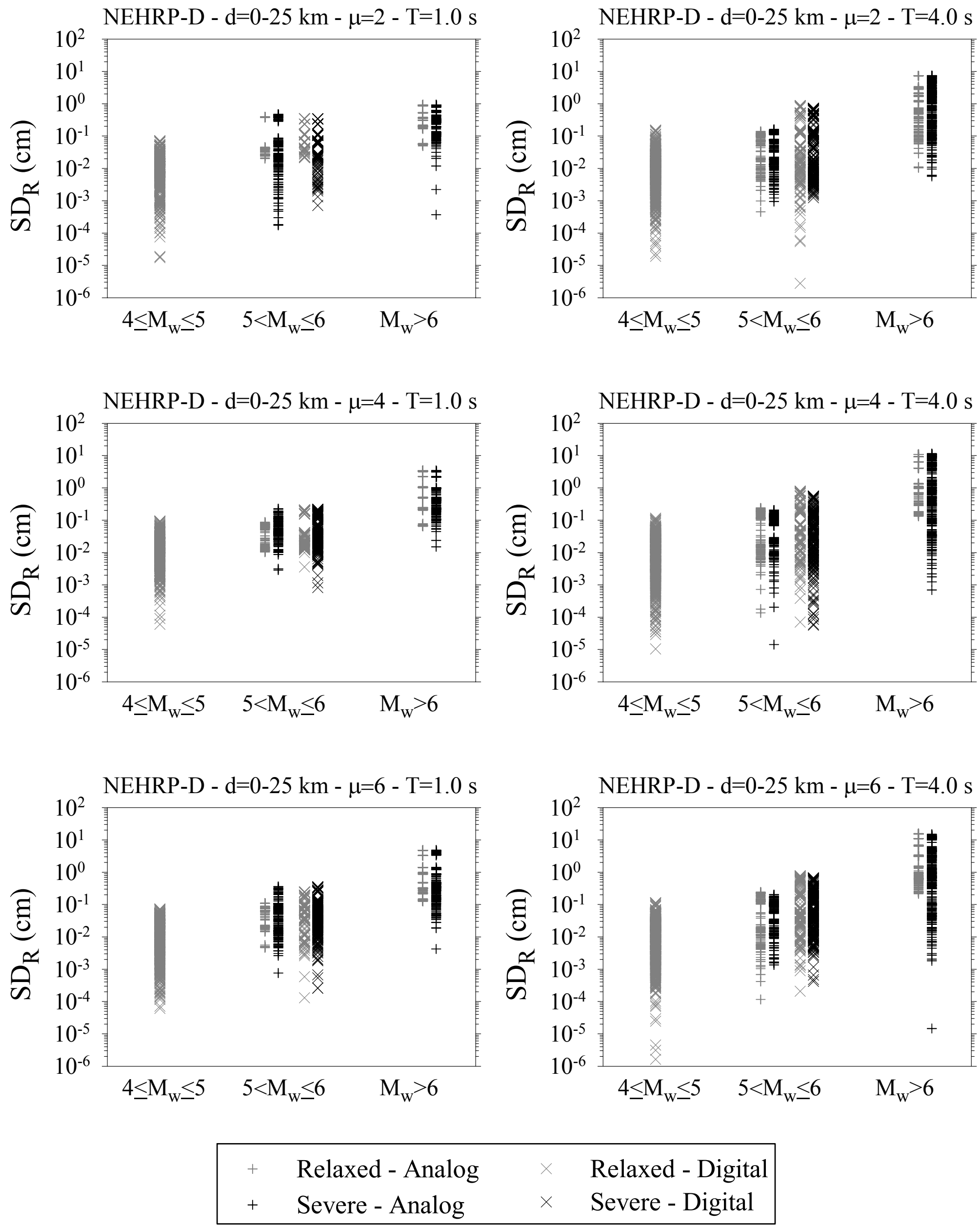

Figure B.9 Scatter plots of residual displacements for SD model.

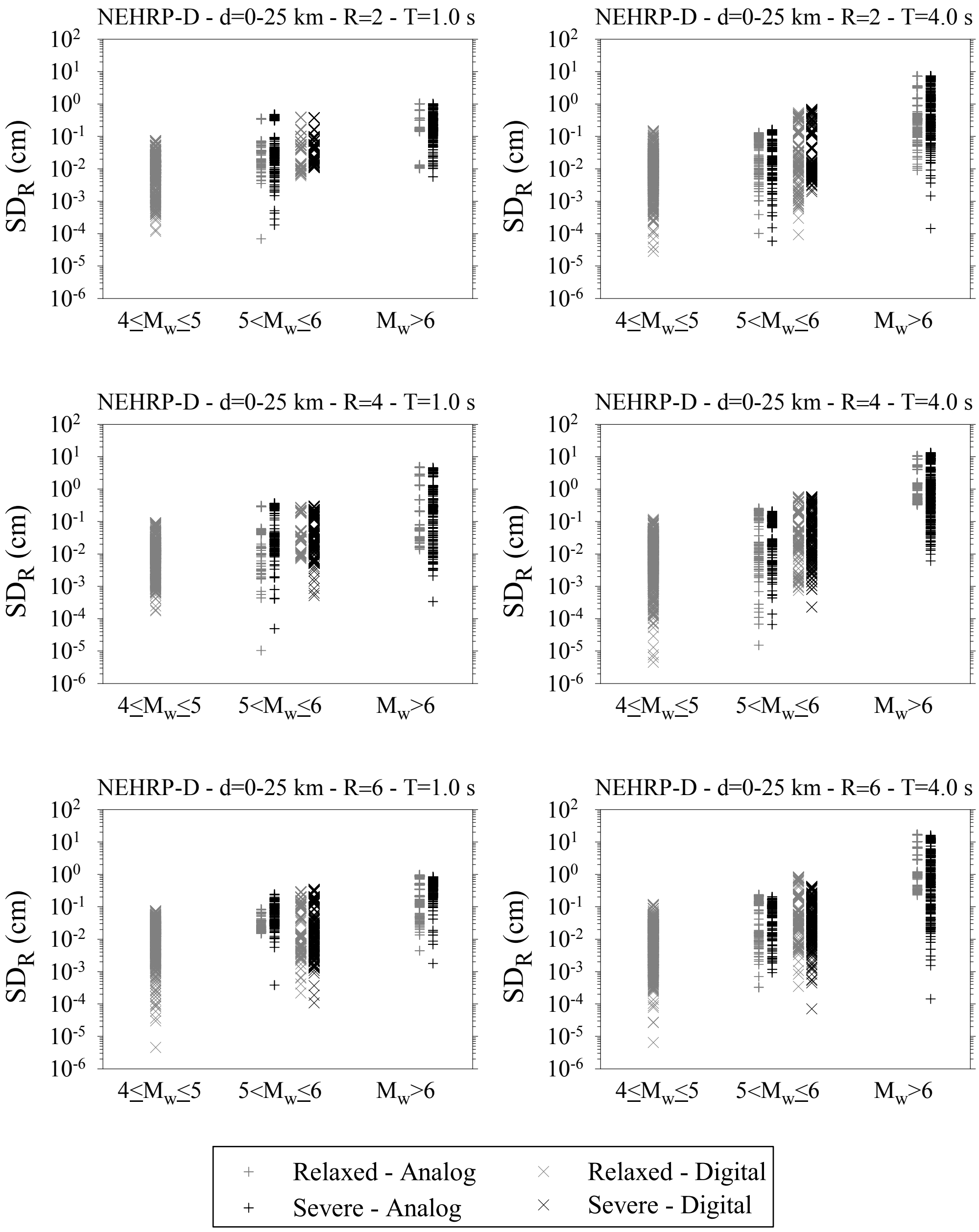

Figure B.10 Scatter plots of residual displacements for SD model.

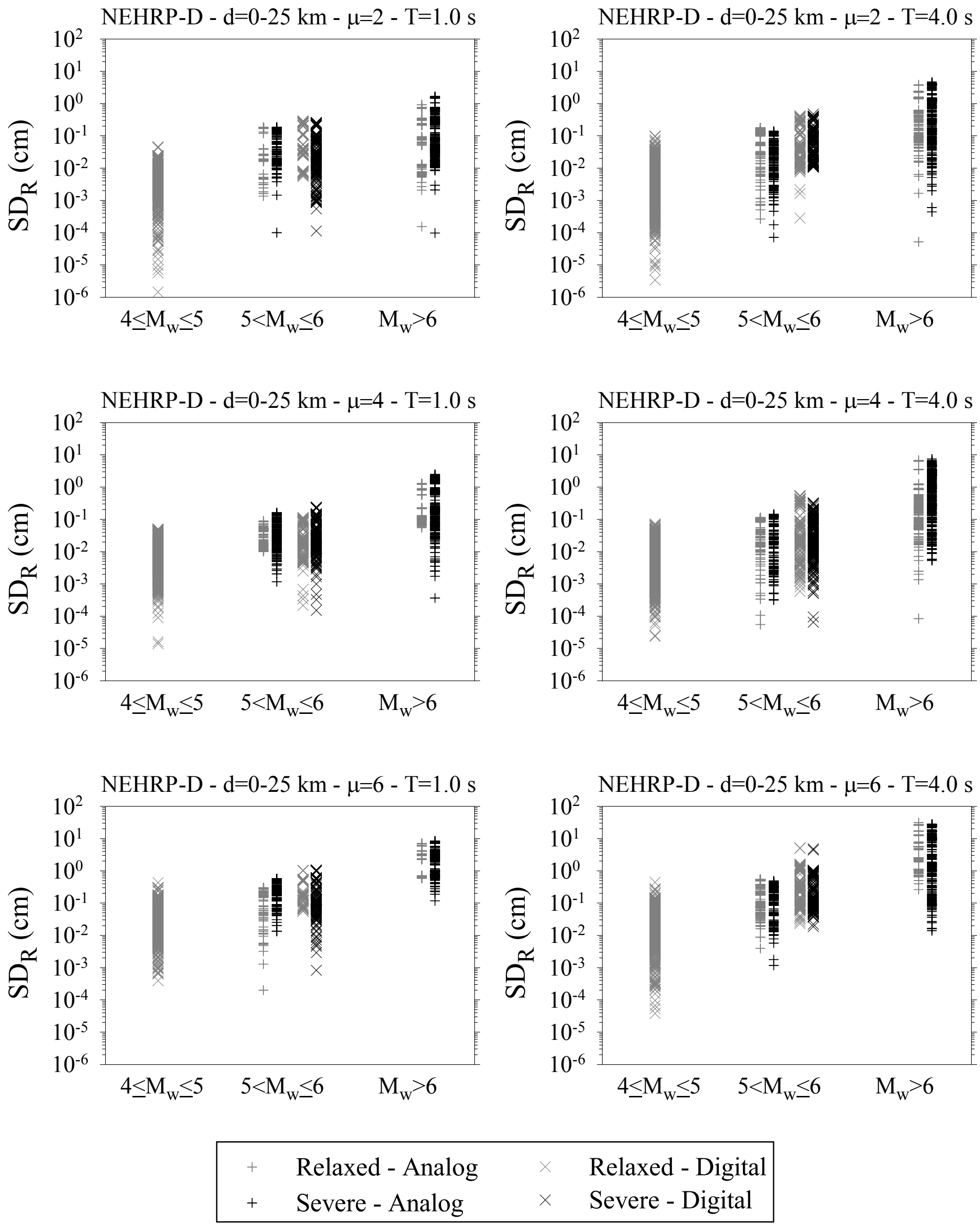

Figure B.11 Scatter plots of residual displacements for SSD model.

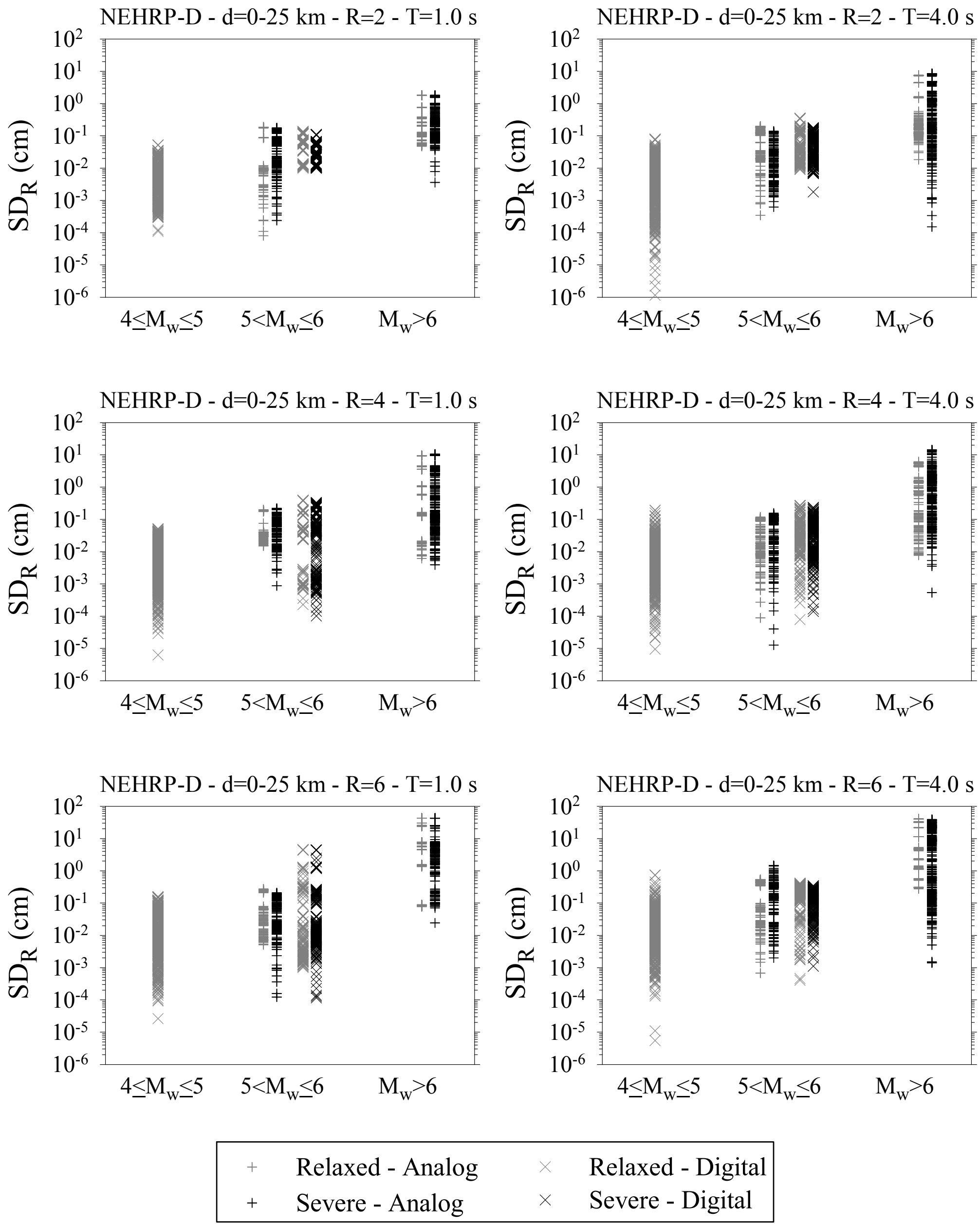

Figure B.12 Scatter plots of residual displacements for SSD model.

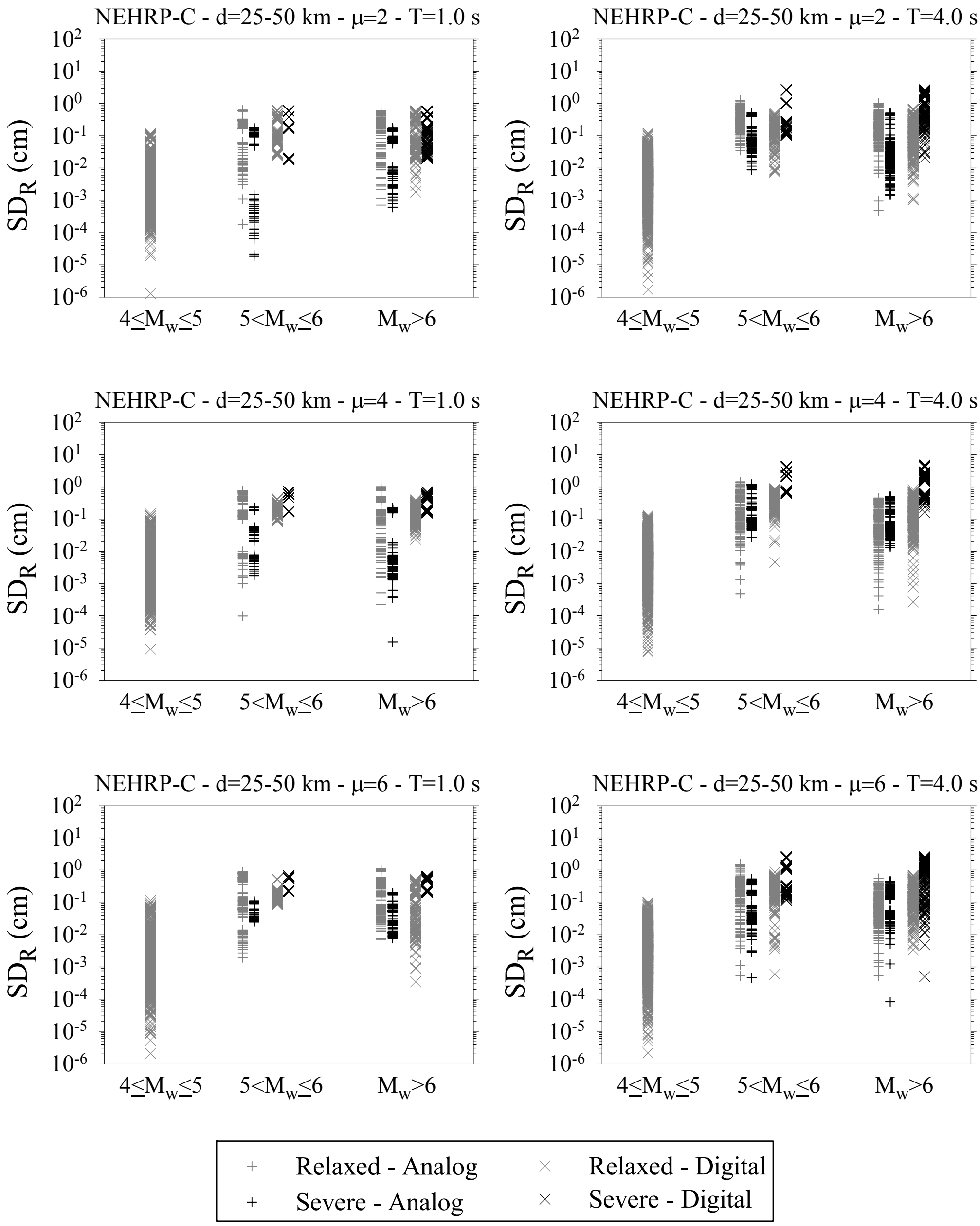

Figure B.13 Scatter plots of residual displacements for ND model.

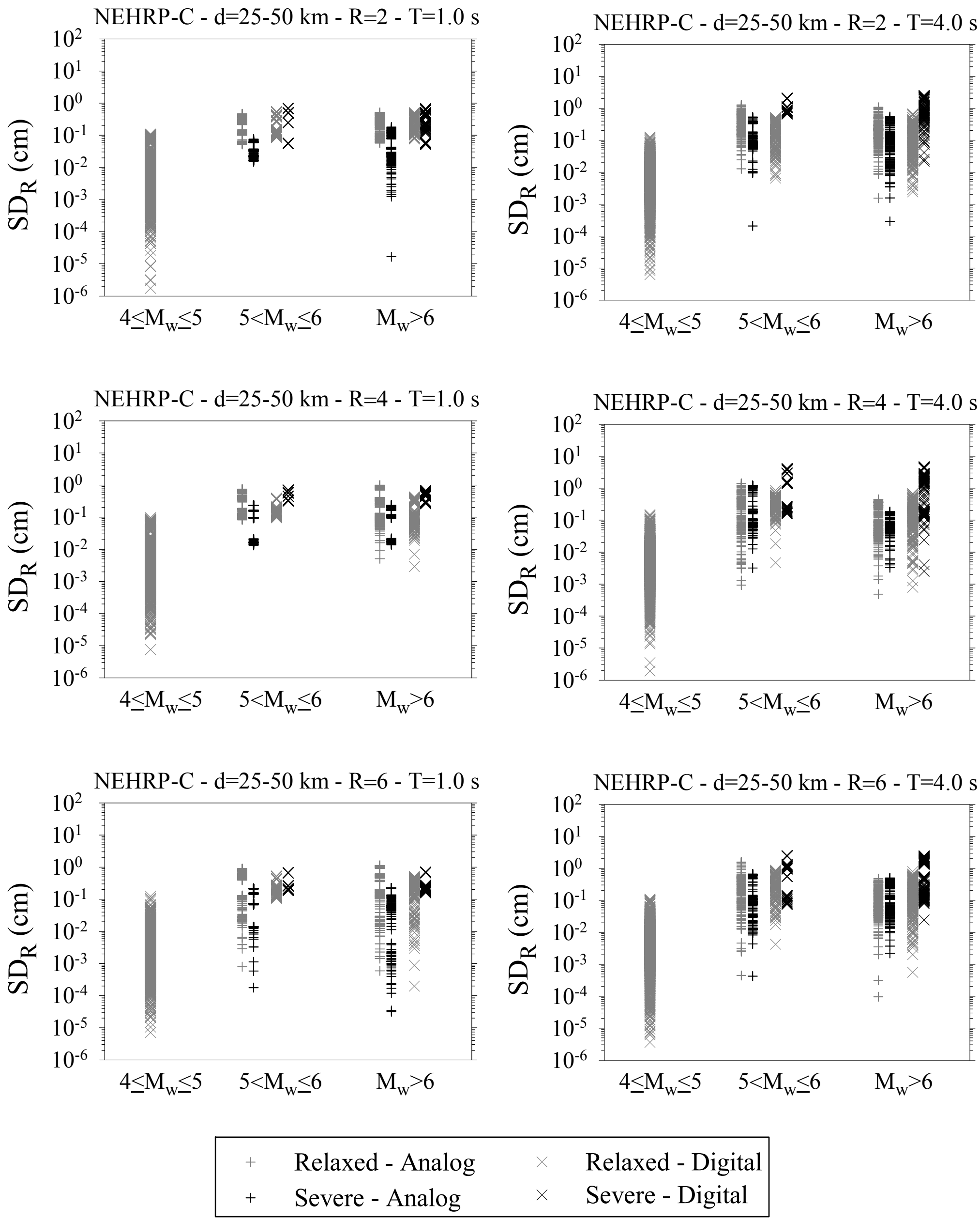

Figure B.14 Scatter plots of residual displacements for ND model.

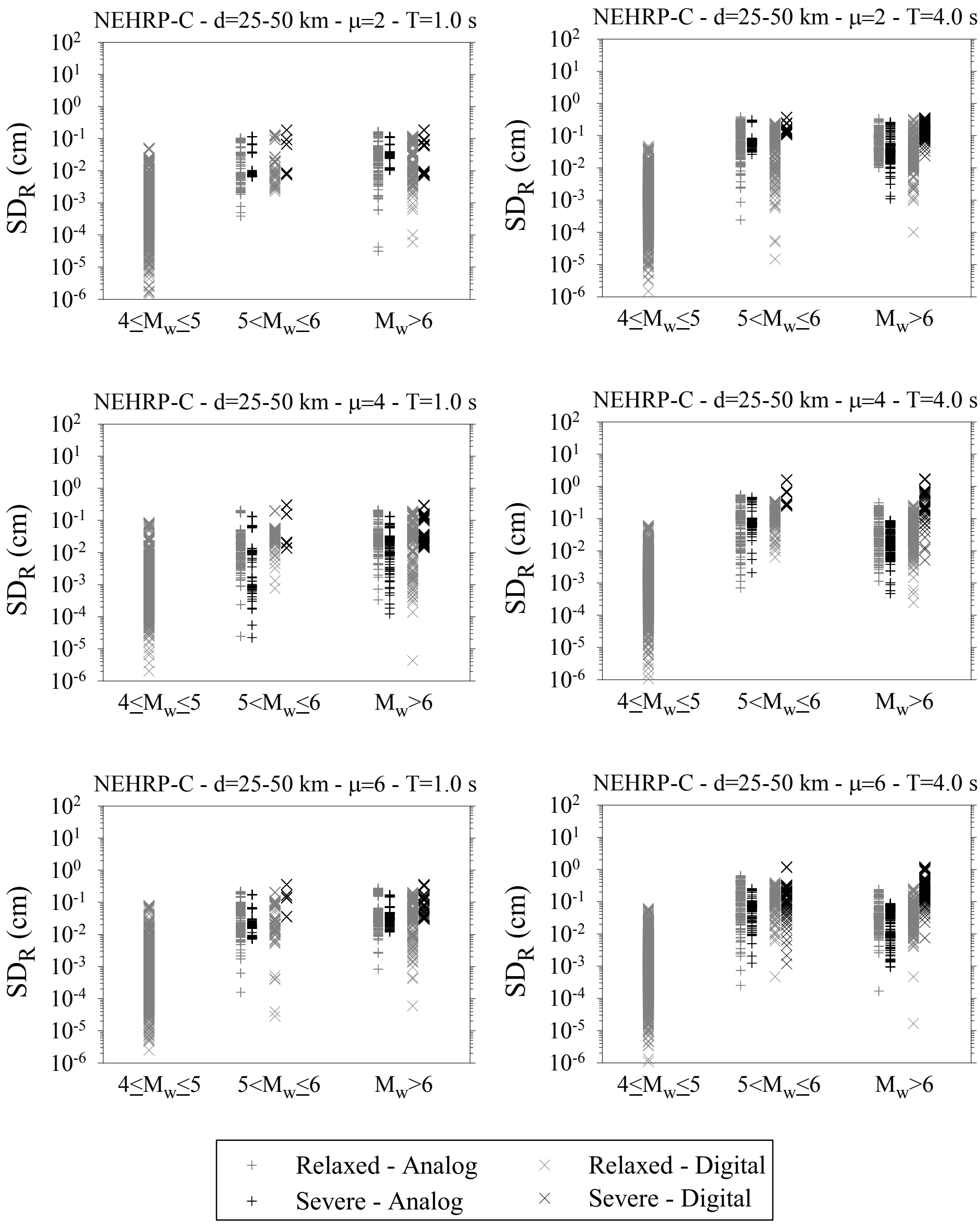

Figure B.15 Scatter plots of residual displacements for SD model.

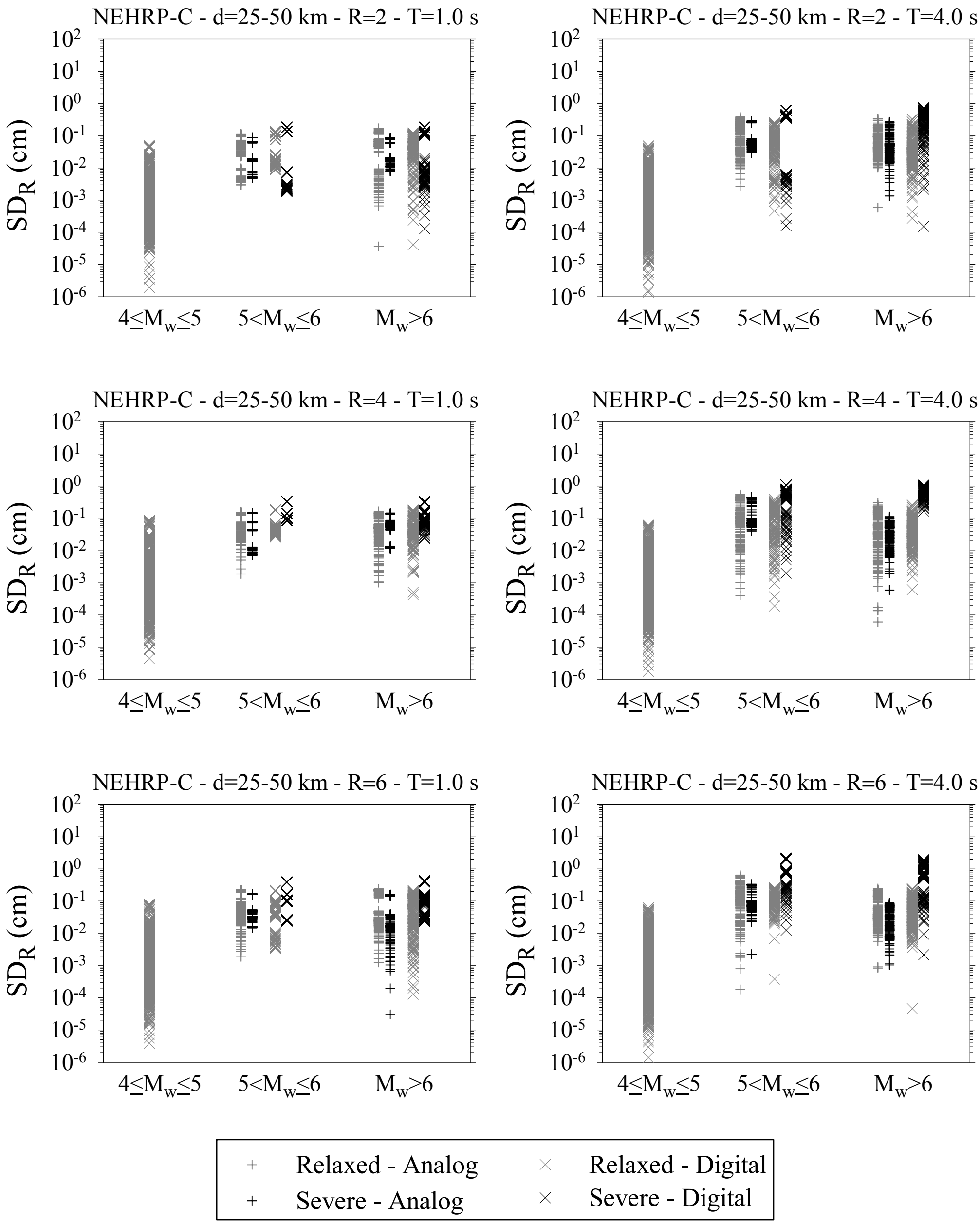

Figure B.16 Scatter plots of residual displacements for SD model.

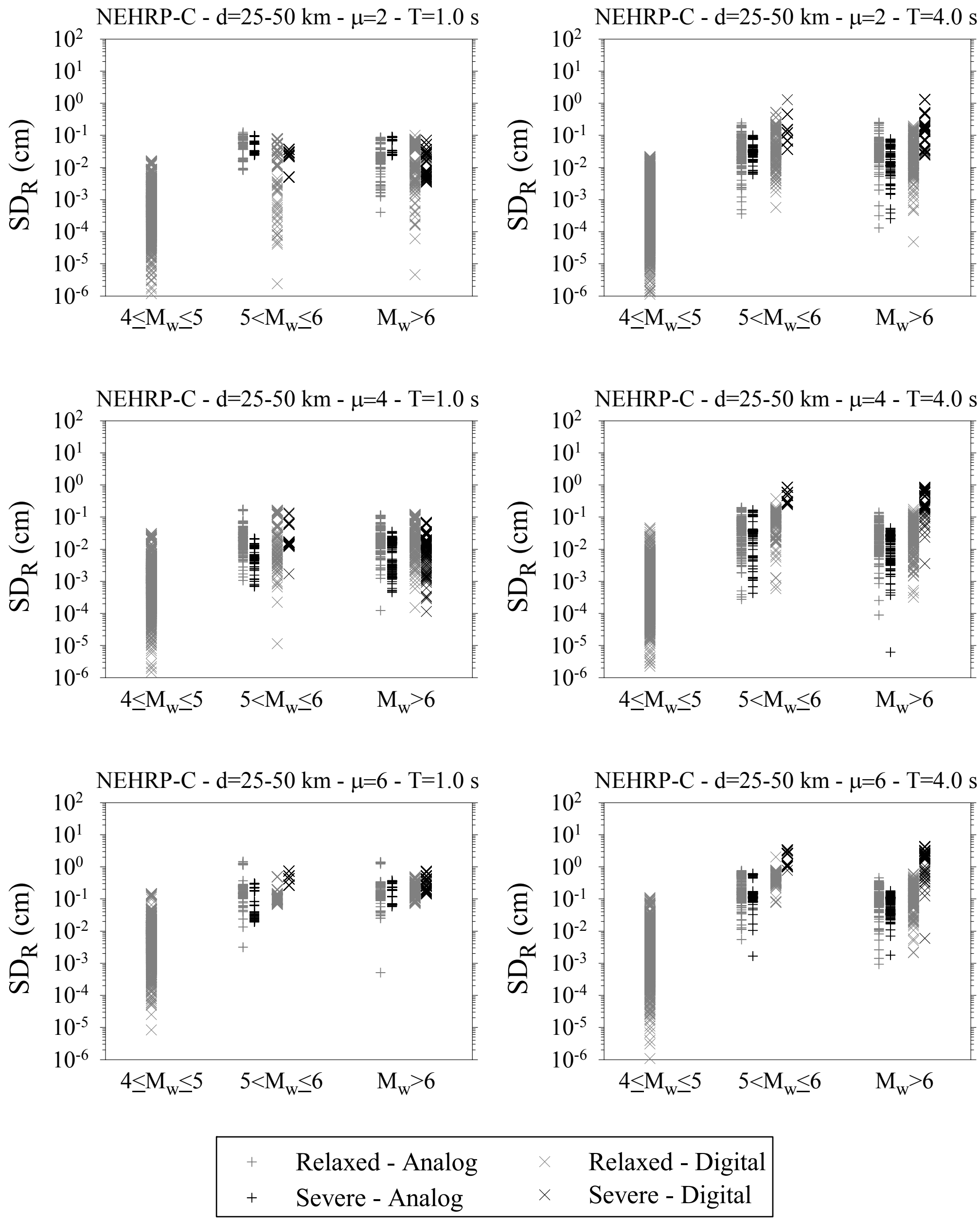

Figure B.17 Scatter plots of residual displacements for SSD model.

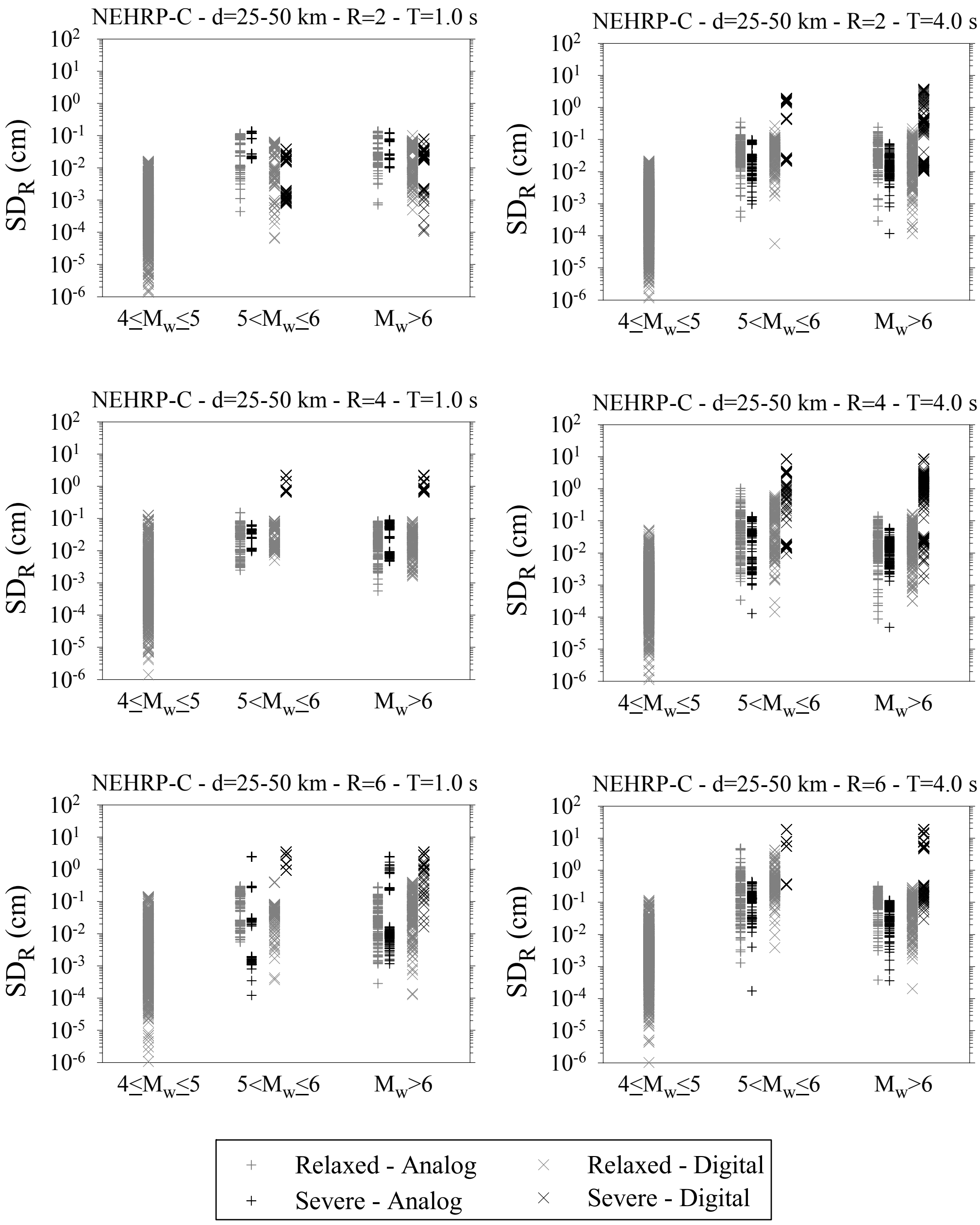

Figure B.18 Scatter plots of residual displacements for SSD model.

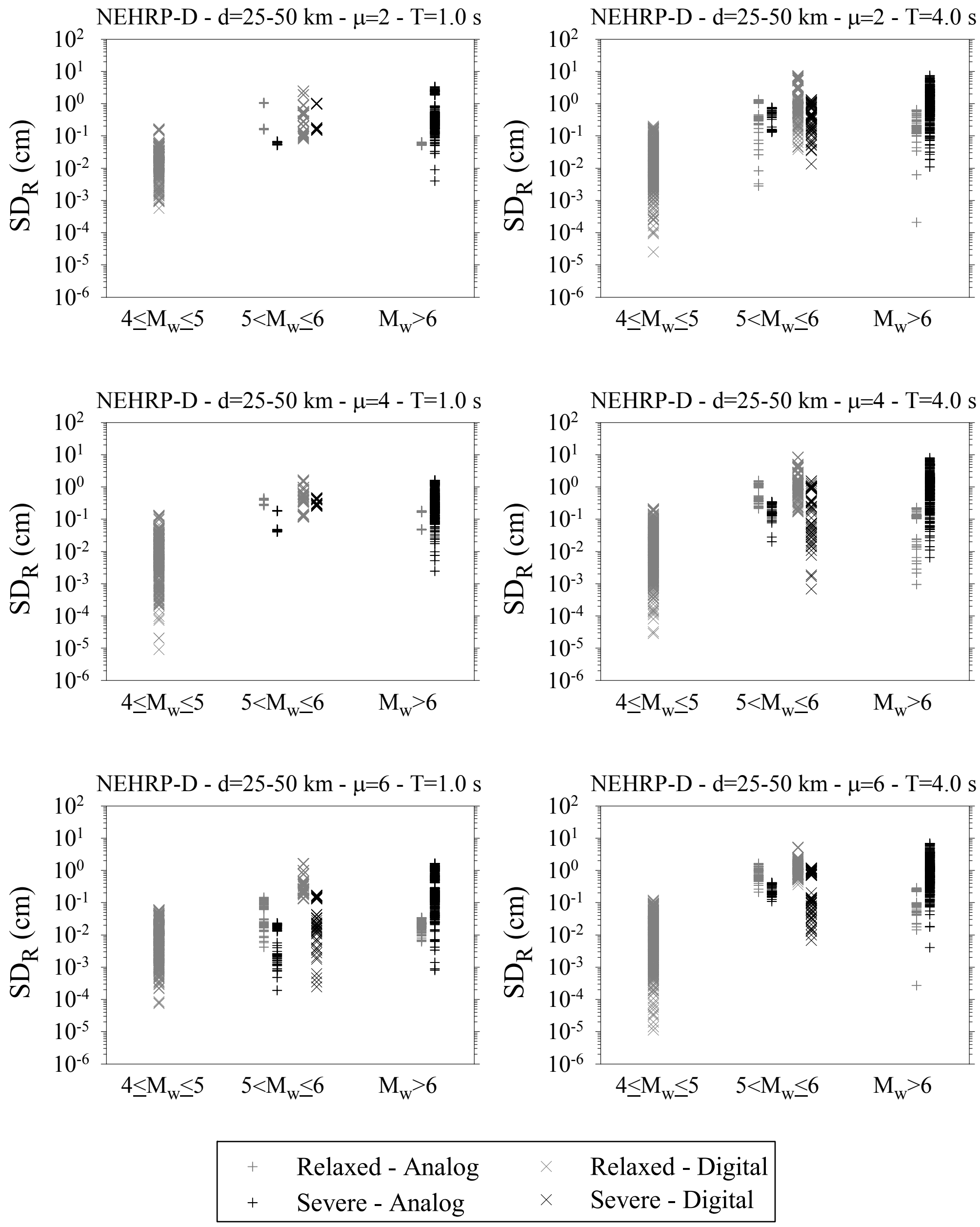

Figure B.19 Scatter plots of residual displacements for ND model.

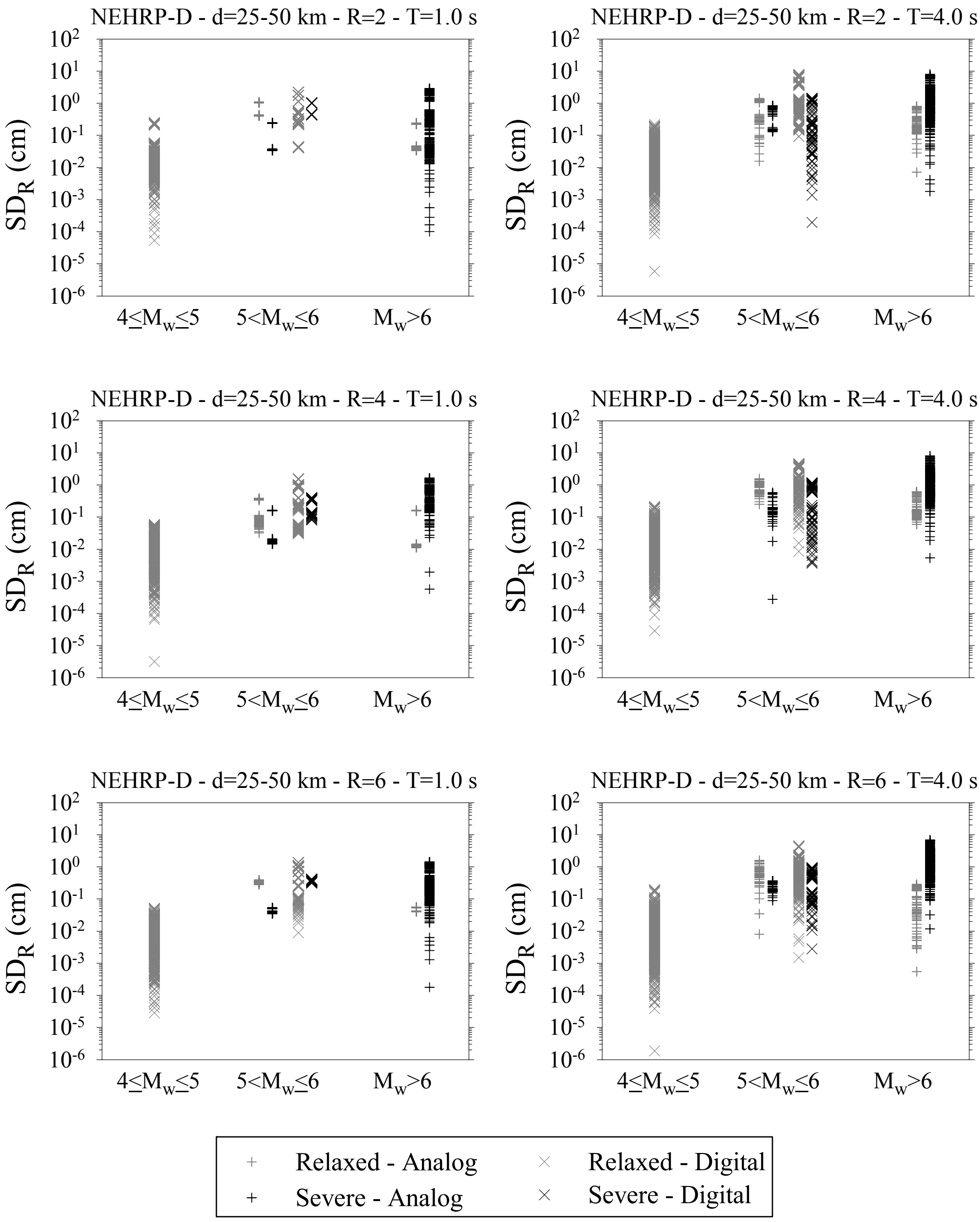

Figure B.20 Scatter plots of residual displacements for ND model.

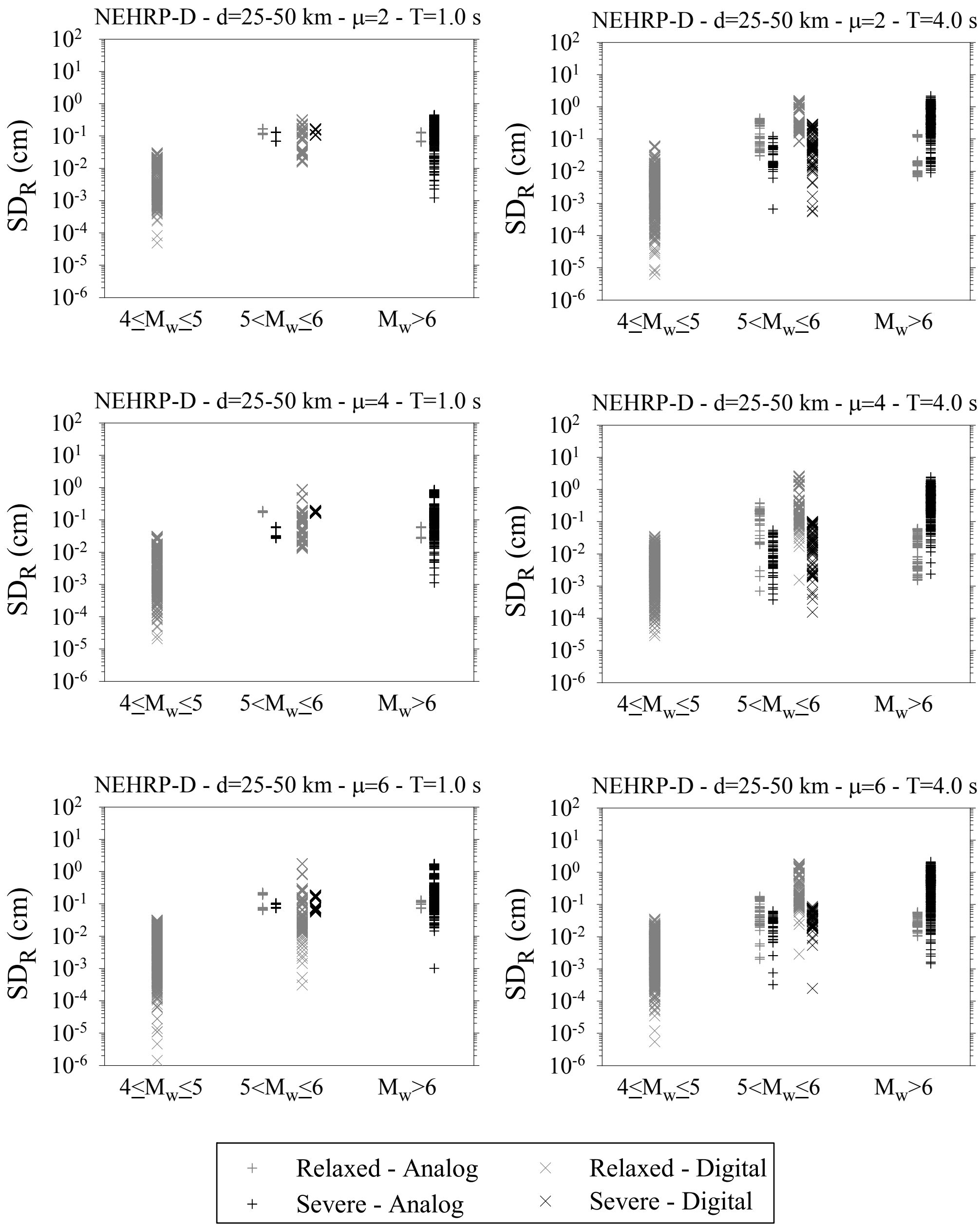

Figure B.21 Scatter plots of residual displacements for SD model.

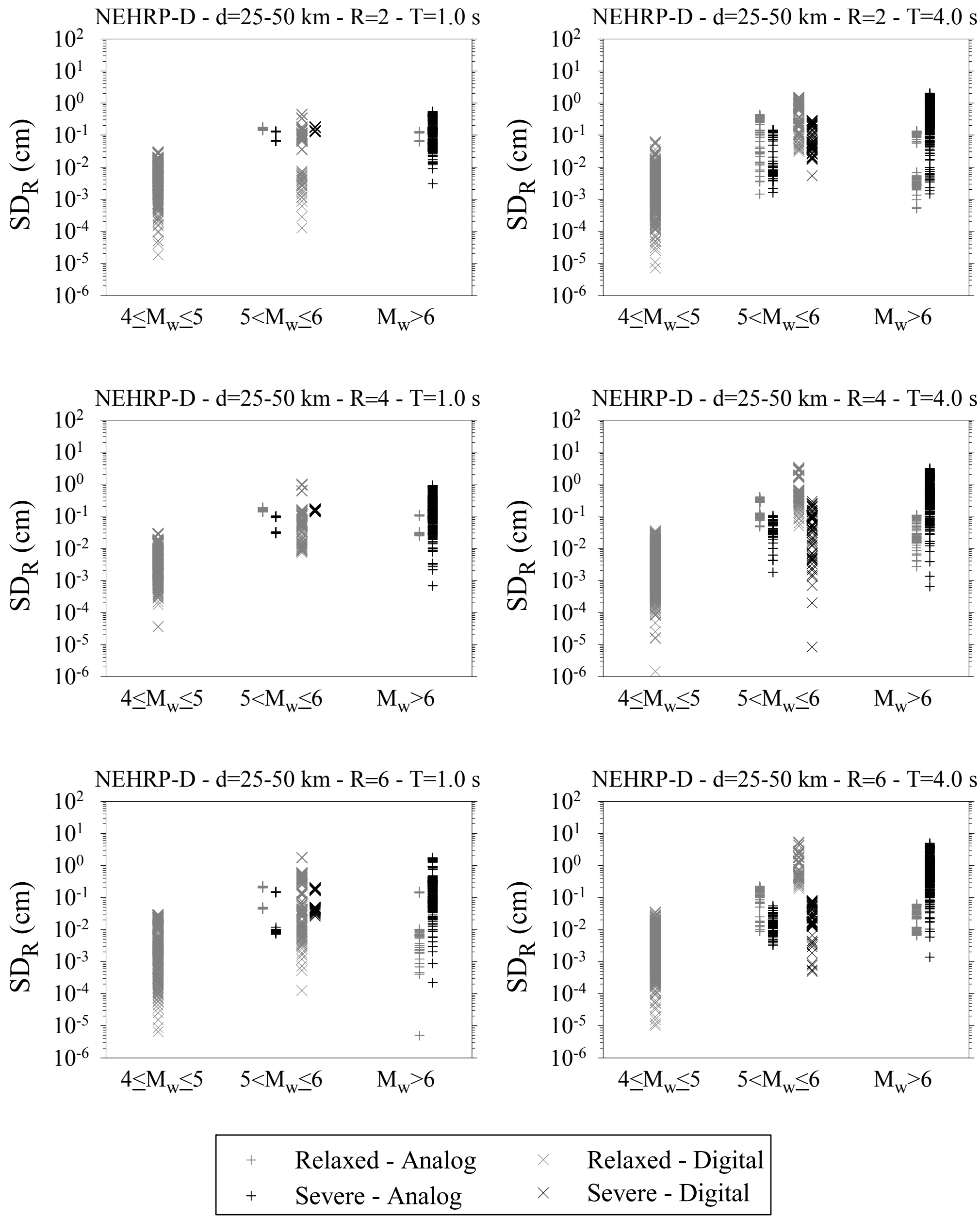

Figure B.22 Scatter plots of residual displacements for SD model.

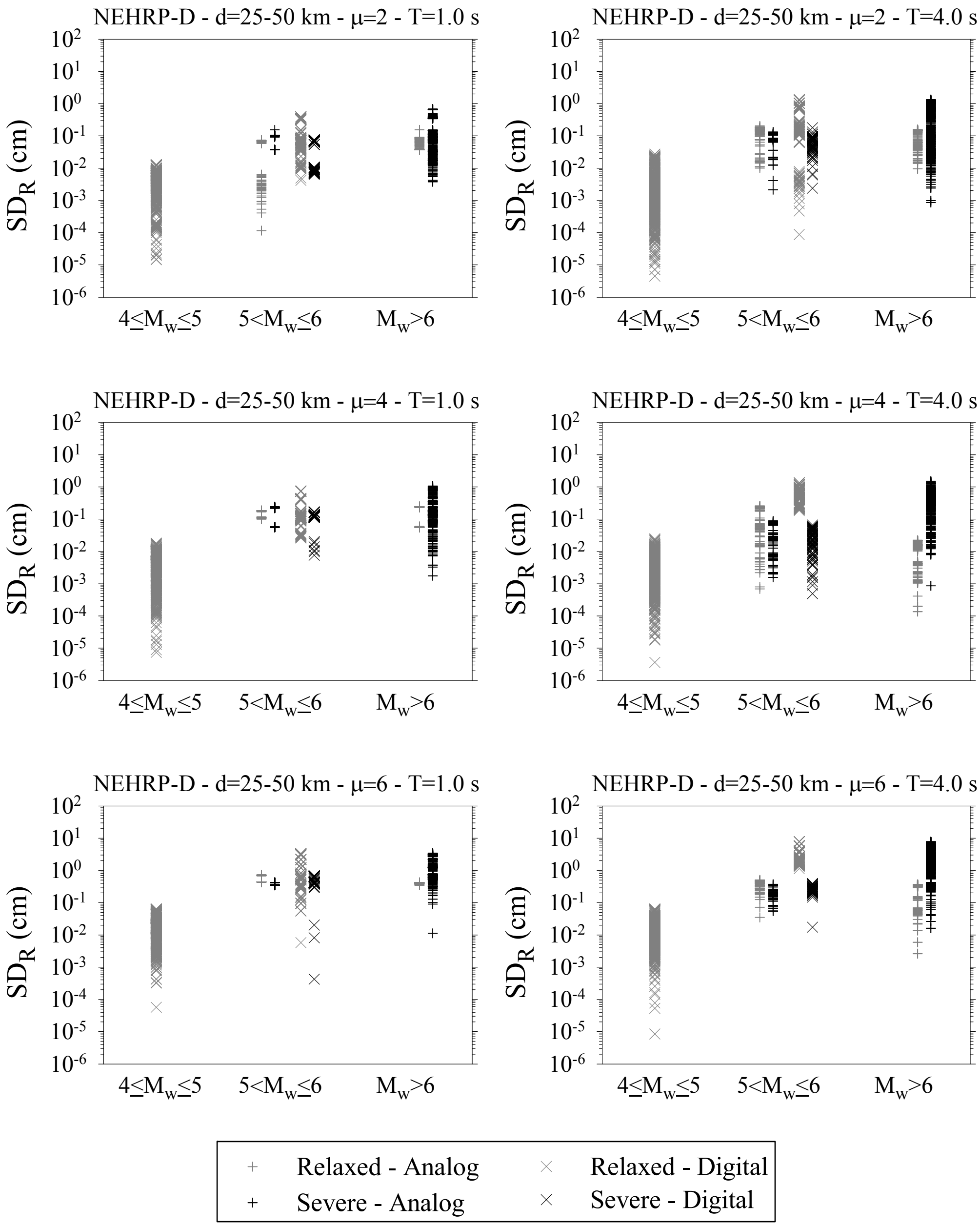

Figure B.23 Scatter plots of residual displacements for SSD model.

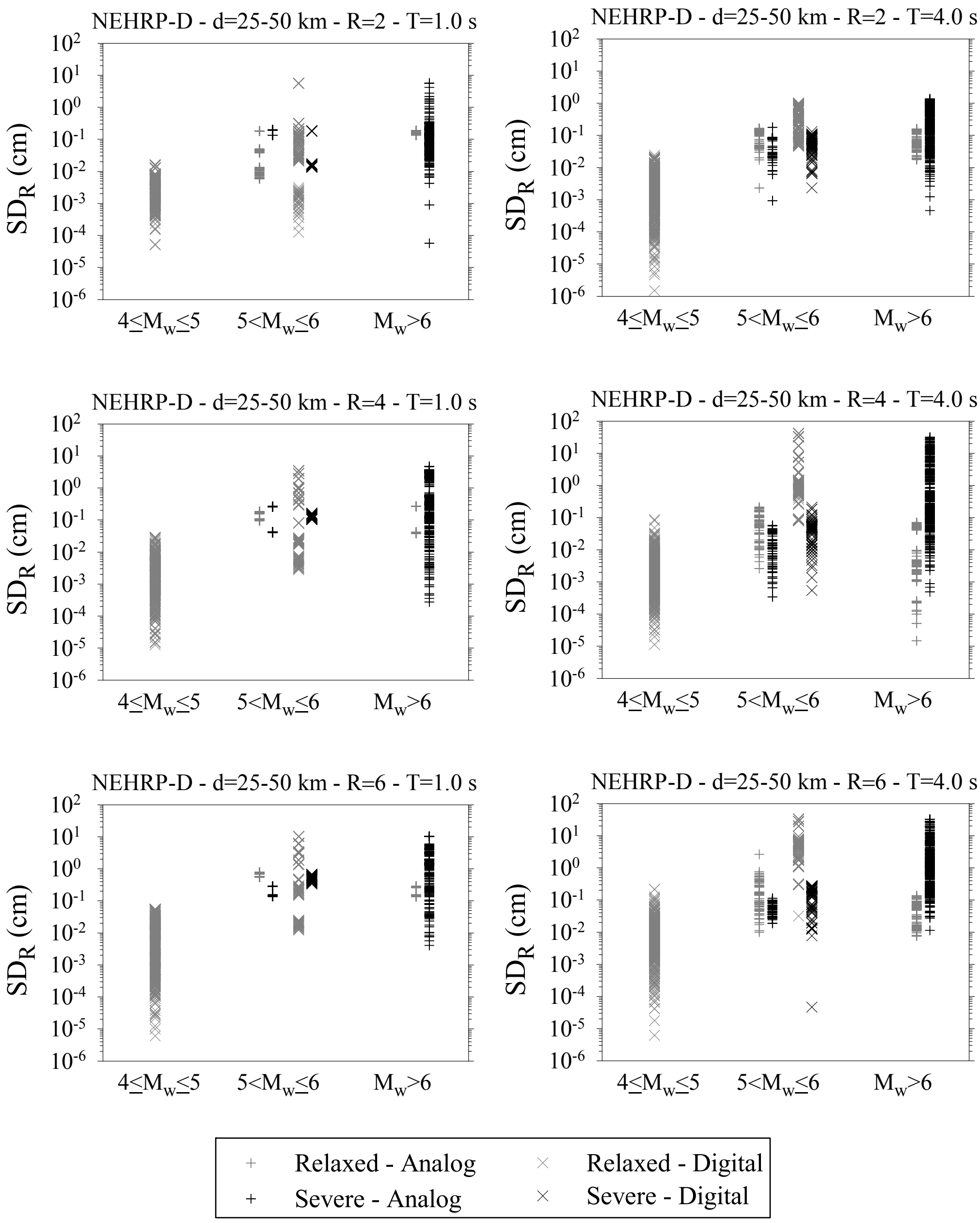

Figure B.24 Scatter plots of residual displacements for SSD model.